NEAR-INFRARED PROPERTIES OF QUASAR AND SEYFERT HOST GALAXIES

by

Kim Katris McLeod

A Dissertation Submitted to the Faculty of the

DEPARTMENT OF ASTRONOMY

In Partial Fulfillment of the Requirements
For the Degree of

DOCTOR OF PHILOSOPHY

In the Graduate College

THE UNIVERSITY OF ARIZONA

1 9 9 4

Order Number 9502621

Near-infrared properties of quasar and Seyfert host galaxies

McLeod, Kim Katris, Ph.D.

The University of Arizona, 1994

U·M·I
300 N. Zeeb Rd.
Ann Arbor, MI 48106

NEAR-INFRARED PROPERTIES OF QUASAR AND SEYFERT HOST GALAXIES

by

Kim Katris McLeod

A Dissertation Submitted to the Faculty of the

DEPARTMENT OF ASTRONOMY

In Partial Fulfillment of the Requirements
For the Degree of

DOCTOR OF PHILOSOPHY

In the Graduate College

THE UNIVERSITY OF ARIZONA

1 9 9 4

THE UNIVERSITY OF ARIZONA
GRADUATE COLLEGE

As members of the Final Examination Committee, we certify that we have read the dissertation prepared by Kim Katris McLeod entitled Near-infrared Properties of Quasar and Seyfert Host Galaxies

and recommend that it be accepted as fulfilling the dissertation requirement for the Degree of Doctor of Philosophy

George H. Rieke	7/13/94 Date
Christopher D. Impey	7/13/94 Date
John H. Black	1994 July 13 Date
Craig B. Foltz	7/13/94 Date
	Date

Final approval and acceptance of this dissertation is contingent upon the candidate's submission of the final copy of the dissertation to the Graduate College.

I hereby certify that I have read this dissertation prepared under my direction and recommend that it be accepted as fulfilling the dissertation requirement.

Dissertation Director George H. Rieke	7/25/94 Date

STATEMENT BY AUTHOR

This dissertation has been submitted in partial fulfillment of requirements for an advanced degree at The University of Arizona and is deposited in the University Library to be made available to borrowers under rules of the Library.

Brief quotations from this dissertation are allowable without special permission, provided that accurate acknowledgment of source is made. Requests for permission for extended quotation from or reproduction of this manuscript in whole or in part may be granted by the head of the major department or the Dean of the Graduate College when in his or her judgment the proposed use of the material is in the interests of scholarship. In all other instances, however, permission must be obtained from the author.

SIGNED: KK McLeod

ACKNOWLEDGMENTS

This work benefitted from the contributions of many people. I am grateful to T. Boroson, J. Bechtold, and D. Friedli for useful discussions; J.B. Hutchings for helpful comments on Chapter 2; D. Williams and W. Latter for observing some of the objects; Tad Morgan for assistance with data reduction; and the 90″operators. Thanks to M. Rieke and E. Montgomery for providing and maintaining the excellent infrared camera. Data processing made extensive use of IRAF. This material is based upon work supported by the NSF (Grant AST-9116442 and a Graduate Student Fellowship).

Particular thanks go to the members of my committee for valuable comments and questions, and for taking it easy on me! I thank Chris Impey; Craig (Cra-ha-ha-haig) Foltz; and especially Johnblack, whose unique talent for asking well-thought-out questions has taught and amazed me for the past 6 years.

I never would have made it to Arizona without the help of Jim Houck; I thank him for giving me my first astronomy job. I was lured to Tucson by the excellent group of grad students who came before me, and I thank them all for showing me how it is done. Special recognition goes to: "Caveman" Doug Kelly for friendship, constant enthusiasm, and 5-ball inspiration; Dennis Zaritsky (yo-ho, yo-ho...) and Hans-Walter Rix (also M.B.) for good advice and friendship on and off the soccer field–you guys are truly the best; and Joe Haller for Zinger breaks and office chats.

For making classes bearable, I thank my classmates Bob, Sally, Karen, and Kim. Gracias Dante Minniti, for teaching me soccer and a FEW words of Spanish, for being a great officemate, and for being a dude.

I am grateful for the friendship of grads who came after me, including Dougw (Did you know he's a blackbelt?), The Patmeister, neighbors Anne, Tim, and Dspray, and my many officemates over the years. I would never have made it through the last few months without the juggling companionship of Chris and Chad. Juggle on, guys! Heartfelt thanks to Jeff "The Ring Guy" Reggie, who has been a true friend since first we met at Fuertes Observatory, Cornell, 10 years ago.

I thank all the faculty and staff of Steward for making this a great place to be. Special thanks to the lunch bunch and their families: Roc, Bill, Gary B., John. I am very sorry to be leaving Jill Bechtold and Ed, Julia, and C.J. Olszewski; I thank them for letting us be part of their family while we were here.

George Rieke. George, George, George...What can I say in order to properly thank you? It has been an honor and a pleasure to be your student. My only regret is that I didn't find you sooner. Thank you for taking care of me, science-wise and otherwise...I'll miss you very much.

DEDICATION

This dissertation is dedicated to my family with all of my love

To my dad Jack, 1933-1979, for turning my gaze upwards

To my mom Ar, for keeping hers there in the face of adversity

To my brother Jeff, for putting it to words

To my grandma Helen, for always smiling

To the Crowes and company, for the music, the beach, and the fun

And to Brian, my sweetheart and my best friend

Contents

List of Figures

List of Tables

ABSTRACT

We present near-infrared images of nearly 100 host galaxies of Active Galactic Nuclei (AGN). Our quasar sample is comprised of the 50 quasars from the Palomar Green Bright Quasar Survey with redshifts $z \leq 0.3$. We have restricted the redshift range to ensure adequate spatial resolution, galaxy detectability, and minimal distance-dependent effects, while still giving a large sample of objects. For lower-luminosity AGN we have chosen to image the CfA Seyfert sample. This sample is composed of 48 Seyferts, rougly equally divided among types 1, 1.5-1.9, and 2. This sample was spectroscopically selected, and, therefore, is not biased towards Seyferts with significant star formation. Taken together, these samples allow a statistical look at the continuity of host-galaxy properties over a factor of 10,000 in nuclear luminosity.

We find the near-infrared light to be a good tracer of luminous mass in these galaxies. The Seyferts are found in galaxies of type S0 to Sc. The radio quiet quasars live in similar kinds of galaxies spanning the same range of mass centered around L^*. However, for the most luminous quasars, there is a correlation between the minimum host-galaxy mass and the luminosity of the active nucleus. Radio-loud quasars are generally found in hosts more massive than an L^* galaxy. We also detect a population of low-mass host galaxies with very low-luminosity Seyfert nuclei.

The low luminosity quasars and the Seyferts both tend to lie in host galaxies seen preferentially face-on, which suggests there is a substantial amount of obscuration coplanar with the galaxian disk. The obscuration must be geometrically thick (thickness-to-radius ~ 1) and must cover a significant fraction of the narrow line region (r $>$ 100 pc).

We have examined our images for signs of perturbations that could drive fuel toward the galaxy nucleus, but there are none we can identify at a significant level. The critical element for fueling is evidently not reflected clearly in the large scale distribution of luminous mass in the galaxy.

We also present an infrared image of the jet of 3C 273 and compare it to visible and radio images from the literature.

Chapter 1

BACKGROUND

1.1 Introduction

The subject of active galactic nuclei (AGN) encompasses a huge range of subfields in astronomy, and in so doing keeps a huge number of astronomers off the streets. In the broadest definition, a galaxy is said to host an AGN if there are energetic phenomena in its nucleus that cannot be produced by normal stellar processes. Members of this class include liners, Seyfert galaxies, BL Lac objects, radio galaxies, and quasars. (In this dissertation the terms quasar and quasistellar object (QSO) are used interchangably.) These objects are characterized by a large bolometric luminosity, up to $\sim$ 15 orders of magnitude higher than that of the Sun in extreme cases, originating from a region whose size is much less than the distance from the Sun to the next nearest star.

Cosmologists are interested in quasars because they (the quasars, not the cosmologists) are the most distant objects ever seen; quasars have been detected to a redshift of nearly $z = 5$, when the universe was less than 20% of its present

age. Their distances and brightnesses also allow them to be used as probes of intervening matter. Astrophysicists are interested in AGN for studying high-energy processes and the physics of compact objects; a massive black hole is presumed to be responsible for AGN activity. Others are interested in AGN from the point of view of galaxy evolution.

In this dissertation, we have chosen to concentrate study on the galaxies in which Seyferts and quasars live. Detailed studies of the host galaxies are needed if we are to understand the AGN phenomenon and galaxy evolution. Host-galaxy studies can help us to understand how QSOs differ from other classes of AGN, what kinds of galaxies are able to "feed" an active nucleus, and whether all galaxies go through an active phase at some point in their lives. They can show us what effects the active nucleus has on star formation in the galaxy, and what kinds of effects might result in correlations between global galaxy properties and nuclear activity. They can also help us test the currently popular hypothesis that QSOs form following the merger of two gas-rich spiral galaxies. To study AGN host galaxies, we will limit ourselves to the nearest examples of this class of objects. But first, a wee bit o' history...

1.2 Fifty Years of AGN Host-Galaxy Studies

The first systematic study of AGN was carried out by Carl Seyfert in 1943 (Seyfert 1943). He described quantitatively the nuclear emission line spectra of 6 nearby galaxies of a class we now call Seyferts. These objects drew his attention because of their high-excitation lines and luminous stellar nuclei. Owing to their proximity, these galaxies were known to be galaxies before they were known to contain AGN. By contrast, other types of AGN were first discovered as radio or

point sources. About ten years after Seyfert's study, Baade & Minkowski (1954) identified the radio source Cygnus A with an "extragalactic nebula" (which they believed to be two colliding galaxies). The visible spectrum showed emission lines somewhat similar to those in Seyferts. Quasars were discovered the following decade. Though there were several radio sources identified with visible stellar features in 1960, the extragalactic nature of quasars was not known until Maarten Schmidt (1963) obtained an visible spectrum of the blue "star" coincident with the radio source 3C 273. The spectrum showed Balmer emission lines with a "large red-shift" of $z = \Delta\lambda/\lambda = 0.158$, which Schmidt suggested could be cosmological.

In the first decade following the discovery of quasars, there was speculation that quasars could be associated with galaxies analogous to Seyferts and radio galaxies. However, proving that assertion was difficult. A galaxy at such a great distance is necessarily faint, and its light is overwhelmed by the bright point source. In a study of extended emission around quasars, Kristian (1973) found that there was "fuzz" only where one would expect it, i.e. around low redshift quasars. Another decade of imaging studies further strengthened the case that the fuzz could be galaxies. Finally, two groups (Balick & Heckman 1983; Boroson & Oke 1984) showed that spectra of the fuzz were consistent with starlight at the same redshift as the quasar.

Thus, the distinction between quasars and Seyferts is largely historical, with those AGN sufficiently nearby enough so that the galaxy is clearly seen being classified as the latter. One working definition distinguishes between quasars and Seyferts based on blue luminosity; objects with $M_B < -22$ ($H_0 = 80$ km s^{-1} Mpc^{-1}) are classified as quasars. We will adhere loosely to that definition, but it is one of the purposes of this dissertation to investigate whether this division is natural from the point of view of the host galaxies.

1.2.1 Quasar Host-Galaxy Imaging

The first attempts to image QSO hosts used photographic plates. These early studies met with limited success because of the nonlinearity inherent in photography; disentangling the galaxian light from the overwhelmingly bright nuclear light requires a highly linear detector. Nonetheless, many galaxies were imaged and several interesting properties were discovered. For example, a photographic survey of 78 quasars (Hutchings, Crampton, & Campbell 1984; Hutchings et al. 1984) indicated that (i) there are differences between galaxies of radio- and optically- selected QSOs; (ii) there may be a correlation between nuclear and galaxian luminosity, in the sense that more luminous quasars reside in more luminous galaxies; and (iii) many of the QSOs appear to be interacting with other galaxies.

More recently, the use of CCD and other electronic detectors has obviated many of the difficulties of photographic imaging. The conclusions based on CCD studies of QSO hosts have been varied and sometimes conflicting (see Véron-Cetty & Woltjer 1990, hereafter VW, for a summary). Many of the results are suspect because of observational selection effects and effects of sample selection. As pointed out by VW, comparing properties of radio-loud and radio-quiet quasars requires caution because the radio-loud quasars are generally more luminous and therefore at higher redshifts in magnitude-limited samples. Also, the apparent correlation between nuclear and galaxian luminosity might result from observational selection effects. Low-luminosity quasars in high-luminosity galaxies might be excluded from quasar studies because these objects would be classified as Seyferts. Low-luminosity galaxies around high-luminosity quasars might escape detection because the quasar light overwhelms that of the galaxy and because these quasars are often at large

redshifts (VW; Malkan 1984; Gehren et al. 1984).

Several recent CCD surveys have avoided some of these problems by careful sample selection. VW studied a complete sample of 36 nearby ($z < 0.5$), high-luminosity ($-24.6 > M_V > -26.6$ mag; $H_0 = 50$ km s^{-1} Mpc^{-1}) quasars from the VV catalog (Véron-Cetty & Véron 1984). Their sample is divided roughly equally between radio-loud and radio-quiet QSOs. Hutchings (1987), Hutchings, Johnson, & Pyke (1988), and Hutchings, Janson, & Neff (1989) imaged a sample of 75 objects in the redshift range $0.1 < z < 0.5$. Their sample included roughly equal numbers of radio-loud QSOs, radio galaxies, and radio-quiet QSOs, well matched in v magnitude and redshift. Though their results differ somewhat in detail, these two groups agree on some general conclusions. (i) Radio galaxies and the hosts of radio-loud quasars have many similarities; both types may be ellipticals, albeit luminous and blue ones. (ii) Host galaxies of radio-quiet quasars are dimmer and many are consistent with being disk galaxies. (iii) Radial luminosity profiles are often ambiguous, with neither a disk model nor an $r^{1/4}$ model preferred.

More recently, Hutchings & Neff (1992, and references therein) have pushed CCD observations to very high (0.″5) spatial resolution through the use of rapid guiding. Such observations have allowed better nuclear point-source removal and luminosity profile analysis than was possible with the earlier studies. The qualitative results point to disturbed morphologies in most of the quasars they observed, with bars present in a large number of the radio-quiet quasar hosts. These authors have interpreted the results in terms of galaxy interactions triggering a flow of fuel to the active nucleus.

1.2.2 Seyfert Galaxy Imaging

Imaging Seyfert host galaxies is a much easier task because the galaxies are closer and the nuclear light is not overwhelming. There have been many in-depth, multiwavelength spectroscopic and imaging studies of individual objects, and there has been considerable effort expended studying nuclear properties. We will not discuss these studies further; however, we will briefly describe several recent imaging studies of large samples of Seyfert host galaxies. Yee (1983) observed 20 Markarian Seyferts with an SIT-vidicon camera and performed surface photometry in r, g, and v. He found the hosts to have radial profiles similar to those of spirals, colors like those of Sa to Sbc galaxies, and luminosities like hosts of quasars. MacKenty (1990) obtained CCD images of $\sim$ 50 Seyferts, mostly Markarian Seyfert 1's. He found disk properties similar to those determined by Yee, but he also noted that most of the galaxies contained some mechanism, such as a bar or interacting companion, that could funnel material to the center of the galaxy. Two other groups have obtained CCD images of Seyfert 1's as part of larger, visible/near-IR studies (Kotilainen, Ward, & Williger 1993; Granato et al. 1993).

1.3 Host-Galaxy Studies with Infrared Arrays

While the Hubble Space Telescope will yield quasar/Seyfert host-galaxy images in the visible at impressive resolutions, the development of infrared array cameras allows us to attack the problem from a different angle. First, the stellar spectral energy distributions (SEDs) of the host galaxies are likely to peak just longward of 1 μm, whereas the nuclear SEDs generally have local minima at about 1 μm (Sanders et al. 1989). Taking advantage of this happy coincidence by observing in the H band, we can observe the galaxian light with less contamination from the nucleus than has been possible at visible wavelengths; thus, removal of

the nuclear point source should be easier. Second, since IR images will show the galaxy's red stellar population, they will show the mass-tracing component of the galaxy. By contrast, CCD studies might ascribe high mass to a galaxy whose visible light output has been boosted by recent star formation. A related argument is that infrared images should yield the underlying galaxy structure with little influence from regions of recent star formation. Third, IR images do not suffer significant contamination from emission lines, which spectroscopy has shown to be substantial in the visible (e.g. Boroson, Persson, & Oke 1985). We note that the VW survey partly circumvented this problem by observing in the i band, where strong visible emission lines such as [O III]5007Å do not contribute for low-redshift objects. Fourth, the IR data can be used along with visible data to determine host-galaxy colors, an important step in investigating the effects of an active nucleus on the star-formation properties of the galaxy.

Because of the development of highly linear, large-format IR arrays, it is now feasible to study active galaxies using near-IR imaging. Dunlop et al. (1993) have presented initial results from a K-band imaging study of 32 quasars, roughly equally divided between radio-loud and radio-quiet objects well-matched in the V-z plane, with $z < 0.4$. They compared the IR properties of the two different kinds of quasars and interpreted the results in terms of the K-z relation for radio galaxies. Two groups have recently published near-IR imaging results for different Seyfert samples. In one series of papers, Kotilainen and collaborators (Kotilainen et al. 1992a,b; Kotilainen, Ward, & Williger 1993; Kotilainen & Ward 1994) analyzed galaxy and nuclear properties derived from visible and IR images of a hard-X-ray-selected sample of $\approx$ 30 Seyferts (nearly all Sy 1's). Another group (Zitelli et al. 1993; Danese et al. 1992; Granato et al. 1993) has carried out a similar analysis for $\approx$ 40 mostly UV-excess-selected Sy 1's. Both groups discuss

host-galaxy luminosities and colors, nuclear colors, and possible sources of the IR emission from these objects. All of these IR studies made use of a 58x62 pixel InSb array camera.

1.4 This Work

In this dissertation, we present near-IR images for nearly 100 AGN host galaxies. We have carefully chosen the samples to avoid the selection biases mentioned above. The quasar sample comprises the 50 quasars from the Palomar Green Bright Quasar Survey (Schmidt & Green 1983) with redshifts $z \leq 0.3$. We have restricted the redshift range to ensure adequate spatial resolution, galaxy detectability, and minimal distance-dependent effects, while still giving a large sample of objects. For lower-luminosity AGN we have chosen to image the CfA Seyfert sample (Huchra & Burg 1992). This sample is composed of 48 Seyferts, rougly equally divided among types 1, 1.5-1.9, and 2. This sample was spectroscopically selected, and, therefore, is not biased towards Seyferts with significant star formation. Taken together, these samples allow a statistical look at the continuity of host-galaxy properties over a factor of 10,000 in nuclear luminosity.

The instrument used for the observations in this work was a 256x256 HgCdTe NICMOS array camera. We used the camera's coarse pixel scale which provides 0.″6 pixels and a 2.′5 field of view. This large field gives us a distinct advantage over the other IR studies mentioned above. For the quasars, the large field means that there is nearly always a suitably bright star in the same frame as each quasar image; such stars are critical for determining the point-spread function and removing the contribution of the bright quasar nucleus. For the Seyfert images, the large field

means that the nearby galaxies will fit on the frames. This allows us to examine the outer parts of the galaxies and, at least as important, to determine reliably the sky level for each frame.

The remaining Chapters are arranged as follows. In Chapter 2 we present and discuss IR images for the low-luminosity half of the quasar sample. In Chapter 3 we present and discuss IR images for the high-luminosity half of the quasar sample. In Chapter 4 we present the Seyfert images. In Chapter 5 we combine the three samples, discuss properties of the ensemble, and present a summary. Finally, in Chapter 6 we investigate some of the implications for our results and plans for future work. We adopt a Hubble constant of $H_0 = 80$ km s^{-1} Mpc^{-1} throughout, unless specified otherwise.

Chapter 2

THE HOST GALAXIES OF LOW-LUMINOSITY QUASARS

We present H-band (1.6μm) images of a complete sample of 24 low-luminosity quasars selected from the Bright Quasar Survey. We detect the quasar host galaxy in at least 22 of these objects. We use a one-dimensional radial profile analysis to remove the contribution of the nucleus to the H-band light and to investigate the properties of the underlying galaxy. In most cases, the galaxy profiles are fitted better by exponential disk models than by de Vaucouleurs models. The average galaxy magnitude is $< M_H >= -24.0$ mag, which is approximately the H magnitude of an L^* galaxy. This result argues against the quasar activity being triggered by the merger of two large galaxies. No quasar host galaxies have inclinations $> 60°$, suggesting that obscuration near the active nucleus hides many of these objects from our view; their space density could be underestimated by a factor of ~ 2. We combine our results with previously published results from CCD imaging to show that the galaxies we detect are about 0.5 magnitudes bluer in

$V-H$ than normal galaxies. Such colors can arise from a heightened level of star formation compared with normal galaxies and are consistent with these galaxies having been the sites of luminous starbursts about 10^8 yrs ago.

2.1 Introduction

In this chapter, we report the first results of a program to study QSO host galaxies with near-infrared imaging. We have selected low-luminosity QSOs from a complete optically-selected sample, the Bright Quasar Survey (Schmidt & Green 1983). We have chosen all of the QSOs between $-23.1 \leq M_B \leq -22$ ($H_0 = 80$ km s^{-1} Mpc^{-1}). The faint cutoff was chosen to exclude objects more commonly labeled as Seyferts; objects dimmer than this might have been excluded from the Bright Quasar Survey because they were seen to be extended. This sample has a total of 24 QSOs with mean redshift $< z > \approx 0.1$ and maximum redshift $z = 0.161$. Because these QSOs are nearby (other studies of low-luminosity QSOs frequently have $< z >= 0.3$), we can achieve high spatial resolution to assist in separating the extended light from the nuclear light.

2.2 Observations

We obtained IR images of the 24 quasars in our sample at the Steward Observatory 2.3m Telescope on Kitt Peak during the period 1992 May to 1993 April. The quasars in our sample, along with redshifts and observation dates, are listed in Table 2.1. The images were taken with a 256x256 IR array camera which used one of two NICMOS HgCdTe detector arrays. The second array, installed in the camera prior to our 1992 September observing run, provided increased quantum

efficiency and greatly reduced the number of bad pixels compared with the first. We used an H-band filter to maximize the galaxian-to-nuclear light contrast and to observe the galaxies where the red stellar light is brightest. We chose the camera's coarse pixel scale, $0\farcs6$ pix^{-1}, because it gave adequate spatial resolution while providing a large enough field of view for us to find stars in the same field as the QSOs. The stars in each quasar field were used to determine the point spread function (PSF) for each image. One object, PG 1612+261, was observed with a slightly different instrument setup, using the camera's fine ($0\farcs23$ pix^{-1}) scale. Typically, the seeing was about $1''$.

The data were obtained by taking a series of exposures with the QSO position varied in a raster pattern across the array. Each frame was offset from the previous frame by about $30''$. The exposure time for each frame was about 40 seconds, which gave background-limited imaging without saturating the array on the bright quasar. Depending on placement of the PSF stars in the field, there were either 9 or 16 frames in each raster pattern. Typically, three rasters were completed for each quasar. Several times throughout each night, IR photometric standard stars from the catalog by Elias et al. (1982) were observed in a similar manner. All of the quasars in our sample were observed during photometric conditions.

2.3 Data Reduction

2.3.1 Image Reduction

To obtain a final image for an object, each set of raster frames was reduced separately and the results were combined afterward. The 9 or 16 frames in each raster set were used along with a dark frame of the same exposure time to

Table 2.1. Low luminosity quasars: the sample

PG #	z[a]	Date	$P_{5\mathrm{GHz}}$[b] (10^{22}W Hz^{-1})
0050+124	0.061	1992 Sep 09	4.2
0804+761	0.100	1992 May 11	10
0838+770	0.131	1992 May 12	≤ 1.1
0844+349	0.064	1992 May 12	0.55
1001+054	0.161	1992 May 13	8.9
1114+445	0.144	1992 May 12	1.9
1115+407	0.154	1992 May 14	3.0
1211+143	0.085	1992 May 13	3.8[c]
1229+204	0.064	1993 Apr 07	1.2
1351+640	0.087	1992 May 11	44
1404+226	0.098	1992 May 12	4.2
1411+442	0.089	1992 May 12	2.1
1415+451	0.114	1992 May 14	2.2
1416−129	0.129	1992 May 13	26
1426+015	0.086	1992 May 13	3.8
1435−067	0.129	1992 May 13	1.3
1440+356	0.077	1992 May 14	4.3
1519+226	0.137	1992 May 11	12
1552+085	0.119	1992 May 14	4.9
1612+261	0.131	1992 May 12	37
1617+175	0.114	1992 May 11	11
1626+554	0.133	1992 May 14	1.3
2130+099	0.061	1992 Sep 09	3.3
2214+139	0.067	1992 Sep 09	0.47

[a]Schmidt & Green 1983
[b]Kellerman et al. 1989, for $H_0 = 50$ km s^{-1} Mpc^{-1}
[c]Derived from Miller, Rawlings, & Saunders 1993

create median sky frames and normalized flat frames. These in turn were used to sky-subtract and flat-field the individual frames in the raster. The images were shifted to align them on the brightest quasar pixel, and combined by averaging to produce a final image for the raster. Bad pixels were excluded from the average through the use of a mask, and the minimum- and maximum-valued pixels at each position were thrown away before the final average was computed. For the four objects observed with the new array, no masking was necessary. Those images were aligned on the centroids of all objects of sufficient signal-to-noise (S/N) rather than on the brightest quasar pixel. Typically, three to four objects were used. Rejection of minimum- and maximum-valued pixels was still used.

A variety of tests confirmed that the procedures used to align the frames would not bias our results. We tried aligning on the brightest quasar pixels, on the quasar images' centroids, on the brightest pixels in stellar images, and on the centroids of a number of objects in the frames. All the results were similar. If anything, the procedure we adopted tended to "tighten up" the quasar image slightly compared with the alternatives, a result which might cause us to overestimate slightly the galaxy contribution to the total image.

To combine the raster sets for each object, we used a weighted average. We determined the weight for each frame by fitting a Gaussian curve to the inner part of the quasar radial profile. The weight was taken to be the square of the peak intensity of the Gaussian curve. In this way, we gave higher weight to frames with smaller widths (the peak intensity times the width was approximately constant). The resulting images have a central region (where the quasar is located) to which all of the original frames contribute, and outlying regions where only some of the original frames contribute because of the image offsets. Contour plots showing the central region of each reduced frame are shown in Figure 2.1. The object is

obviously extended in most cases.

2.3.2 Profile Extraction

We used a one-dimensional technique to remove the contribution of the nucleus from each reduced quasar image. The 1D radial profile for each object was obtained by using the ellipse-fitting task in IRAF to compute the average pixel value in an elliptical annulus at each radius. The ellipse fits were carried out down to a surface brightness level at which S/N ≈ 1, where S/N is the mean value of intensity around an isophote divided by the rms deviation of intensities along the isophote. For most of the frames, this corresponded to $H \approx 21.3$ mag arcsec^{-2}.

We used the same technique to extract the radial profiles of stars from each image to determine the PSF. In each case, we selected a star that (i) was near the quasar, (ii) had good S/N, and (iii) was not saturated on the original frames. Here, "near the quasar" means the star was located in the central overlap region of all frames. In about half of the images, there was no suitable star in the central region. In these cases, we averaged normalized profiles of two or three stars from outlying parts of the image. Tests of this procedure on images which had both outlying stars and central stars gave excellent agreement. The radial profiles of our quasars and PSF stars are shown in Figure 2.2.

2.3.3 Profile Fitting

To determine the properties of each galaxy, we first had to remove the contribution of the nucleus. We assumed that the nucleus was a point source with radial profile represented by the PSF profile. The PSF was normalized to

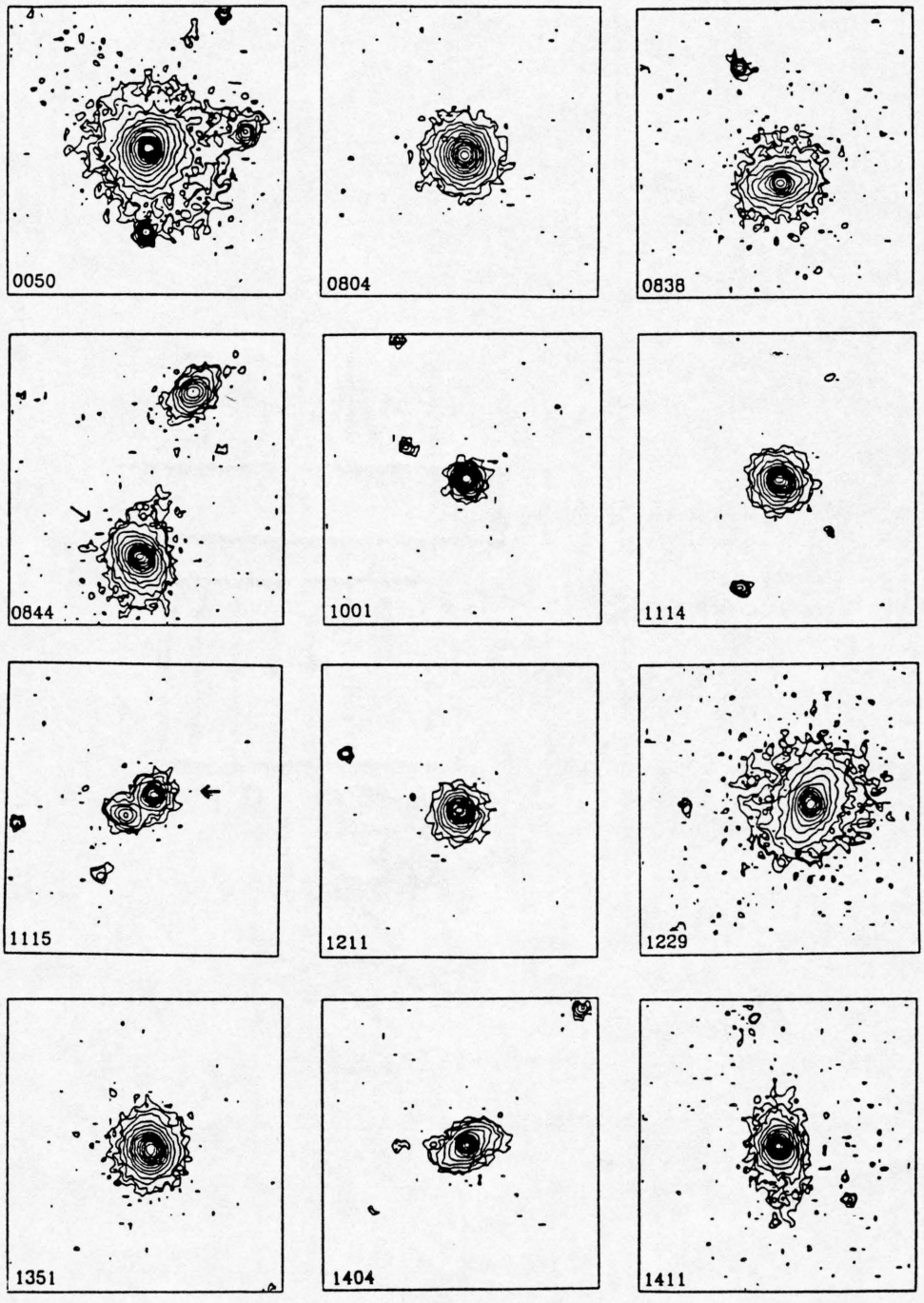

Fig. 2.1.—
Contour plots showing the central $38 \times 38''$ region of each quasar image. Contours are in steps of 0.5 H mag arcsec^{-2}. The lowest contour level and peak surface brightness for each object are given in Table 2.2. North is down and East is to the left.

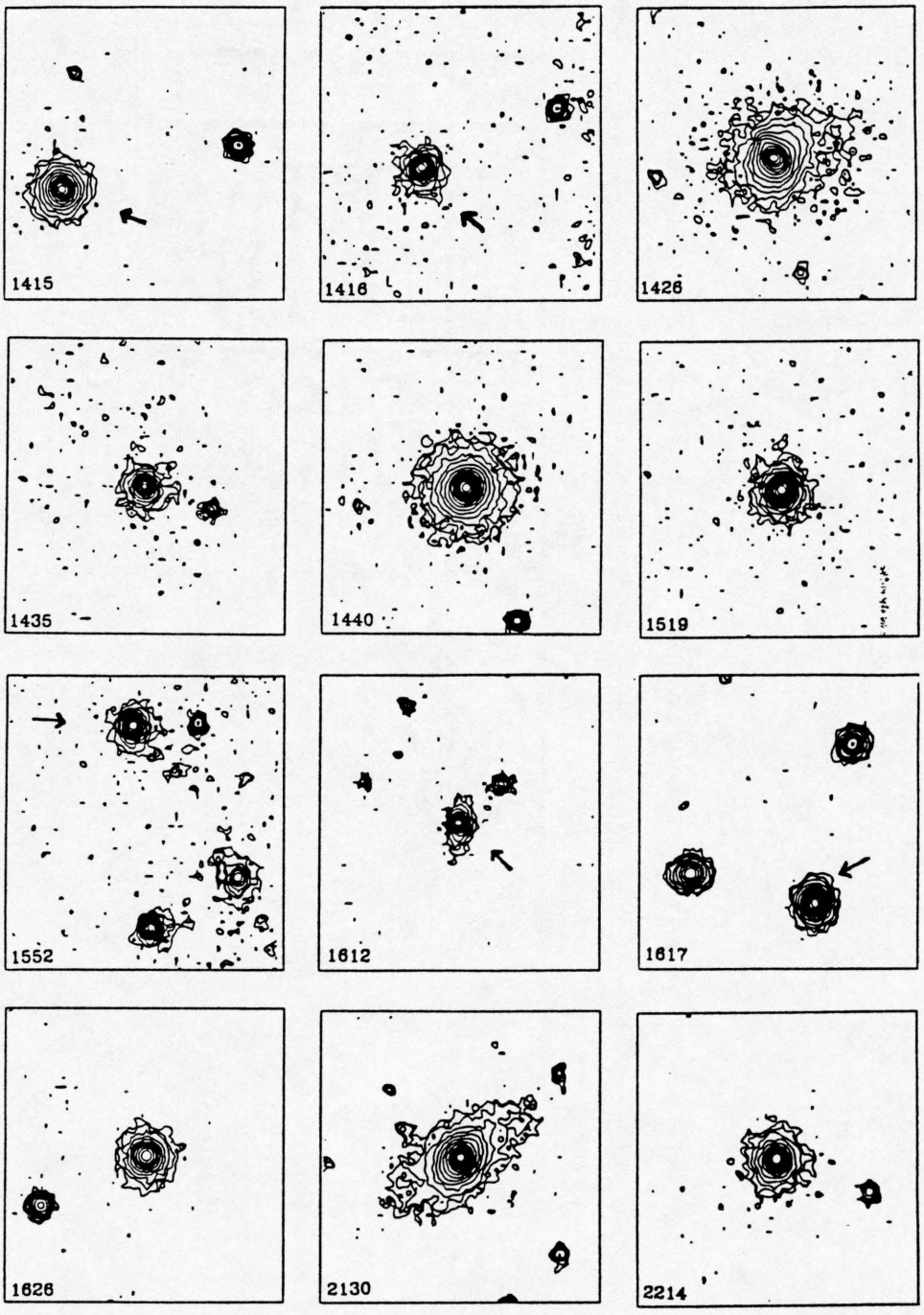

Fig. 2.1—continued

Table 2.2. Low-luminosity quasars: contour legend

	Contour (H mag arcsec^{-2})	
PG #	Low	High
0050+124	21.0	12.8
0804+761	21.0	14.1
0838+770	21.0	15.3
0844+349	21.0	14.1
1001+054	21.0	15.1
1114+445	21.0	14.3
1115+407	20.5	15.0
1211+143	20.5	13.7
1229+204	21.0	14.9
1351+640	21.0	14.9
1404+226	21.0	14.9
1411+442	20.5	13.4
1415+451	21.0	14.7
1416−129	21.0	15.3
1426+015	20.5	14.0
1435−067	21.0	14.8
1440+356	21.0	13.4
1519+226	21.5	14.8
1552+085	21.0	15.1
1612+261	21.0	14.8
1617+175	21.0	14.5
1626+554	21.0	15.8
2130+099	21.0	13.5
2214+139	20.0	14.3

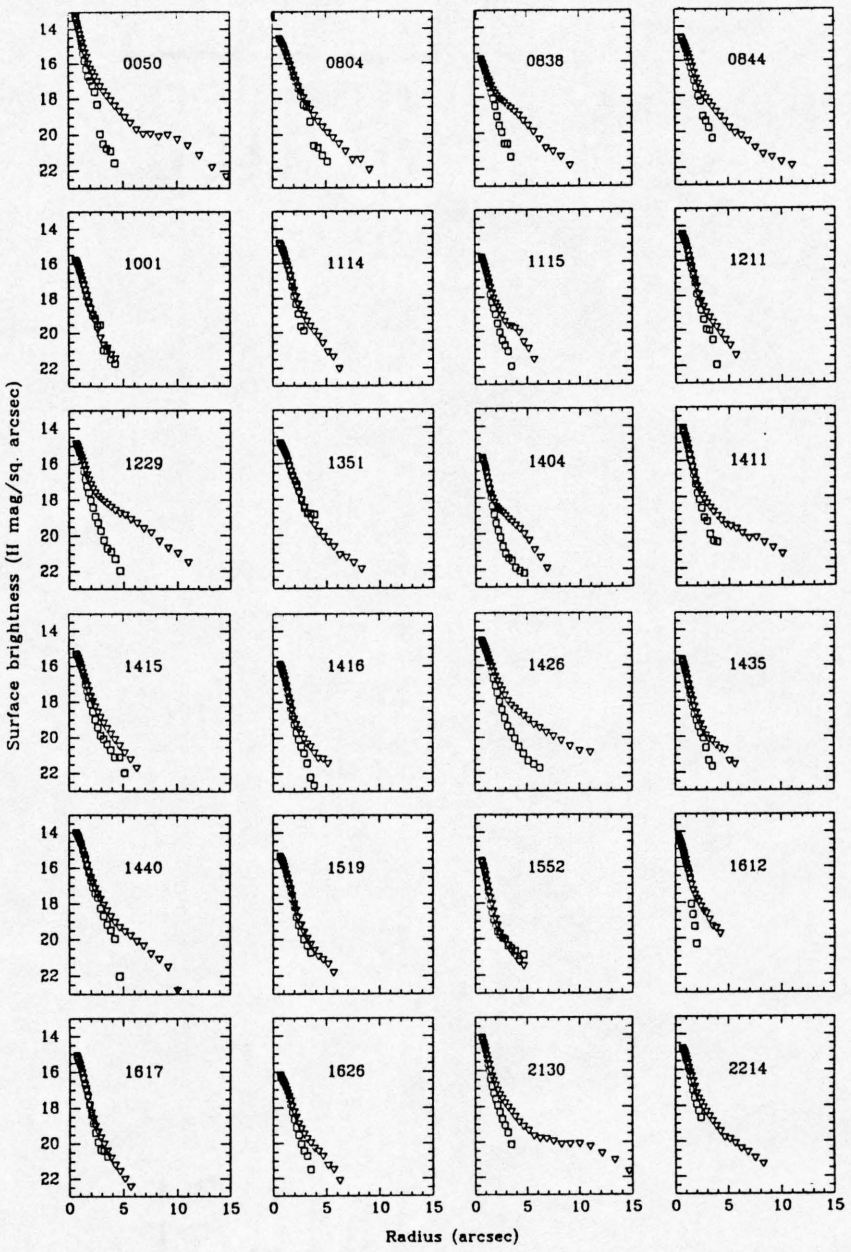

Fig. 2.2.—
Radial profiles of QSOs (triangles) and normalized PSF stars (squares) plotted to S/N $\approx$ 1. Pixel scale is 0.6″ (0.23″ for PG 1612+261). PG 1001+054 and PG 1552+085 are unresolved.

have the same flux as the quasar at the innermost point of the profile, a radius of 1 pixel. We then subtracted progressively larger fractions of the PSF profile from the quasar profile. We stopped subtracting just before the resulting profile became nonmonotonic with radius, i.e. before the profile turned over at small radii. The resulting profile was then fitted with an exponential disk model with free parameters r_0 and s_0, the disk scale-length and central surface brightness, respectively. Finally, the total amount of light in the galaxy was computed from these parameters as $I_{tot} = 2\pi r_0^2 s_0$. The results of these fits are listed in Table 2.3.

To check our results, we also experimented with subtracting the fraction of the PSF that minimized the rms residuals for an exponential disk model of the galaxy. The enclosed flux was the same to within about $15 \pm 10\%$. In addition, the disk scale-lengths and central surface brightnesses matched the original values very well. As another check, we also fitted an exponential disk law to only the outer parts of each unsubtracted quasar profile, outside the radius where the nucleus contributes. While the central surface brightnesses and disk scale-lengths were sometimes different than for the subtracted fits, the enclosed fluxes were the same to within about 20%.

The disk fits we used did not include an $r^{1/4}$ contribution from a central bulge because there are not enough pixels across the inner parts of the galaxies to justify fitting an extra component. As a result, the disk scale-lengths and central surface brightnesses derived are possibly in error. Any contribution of the bulge to the light of the PSF-subtracted profile will tend to decrease artificially the disk scale-length while boosting the central surface brightness. As we show below, the disk scale-lengths are typical of spiral galaxies, whereas the central surface brightnesses are slightly brighter than normal. We estimated the possible error due to neglect of the bulge component based on the study of Kent (1985). For

Table 2.3. Low-luminosity quasars: disk fits to profiles

PG #	f[a]	s_0[b]	r_0[c]	H_{gal}[d]	H_{tot}[e]	H_{nuc}[f]	$\frac{L_{gal}(H)}{L_{tot}(H)}$ [g]
0050+124	0.85	15.0	1.33	12.4	11.4	11.9	0.38
0804+761	0.80	15.8	1.03	13.7	12.3	12.6	0.26
0838+770	0.70	17.0	2.05	13.4	13.4	17.7	0.98
0844+349	0.80	16.2	1.54	13.3	12.6	13.5	0.54
1001+054	0.80	$\geq$16.1	0.56	$\geq$15.4	14.0	$\leq$14.3	$\leq$0.27
1114+445	0.80	16.0	1.02	13.9	13.1	13.7	0.46
1115+407	0.75	16.9	1.23	14.5	13.7	14.5	0.51
1211+143	0.80	15.9	0.91	14.1	12.8	13.2	0.30
1229+204	0.85	16.9	2.70	12.7	12.5	14.2	0.80
1351+640	0.60	14.8	0.68	13.6	12.7	13.3	0.43
1404+226	0.75	17.7	2.09	14.1	13.8	15.4	0.76
1411+442	0.90	17.5	2.66	13.4	12.4	13.0	0.41
1415+451	0.85	16.6	1.16	14.3	13.2	13.7	0.38
1416−129	0.85	17.0	0.84	15.3	14.1	14.5	0.31
1426+015	0.90	16.5	2.15	12.8	12.1	13.0	0.54
1435−067	0.85	17.3	1.04	15.2	13.9	14.3	0.31
1440+356	0.85	16.6	1.82	13.3	11.9	12.2	0.27
1519+226	0.90	16.9	0.99	15.0	13.4	13.7	0.24
1552+085	0.85	$\geq$16.1	0.59	$\geq$15.3	13.9	$\leq$14.3	$\leq$0.28
1612+261[h]	0.45	14.5	0.61	13.6	13.3	14.8	0.75
1617+175	0.80	15.6	0.62	14.7	13.4	13.8	0.30
1626+554	0.85	17.9	1.70	14.7	13.9	14.5	0.46
2130+099	0.90	16.3	1.84	13.0	12.0	12.6	0.43
2214+139	0.90	16.6	1.73	13.4	12.7	13.4	0.52

[a]Fraction of normalized PSF subtracted
[b]Central surface brightness of fitted galaxy (H mag arcsec^{-2})
[c]Disk scale length of fitted galaxy (arcsec)
[d]Total H magnitude of fitted galaxy
[e]H magnitude of system (galaxy plus quasar nucleus)
[f]H magnitude of fitted PSF (i.e. quasar nucleus)
[g]Fraction of total H band emission contributed by the host galaxy
[h]Fine pixel data; flux calibration based on Neugebauer et al. 1987 photometry

the early-type spirals in his sample, the bulge contributes about 40% of the total r band light, albeit with large scatter. For later types, the contribution is much less. We assume the bulge-to-disk ratio at H will be similar. While the disk models may not have the correct functional form to use at all radii, they account for at least some of the bulge light. Thus, we estimate that the total galaxy H fluxes are likely accurate to about 25%.

We experimented with fitting a de Vaucouleurs $r^{1/4}$ model for each galaxy, subtracting a fraction of the PSF that gave the best fit. The derived galaxy flux was in general approximately twice the flux from the disk fit. In most cases, the disk fits were clearly very good, whereas the de Vaucouleurs fits were unacceptable in the outer parts of the profile. In several cases, disk and $r^{1/4}$ fits worked equally well. In three cases, however, the disk fits were poor whereas the de Vaucouleurs fits were much better. For the purposes of comparison with the rest of the sample, we have used the disk fits for these three objects. However, we will discuss these cases further below.

2.4 Results

We have detected the quasar host galaxy in at least 22 out of the 24 cases. We estimate the errors in our total magnitudes to be about 0.1 mag, which is smaller than the uncertainty from the disk fits to the galaxies. Thus, based on the tests described above, we estimate that the galaxy H magnitudes are accurate to about 0.30 mag.

We have checked our photometry against the H photometry in Neugebauer et al. (1987) by adding up the light in a 5″ diameter aperture. Our magnitudes agree well with theirs, ours being on average 0.17 mag dimmer with 1σ scatter about

that average of 0.25 mag. The agreement is well within limits expected from the combined uncertainties and possible quasar variability except in the case of PG 1211+143 which we measure to be 0.7 mag dimmer than their value. We have used the Neugebauer et al. H fluxes to calibrate our data for PG 1612+261, because we did not observe a standard star with the fine pixel scale.

We have calculated absolute H magnitudes and sizes for the host galaxies assuming $H_0 = 80$ km s^{-1} Mpc^{-1} and $q_0 = 0$, and applying a small k-correction of $H(z) - H(0) = -0.02$ to -0.04 mag that is appropriate for the range of redshifts in our sample. The results are listed in Table 2.4, and we plot galaxy vs. total absolute magnitude in Figure 2.3. We estimated $M_H = -23.9$ for an L^* galaxy in a Schechter function description of the local field galaxy luminosity function, using an L^* magnitude of $M_V = -21.0$ (from, e.g., data of Efstathiou, Ellis, & Peterson 1988) and normal galaxy colors of $V-H = 2.9$. This color is appropriate for all but the latest-type galaxies (Griersmith, Hyland, & Jones 1982; Aaronson 1977). By inspection of the Griersmith et al. data, we estimate the scatter in the $V-H$ color to be less than 0.2 mag (note, however, that these colors may be inappropriate for the outer disk regions). For the quasar host galaxies, $< M_H >= -24.0 \pm 0.6$, where the quoted error is the 1σ scatter around the mean. (In computing this value, we have set M_H for the two undetected galaxies equal to the upper limits on their luminosities.) Therefore, a typical low-luminosity quasar lies within an L^* galaxy as measured at H. Since the H luminosity traces the stellar mass, it appears that the host galaxies are of typical mass for field spirals.

The average disk scale-length and central surface brightness are $< r_0 > \approx$ 2.5 kpc and 16.6 H mag arcsec^{-2} (but see caveats in §2.5.1 below; surface brightness includes a small correction for galaxy inclination). The corresponding central surface brightness in V, 19.5 V mag arcsec^{-2}, is on the bright

Table 2.4. Low-luminosity quasars: absolute magnitudes

PG #	M_H(gal)[b]	M_H(tot)[c]	s_0[d]	r_0[e]
0050+124	−24.4	−25.4	15.3	1.47
0804+761	−24.1	−25.6	15.9	1.87
0838+770	−25.0	−25.1	17.6	4.89
0844+349	−23.6	−24.3	16.5	1.80
1001+054	$\geq$ −23.5	−25.0	$\geq$16.2	1.64
1114+445	−24.7	−25.6	16.0	2.67
1115+407	−24.3	−25.1	17.1	3.45
1211+143	−23.4	−24.7	15.9	1.41
1229+204	−24.2	−24.4	17.4	3.15
1351+640	−23.9	−24.9	14.8	1.08
1404+226	−23.7	−24.0	18.3	3.73
1411+442	−24.2	−25.2	18.1	4.32
1415+451	−23.8	−24.9	16.6	2.40
1416−129	−23.0	−24.3	17.1	1.97
1426+015	−24.7	−25.4	16.8	3.36
1435−067	−23.2	−24.5	17.5	2.44
1440+356	−23.9	−25.4	16.7	2.55
1519+226	−23.6	−25.2	17.0	2.47
1552+085	$\geq$ −22.9	−24.3	$\geq$16.3	1.27
1612+261	−24.8	−24.9	14.8	1.45
1617+175	−23.4	−24.8	15.7	1.28
1626+554	−23.7	−24.6	17.9	4.12
2130+099	−23.8	−24.8	17.1	2.04
2214+139	−23.6	−24.3	16.6	2.11

[a] $H_0 = 80$ km s^{-1} Mpc^{-1} and $q_0 = 0$

[b] Absolute magnitude of fitted galaxy; includes k-correction

[c] Total magnitude of system

[d] Central surface brightness of fitted galaxy (H mag arcsec^{-2}); includes inclination correction

[e] Disk scale length of fitted galaxy (kpc)

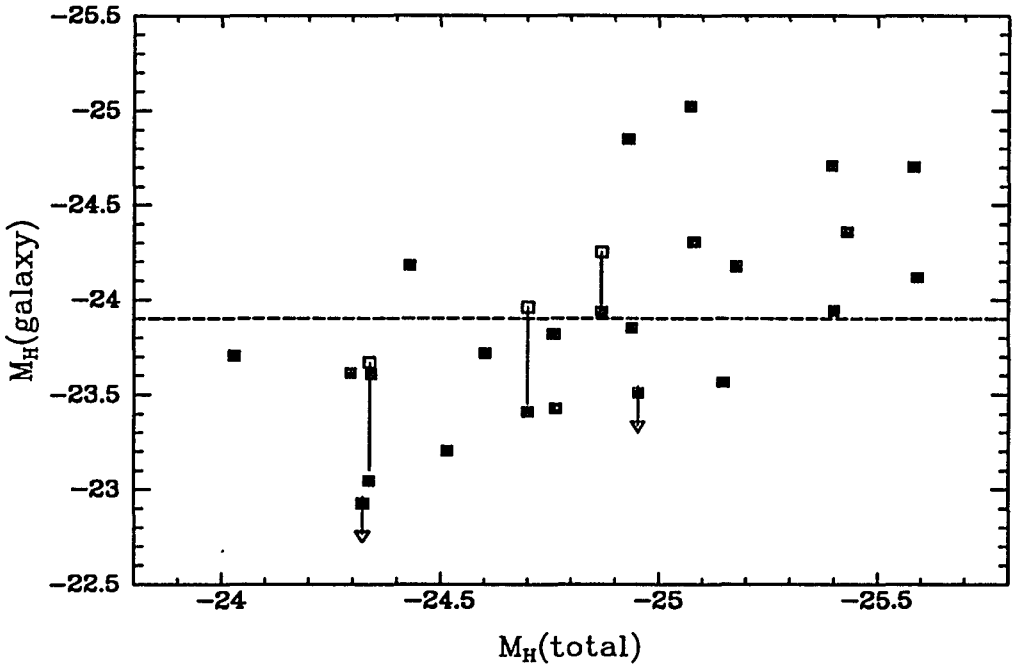

Fig. 2.3.—
Plot of galaxy vs. total magnitude in the H band ($H_0 = 80$ km s^{-1} Mpc^{-1}). The dotted line shows the magnitude of an L^* galaxy. Filled squares represent disk fits; open squares represent the preferred $r^{1/4}$ fits for three galaxies discussed in the text.

end of the distribution measured by Kent (1985), whereas the disk scale-length we have measured is typical of his sample. Those results reinforce the conclusion that the host galaxies are typical spirals.

We have also used the normal galaxy colors described above to determine our surface brightness detection limit, $B \approx 25$ mag arcsec^{-2}. Though CCD studies can go several magnitudes deeper, our limit is sensitive enough for comparison with other galaxy studies, which often quote results to a surface brightness $B = 25$ mag arcsec^{-2}. Based on the data given in Smith et al. (1986), we find that the average nuclear-to-galaxy luminosity ratio at visible wavelengths is nearly 5,

while our H-band results give a value less than 2; thus, the behavior of the SEDs favors the use of IR imaging to study host galaxies.

2.5 Discussion

2.5.1 Disk Fits

The exponential disk models should be considered only a first approximation to the galaxy luminosity profiles. With high-resolution visible images, many quasars are seen to be morphologically disturbed by tidal interactions (e.g. Hutchings & Neff 1992), so we might not expect an exponential disk or $r^{1/4}$ model to be appropriate. Where the galaxy is faint, very deep images are required to distinguish between these models, even if the galaxy is undisturbed.

There are, however, reasons to expect that disk models are an appropriate approximation. First, adopting the radio-quiet/radio-loud quasar cutoff as defined by Woltjer (1990), $P_{5GHz}(H_0 = 50) = 10^{24.7}$ W Hz^{-1}, we find that all of the objects in our sample are radio quiet and hence possibly associated with disk galaxies. The radio power of each quasar, taken from Kellerman et al. (1989), is listed in Table 2.1. Second, we might expect a disturbed galaxy to look less peculiar in near-IR, mass-tracing light than in visible light. Third, the redshift of these objects is so very low that the $\sim 1''$ resolution of our data may be adequate. Finally, the disk models do fit most of the profiles well, whereas $r^{1/4}$ models were often unacceptable.

Thus, we caution that it may be dangerous to interpret the scale-lengths and central surface brightnesses as spiral galaxy parameters. However, we believe that the fits accurately account for the galaxy light, so that the end products of the fits, namely the galaxy magnitudes, are robust.

Interestingly, we find that two of the three galaxies in which a de Vaucouleurs profile was preferred over a disk profile are associated with relatively strong radio emitting quasars: PG 1351+640, and PG 1416−129. Even with the $r^{1/4}$ fits, the three galaxies have luminosities near those of L^* galaxies. The average M_H for these galaxies assuming $r^{1/4}$ fits is $< M_H >= -24.0$, the same as that for the whole sample. If these galaxies are included in the sample average at their $r^{1/4}$ fit values, we still obtain $< M_H >= -24.0$, i.e. approximately the L^* value.

2.5.2 Galaxy Ellipticities

From the elliptical isophote fits to the quasar images, we are able to determine the ellipticity $\epsilon = 1 - b/a$ from the axis ratio b/a. We find on average $\epsilon = 0.2$ with all galaxies having $\epsilon < 0.5$. This lack of flattened galaxies was also found for the sample of quasars imaged at K by Dunlop et al. (1993), who note that there "appears to be a selection bias against finding active nuclei in an edge-on disc" galaxy. Given the minimal overlap of their sample with ours, our result provides an independent confirmation of the effect. Hutchings et al. (1989) had also noted this tendency from imaging in the visible. Presumably, it indicates that quasars in edge-on galaxies are too reddened to be included in visible light surveys such as the PG survey. Assuming a simple geometry where there is a sharp cutoff in quasar visibility at $\epsilon = 0.5$ and no effect for $\epsilon < 0.5$, only 50% of the sky is visible to the quasar in the usual visible search techniques. Therefore, typical searches must underestimate the space density of quasars like the low-luminosity ones we have studied by a factor of ~ 2.

Based on new multicolor quasar surveys, two groups have recently concluded that the PG survey is incomplete by factors of 2-3 for bright quasars (Savage et

al. 1993; Goldschmidt et al. 1992). That is, applying the PG survey's selection criteria yields more than twice the surface density of quasars in the new surveys. The degree of incompleteness is uncertain for the extremely low redshifts of quasars in our sample. In any case, we note that it is independent of the incompleteness we infer from the axial ratios; our factor of 2 applies in addition to any other factors deduced from the new surveys.

It is interesting to speculate where the obscuration of the quasar occurs. An ellipticity $\epsilon = 0.5$ corresponds to an inclination angle of 60°. Given their small scale-heights, disks do not extend close enough to the galaxy nucleus to obscure the nuclei at this inclination. Thus, the obscuration is probably close to the active nucleus.

2.5.3 Comparison to CCD Studies

We now compare our results to previously published information about QSO host galaxies. In the following discussion, we have adjusted all results to $H_0 = 80$ km s^{-1} Mpc^{-1}. We refer to the summary by VW, who have assembled data for approximately 40 radio quiet quasars and Seyferts from their own sample and the samples of Malkan (1984), Malkan, Margon, & Chanan (1984), Smith et al. (1986), & Gehren et al. (1984). These data provide a good comparison to our sample because the objects have low redshifts and because the galaxy magnitudes are based on disk fits to the profiles. The 12 QSOs with the same luminosity as the QSOs in our sample have mean redshift $< z >= 0.167$ and mean galaxy magnitude $< M_V > \approx -21.5$, with a scatter of 0.8 mag. By comparison, in our sample the average magnitude would correspond to $< M_V > \approx -21.1$ with normal galaxy $V-H$ colors. Thus, if the two samples represent the same population of objects, we

find that the $V-H$ colors we assumed are inappropriate and that the host galaxies are about a half a magnitude bluer in $V-H$ than normal early-type galaxies.

The sample of radio-quiet QSOs observed by Hutchings et al. (1989) unfortunately does not provide as good a comparison for our sample; only eight of those objects have a B luminosity in the range represented in our sample, and their average redshift is nearly 0.3. The average galaxy magnitude of these objects is $< M_V > \approx -21$ with a large scatter of 1.5 mag (derived from B magnitudes, including an uncertain k-correction). The large scatter and different sample properties make this result difficult to interpret.

In several cases, magnitudes for galaxies in our sample have been measured using CCDs. As reported in VW, the QSO PG 2130+099=II Zw 136 has been imaged by three different groups (Smith et al. 1986; Gehren et al. 1984; Malkan 1984) with an average galaxy magnitude measured to be $M_V = -21.4$. Using our value $M_H = -23.8$ for this galaxy we compute $V-H = 2.4$, which is half a magnitude bluer than normal early-type galaxies. Similarly, using published visible magnitudes for the hosts of PG 0050+124, PG 1440+356, PG 2214+139, and PG 1626+554 (Smith et al. 1986; Malkan 1984; Hutchings et al. 1988), we find that these galaxies are about a magnitude bluer in $V-H$ than normal early-type galaxies. Two quasars, PG 0844+349 and PG 1612+261, are found to have normal or slightly red hosts (Hutchings & Crampton 1990; Hutchings et al. 1988).

These colors suggest that many, but not all, of the galaxies have undergone strong star formation, making them bluer than normal galaxies. Any correlations seen in CCD studies between galaxy and nuclear luminosity apply only to the blue stellar component; CCDs probably trace out a young, blue, stellar population that is somehow associated with the activity in the nucleus. Indeed, visible spectroscopy

of the host galaxies of some of our objects shows evidence for a young stellar component (Hickson & Hutchings 1987; Hutchings & Crampton 1990).

2.5.4 Galaxy Mergers

In normal galaxies, the near-IR output arises from red giant stars that have evolved from the stellar population that dominates the galaxy mass. Therefore, the luminosity at H is a measure of the stellar mass of the galaxy. In galaxies which have undergone large starbursts, massive red giants and red supergiants can increase the H luminosity temporarily. Hence, for the quasar host galaxies, which have evidence for some degree of active star formation, we take the H luminosities to provide an upper limit to the stellar masses when compared with normal galaxies.

It is therefore remarkable that the host galaxies in our sample typically have the H luminosities of L^* galaxies. Out of the 24 galaxies, 16, or $\approx$70%, have M_H fainter than $M_{L^*} - 0.3$ (where 0.3 mag is the size of the galaxy magnitude uncertainties). Even if our photometry is subject to a 0.17 mag zero-point shift as might be indicated by the Neugebauer et al. (1987) photometry, 15 galaxies still satisfy this criterion. This result appears *not* to be compatible with the hypothesis that these quasars originate from the activity triggered by the merger of two large, gas-rich spiral galaxies.

To make a more detailed comparison with merger/starburst expectations, we have used the starburst program described by Rieke et al. (1993). We computed a model of a short duration starburst using the initial mass function of Scalo (1986) and let it evolve for 10^8 yrs. We then combined it with normal galaxy colors to reproduce the observed $V-H \approx 2.4$ for the quasar hosts. The starburst has

$V-H \approx 1.65$ at this age, and we assumed $V-H = 2.9$ for the underlying galaxy.

Using these colors, we divided the average $< M_H >= -24$ for our sample into underlying and starburst components. We determined the average H luminosity for the underlying galaxies to be $< M_H >= -23.65$. Therefore, the possibility that the hosts represent mergers of two "normal" L^* galaxies is even less likely. For the starburst component, $< M_H >= -22.6$, which corresponds to a bolometric luminosity at the peak of the starburst of $L_{bol} = 9 \times 10^{11} L_\odot$. L_{bol} would exceed $4 \times 10^{11} L_\odot$ for 10^7 yrs in these models. If the starburst IMF were biased toward massive stars, these luminosities would increase.

If the age of the starburst is increased beyond 10^8 yrs, its stellar population becomes redder. To match the total colors, the host-galaxy luminosity must then be significantly less than that of a single L^* galaxy. If the age of the starburst is 5×10^7 yrs, the $V-H$ colors can be reproduced with an average of $< M_H >= -23.75$ for the underlying galaxy. Making the starburst younger than 5×10^7 yrs results in decreasing the permitted host H luminosity (because the starburst emission is dominated by extremely luminous red stars), unless it is only a few million years old. Such young starbursts are not plausible for the average properties of our sample. We conclude that the galaxy properties are consistent with the host having been the site of a very luminous starburst about 10^8 yrs ago. However, this event must have occurred within a single $\sim L^*$ galaxy, not through the merger of two such galaxies. One possibility is that star formation and quasar activity was triggered by the interaction of an L^* galaxy with a substantially less massive companion. Such interactions have been described by Hutchings (1987), who found that companions to quasars in his sample are always fainter and smaller than the host galaxies (note, however, that those are radio-loud quasars). Alternately, the relatively blue $V-H$ colors may result from an ongoing episode of

star formation rather than a burst.

2.5.5 Comparison to Other Near-IR Studies

Combining our H data with the Dunlop et al. (1993) K data for the three objects common to both studies gives puzzling results. They have given K magnitudes for the galaxies surrounding PG 1211+143, PG 1440+356, and PG 2130+099. The technique they use to obtain the galaxy magnitude is to subtract the PSF so that the flux in the central pixel goes to zero. To compensate for this oversubtraction, they suggest a 0.75 mag adjustment to the galaxy magnitudes. The resulting magnitudes give $H-K \approx 1$ mag, which is surprisingly higher than the k-corrected value for "normal" galaxies, ≈ 0.45.

Zitelli et al. (1993) have recently presented K-band radial profiles for a sample of Seyfert 1 galaxies, including four of the galaxies in our sample: PG 0050+124 (I Zw I), PG 1440+356 (Markarian 478), PG 2130+099 (II Zw 136), and PG 2214+139 (Markarian 304). The K radial profiles agree fairly well with our H profiles outside the region where the nucleus contributes. However, the galaxy colors implied by these profiles are $H-K \approx 1$ mag. These authors also obtained H-band photometry in a 5″ diameter beam for the latter two of these objects; their photometry agrees with ours to within 0.2 mag. The photometric agreement makes the peculiar colors difficult to interpret.

We feel that the very red colors may result from the different ways the data were obtained and reduced. To test this hypothesis, we obtained K images of four quasars in our sample. The data were obtained with the same instrument setup and telescope as the H data, and were reduced and processed using the same techniques. The resulting $H-K$ colors are consistent with the expected values;

they are not anomalously red.

2.6 Summary

We have taken H-band images for a complete sample of 24 low-luminosity QSOs with redshift $z \lesssim 0.15$. We have detected the host galaxy for at least 22 of these objects. We find that:

(i) most of the galaxies have surface brightness profiles that follow an exponential disk law

(ii) on average, the galaxy contributes about 40% of the total light in the H band

(iii) the average galaxy H magnitude, and hence mass, is that of an L^* galaxy

(iv) the galaxies are bluer than normal early-type galaxies by about 0.5 mag in $V-H$

(v) the blue colors are consistent either with the galaxies having undergone very luminous starbursts about 10^8 yrs ago, or with an ongoing episode of star formation in the galaxies

(vi) most of these sources cannot arise from mergers of two normal L^* spiral galaxies

(vii) about half of the low-luminosity quasars are hidden by obscuration that is probably close to the active nucleus; the space density of these sources is probably underestimated by a factor of ~ 2, *beyond the factor of 2-3 incompleteness recently inferred for the PG survey from newer surveys.*

Chapter 3

THE HOST GALAXIES OF HIGH-LUMINOSITY QUASARS

We present H-band images of a complete sample of 26 high-luminosity quasars selected from the Bright Quasar Survey. We detect the quasar host galaxy in at least 23 of these objects. We compare these galaxies with host galaxies from a complementary sample of low-luminosity quasars, and find the hosts of the high-luminosity quasars to be significantly brighter at H, and possibly more massive. The average galaxy magnitude corresponds to a luminosity (and approximate mass) twice that of an L^* galaxy. The high-luminosity quasars are possibly more likely to have brighter interacting companions than their low-luminosity counterparts. These results are consistent with suggestions that the highest levels of activity in radio-quiet quasars require a large host galaxy or a close interaction with a massive galaxy, and that some of these interactions result in mergers.

We also present what we believe is the first published infrared image of the jet of 3C273, and we compare this image to visible and radio images from the

literature. The results are consistent with suggestions that the knots at the end of the jet are due to rapid energy loss where the jet is burrowing into the surrounding medium.

3.1 Introduction

In this chapter, we report results of an IR imaging study of 26 high-luminosity quasars. This new sample consists of all BQS quasars with $M_B < -23.1$ and $z \leq 0.3$, whereas the sample in Chapter 2 included all BQS quasars with $-23.1 \leq M_B \leq -22$ (adjusted to $H_0 = 80$ km s^{-1} Mpc^{-1}). The new sample is the high-luminosity sample most complementary to Chapter 2; the objects were chosen with the same initial selection criteria (apparent brightness, compactness, and $U-B$ color), and we have selected a subset to get a complete sample at nearly the same redshift. The mean redshift of the new sample is $< z >= 0.2$.

3.2 Observations

The 26 quasars in our sample, along with redshifts and observation dates, are listed in Table 3.1. We obtained H-band images of these quasars using a 256x256 NICMOS array camera on the Steward Observatory 2.3m telescope on Kitt Peak. The camera was operated within its linear regime ($< 240,000$ e$^-$, derived from M. Rieke et al. 1993). We acquired the images using the rastering procedure described in Chapter 2. For these observations, the pixel scale was about $0\farcs65$ pix^{-1} and the seeing was $1\farcs0$ to $1\farcs5$. We note that the large field of view of this camera allows accurate determination of the sky level around each galaxy, something that has been a problem for studies with smaller IR arrays. Once again, the stars in

each quasar field were used to determine the point spread function (PSF) for each image, and standard stars from the catalog of Elias et al. (1982) were observed several times throughout each night. All of the quasars except PG 0923+201 were observed during photometric conditions; for this object, a set of short calibration images was taken on a photometric night.

3.3 Data Reduction

3.3.1 Image Reduction

The raster sets were reduced using a procedure nearly identical to the one described in Chapter 2. The 16 frames in each raster set were used along with a dark frame of the same exposure time to create median sky frames and normalized flat frames. These in turn were used to sky-subtract and flat-field the individual frames in the raster. The images were then shifted to align them on the centroids of the quasar and two or three other objects of sufficient signal-to-noise. The registered images were combined by averaging to produce a final image for the raster. Bad pixels, which make up less than a tenth of a percent of the total number of pixels, were excluded from the average through the use of a mask. The minimum- and maximum-valued pixels at each position were thrown away before the final average was computed. To combine the reduced raster sets for each object, we used a weighted average with the weight taken to be the square of the peak intensity of a Gaussian curve fit to the quasar; this helped us to eliminate the few frames with minor tracking errors. The central region of each reduced frame is shown in Figure 3.1; most of the quasars are seen to be extended, and many are part of interacting systems.

Table 3.1. High-luminosity quasars: the sample

PG Number	z[a]	Date	P_{5GHz}[b] (10^{22}W Hz^{-1})
0026+129	0.142	92 Sep 09	44
0052+251	0.155	92 Sep 10	7.6
0157+001	0.164	92 Sep 09	93
0923+201	0.190	93 Feb 12	3.9
0947+396	0.206	93 Apr 07	5.6
0953+414	0.239	93 Apr 07	47
1004+130	0.240	93 Apr 08	11000
1012+008	0.185	93 May 27	15
1048+342	0.167	93 May 28	<2.3
1116+215	0.177	93 Apr 08	38
1121+422	0.224	93 May 26	<4.0[c]
1151+117	0.176	93 May 27	<2.6
1202+281	0.165	93 Apr 07	9.8
1226+023	0.158	93 May 28	400000
1302−102	0.286	93 Apr 09	28000
1307+085	0.155	93 May 27	3.6
1309+355	0.184	93 May 26	780
1322+659	0.168	93 Apr 09	2.4
1352+183	0.158	93 May 26	2.7
1354+213	0.300	93 Apr 09	<6.5
1402+261	0.164	93 Apr 09	7.1
1427+480	0.221	93 Apr 07	<4.5
1444+407	0.267	93 Apr 09	<10
1545+210	0.266	93 May 27	22000
1613+658	0.129	92 Sep 09	22
1700+518	0.292	92 Sep 09	2600

[a]Schmidt & Green 1983.

[b]Kellerman et al. 1989 ($H_0 = 50$ km s^{-1} Mpc^{-1}).

[c]Possible position error but still radio quiet with new upper limit (Miller, Rawlings, & Saunders 1993).

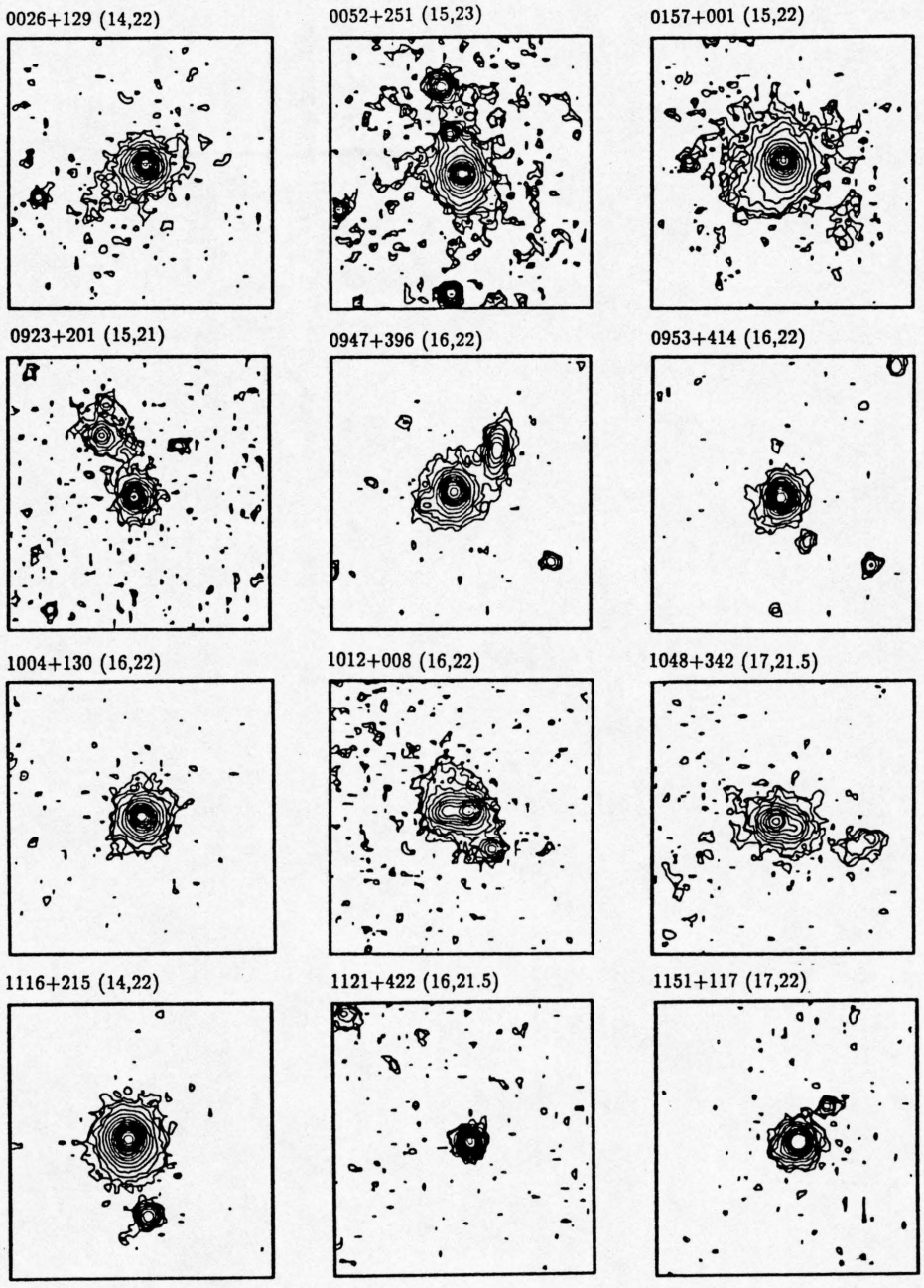

Fig. 3.1.—
Contour plots showing the central 40 × 40″ region of each quasar image. North is down and East is to the left. Contours are in steps of 0.5 H mag arcsec^{-2}. The lowest contour level and peak surface brightness for each object are given above each plot.

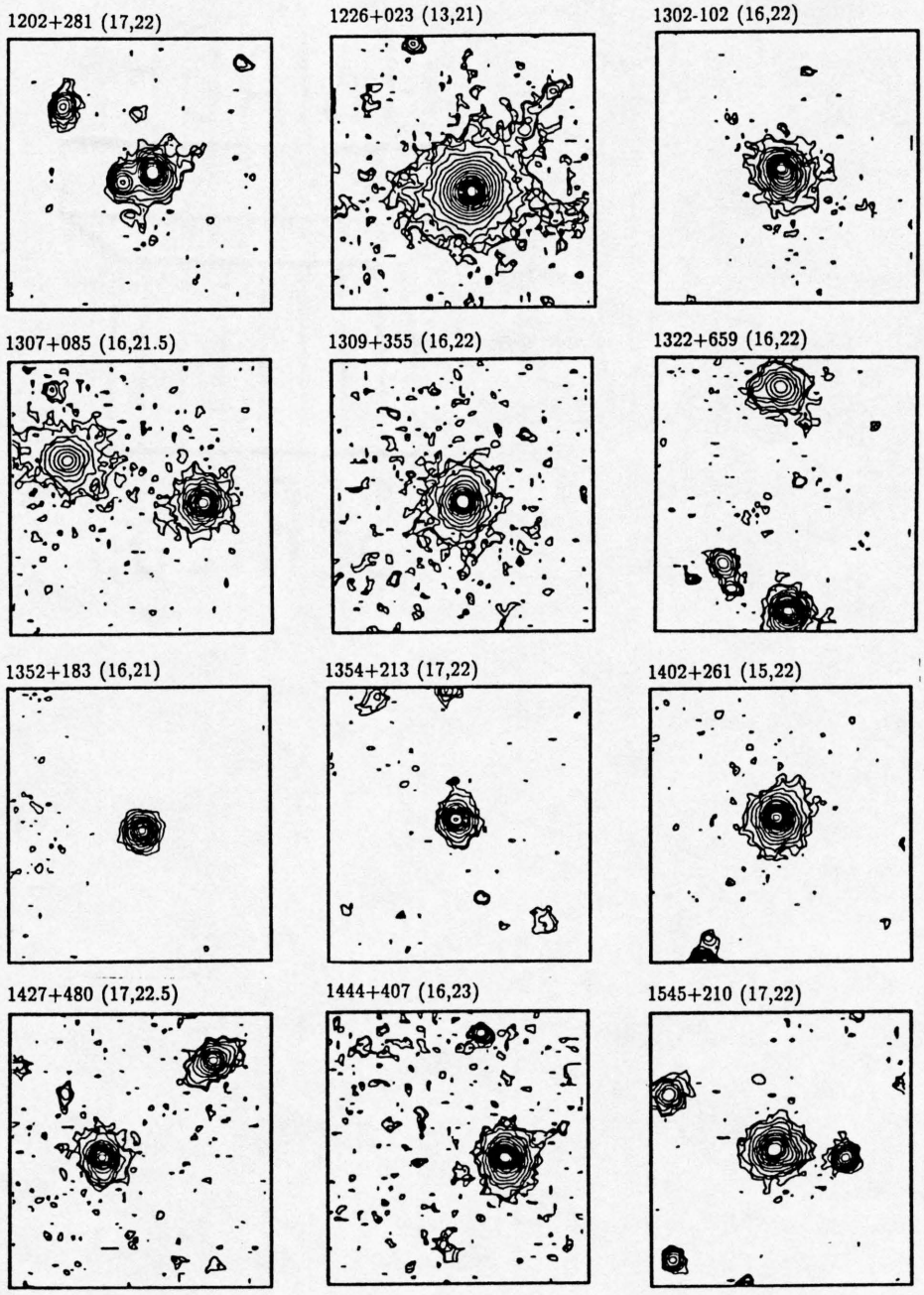

Fig. 3.1—continued

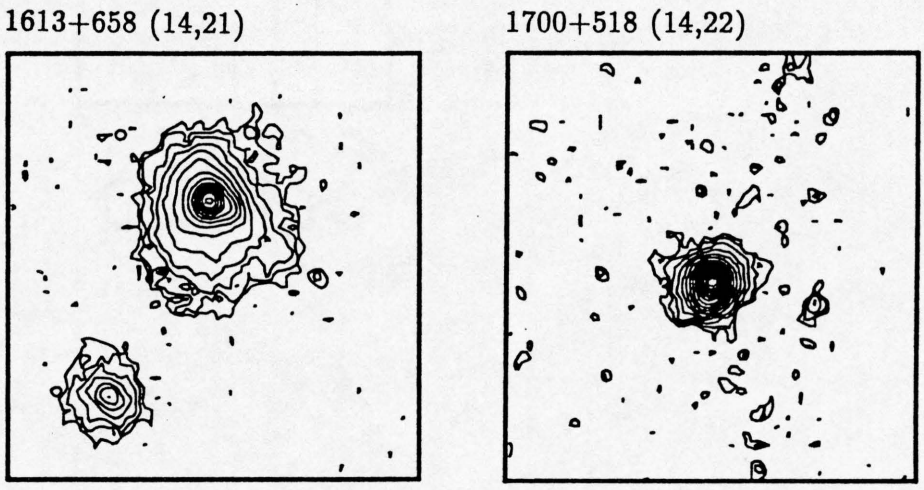

Fig. 3.1—continued

3.3.2 Point Source Removal

One-Dimensional Analysis

For most of the objects, we were able to use the one-dimensional (1-D) technique described in Chapter 2 to remove the contribution of the nucleus from each reduced quasar image. Briefly, we used elliptical isophote fitting to determine the the 1-D radial profile for the quasar and for the point spread function (PSF) for each frame. The PSF for a frame was determined from stars of comparable brightness to the quasar. The ellipse fits were carried out down to a surface brightness level at which the signal-to-noise S/N ≈ 1, where S/N is the mean value of intensity around an isophote divided by the rms deviation of intensities along the isophote. For most of the frames, this corresponded to $H \approx 23$ mag arcsec^{-2}, an improvement of approximately 1.5 mag arcsec^{-2} over the Chapter 2 observations, owing to slightly longer integration times and a new detector with better quantum efficiency. For a normal galaxy color of $B-H \approx 3.7$, our minimum surface brightness would correspond to $B \approx 26.7$ mag arcsec^{-2}; therefore, for normal host galaxies our images are of similar depth to those available at B. The radial profiles of our quasars and PSF stars are shown in Figure 3.2.

To determine the magnitude of the galaxy underlying each quasar, we first had to remove the contribution of the nucleus, assumed to be a point source with the shape of the PSF. We did this by normalizing the PSF to the quasar and then subtracting progressively larger fractions of this normalized PSF until the resulting profile started to turn over at small radii; typically, 0.8 to 0.9 of the normalized PSF was subtracted. The resulting profile was then fitted with both an exponential disk model and a de Vaucouleurs $r^{1/4}$ model. On average, the de Vaucoulers fits

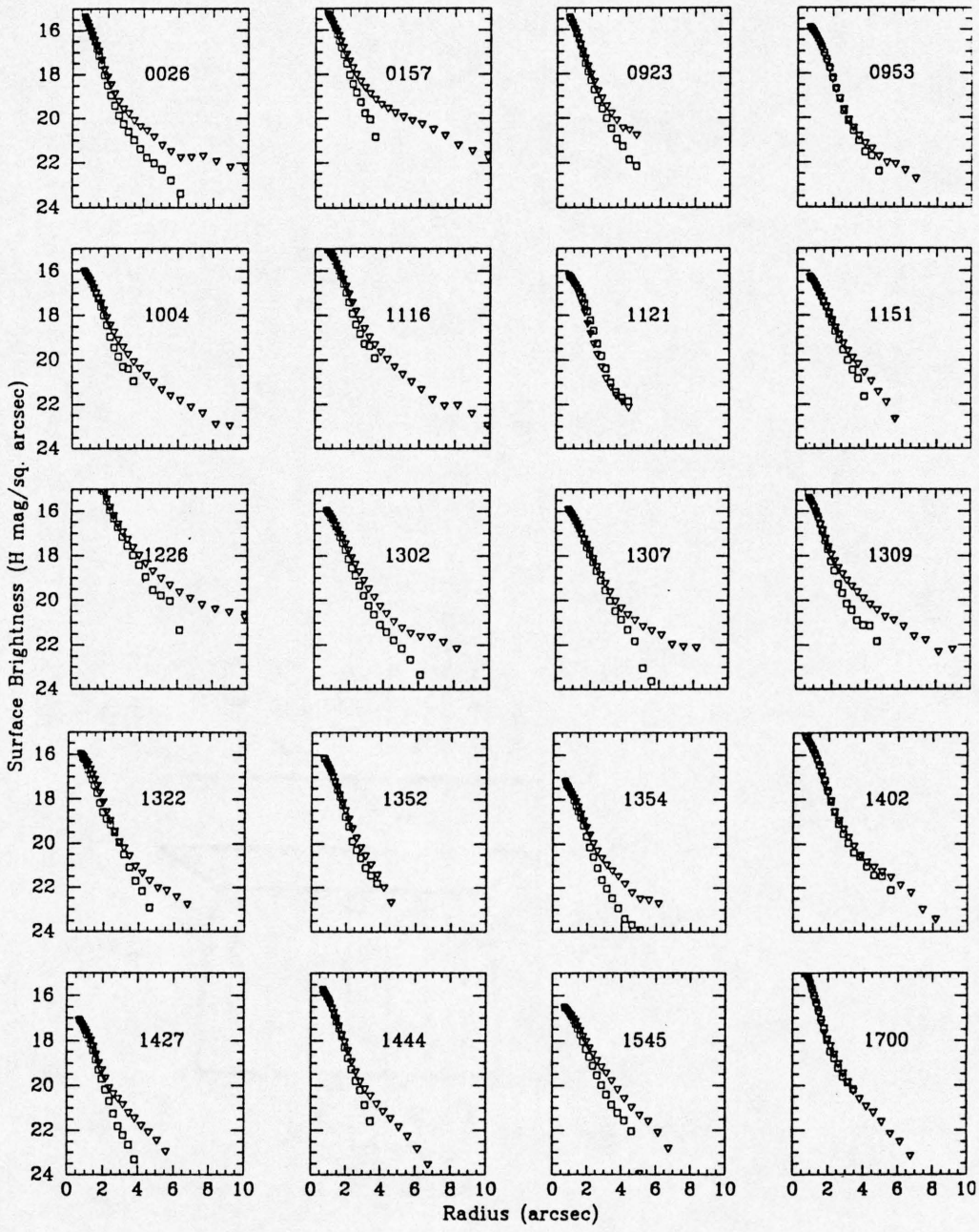

Fig. 3.2.—
Radial profiles of QSOs (triangles) and normalized PSF stars (squares) plotted to $S/N \approx 1$. Pixel scale is 0.″65. PG 1121+422, PG 1352+183, and PG 1700+518 are unresolved.

gave a galaxy flux approximately twice that determined from the disk fits. This procedure is the same as that used in Chapter 2 to permit comparison between the two samples. More details of this procedure as well as tests performed to estimate galaxy magnitude uncertainties can be found in Chapter 2. Here we simply state that the fits give a reasonable estimate of the light under the subtracted profiles.

Two-Dimensional Analysis

Six of the quasars either were too perturbed or had interacting companions too nearby for the 1-D analysis to work. In these cases, we resorted to a 2-D technique to remove the nuclear contribution. A PSF image was created using stars of good S/N in each frame. We subtracted progressively larger fractions of the normalized PSF while examining the resulting profile, determined by taking line and column cuts through the quasar image. Again, we stopped subtracting just before the profile turned over in the center. The galaxy flux was then determined by aperture photometry, and included the flux of the companion when the two could not be separated. Contour plots of the PSF-subtracted images are shown in Figure 3.3. Any detail in the central region of a galaxy is likely to be an artifact of the technique and is not significant.

We found this approach to be somewhat noisier than the 1-D procedure; the 2-D technique does not have the advantage of azimuthal averaging of the luminosity profile. To test for consistency in our galaxy magnitude estimates, we compared several quasars using both procedures. We found that the galaxy fluxes from the 2-D technique agreed with those from the 1-D analysis (and exponential disk fits) to within $\sim 15\%$.

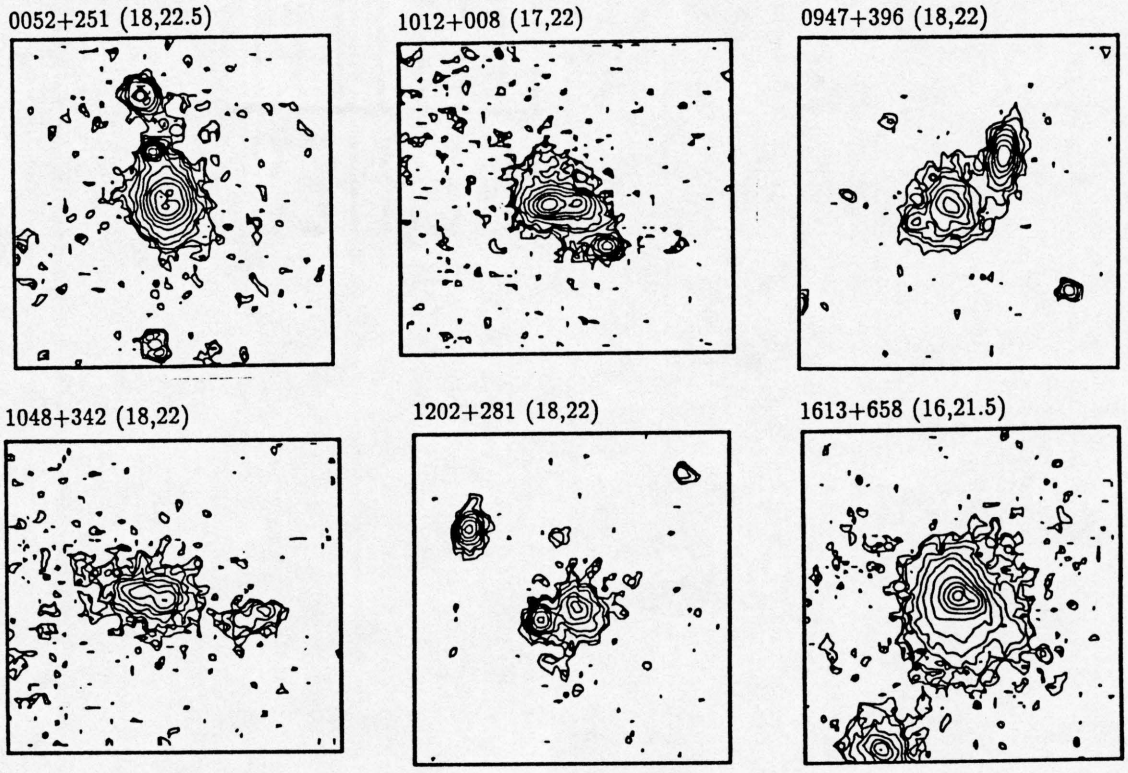

Fig. 3.3.—
Contour plots of PSF-subtracted quasars (see Fig. 3.1 caption). Structure seen in the quasar centers is not significant.

3.4 Results

We have detected the quasar host galaxy in at least 23 out of the 26 cases. This high detection rate and the similarly high one in Chapter 2 (22 out of 24) mean that our conclusions will not be significantly affected by incompleteness.

The photometric errors in our total quasar magnitudes are less than 0.1 mag, which is much smaller than the uncertainty from PSF subtraction. In Chapter 2 we found that disk models generally gave good fits to the galaxy luminosity profiles whereas the $r^{1/4}$ fits were unacceptable. For this high-luminosity sample, however, the situation is less clear. In many cases we cannot distinguish between the two types of profiles because the nuclei are more luminous, the objects are at

somewhat higher redshifts, and the seeing was sometimes poorer. For the purpose of comparison with the low-luminosity quasar sample of Chapter 2, we have chosen to report here only the magnitudes determined from the disk fits for 1-D analyses and aperture photometry for the 2-D analyses.

Based on tests described in Chapter 2, we believe that the galaxy H magnitudes are accurate to about 0.30 mag for spiral galaxies. For elliptical or disturbed hosts, the accuracies will be worse than 0.30 mag, but we believe we have used a measure of the galaxy light that is consistent from object to object and with that used in Chapter 2. Six of the quasars in our sample have been imaged in the K band by Dunlop et al. (1993). Though the methods of analysis are different, the inferred galaxy magnitudes agree to within the uncertainty. Note the difference between this situation and that in Chapter 2; for the Chapter 2 (low-luminosity) sample, we found that our galaxy magnitudes were much dimmer than the Dunlop et al. values. The difference lies in their method of estimating galaxy magnitudes, namely subtracting the PSF so that the central flux goes to zero, then adjusting the galaxy magnitude by 0.75 magnitudes to compensate for the oversubtraction. We believe the 0.75 magnitude adjustment is appropriate for the more luminous galaxies but not for the less luminous galaxies of Chapter 2.

We have calculated absolute H magnitudes and sizes for the host galaxies assuming $H_0 = 80$ km s^{-1} Mpc^{-1} and $q_0 = 0$, and applying a small k-correction of $H(z) - H(0) = -0.02\ to\ -0.08$ mag that is appropriate for the range of redshifts in our sample. The results are listed in Table 3.2, and we plot galaxy vs. quasar absolute B magnitude for both the high- and low-luminosity samples in Figure 3.4. We take from Chapter 2 our estimate $M_H = -23.9$ mag for an L^* galaxy, which represents a characteristic galaxy in a Schechter function description of the local field galaxy luminosity function. This value, derived from a visible luminosity

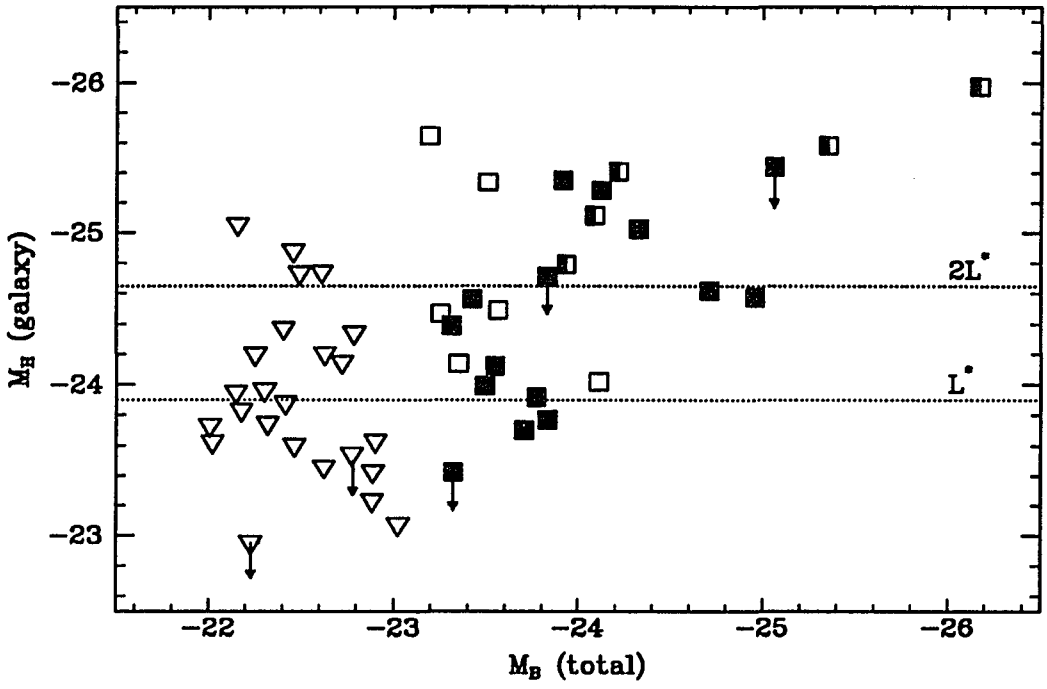

Fig. 3.4.—
Plot of galaxy absolute H magnitude (k-corrected) v. quasar absolute B magnitude ($H_0 = 80$ km s^{-1} Mpc^{-1}). Dotted lines show the magnitudes of $L^*$and $2L^*$ galaxies. Triangles represent low-luminosity quasars from Chapter 2. Squares represent high-luminosity quasars (this chapter). Half-filled squares denote radio-loud quasars, and open squares denote galaxy magnitudes derived from 2-D PSF subtraction.

function assuming normal galaxy colors, is identical to the the value determined from a new, K-band luminosity function (Mobasher, Sharples, & Ellis 1993). The mean host-galaxy magnitude in our sample is $< M_H >= -24.6$ mag with 1σ scatter about the mean of 0.7 mag (properly accounting for the nondetections using the techniques of survival analysis). The corresponding galaxy luminosity is roughly $2L^*$.

The sizes listed in Table 3.2 are the host-galaxy isophotal diameters after removal of the nuclear light. They were determined from the quasar rest frame

Table 3.2. High-luminosity quasars: magnitudes and sizes

PG Number	f[b]	H_{tot}[c]	H_{gal}[d]	$\frac{L_{gal}}{L_{tot}}$[e]	$M_{H,tot}$[f]	$M_{H,gal}$[g]	D[h]
0026+129	0.90	13.31	14.97	0.22	-25.5	-23.8	25
0052+251	0.90	13.39	14.46	0.37	-25.6	-24.5	20
0157+001	0.90	12.80	13.73	0.43	-26.3	-25.3	50
0923+201	0.85	13.40	14.86	0.26	-26.1	-24.6	38
0947+396	0.90	14.07	15.14	0.37	-25.6	-24.5	25
0953+414	0.80	13.77	15.38	0.23	-26.2	-24.6	39
1004+130	0.90	13.68	14.86	0.34	-26.3	-25.1	46
1012+008	0.80	13.57	14.02	0.66	-25.8	-25.3	15[i]
1048+342	0.80	14.22	14.98	0.50	-24.9	-24.1	25[i]
1116+215	0.90	12.64	13.97	0.29	-26.7	-25.3	41
1121+422	...	14.34	>15.10	<0.50	-25.5	>-24.7	~ 23
1151+117	0.80	14.07	15.32	0.32	-25.2	-23.9	25
1202+281	0.90	14.07	15.07	0.40	-25.1	-24.0	16
1226+023	0.90	10.82	13.01	0.13	-28.2	-26.0	53
1302−102	0.90	13.52	14.79	0.31	-26.9	-25.6	62[i]
1307+085	0.90	13.68	15.24	0.24	-25.3	-23.7	30
1309+355	0.85	13.34	14.55	0.33	-26.0	-24.8	40
1322+659	0.80	13.84	14.74	0.43	-25.3	-24.4	23
1352+183	...	14.21	>15.56	<0.29	-24.8	>-23.4	~ 19
1354+213	0.80	14.11	15.86	0.20	-26.5	-24.6	35
1402+261	0.80	13.17	14.95	0.19	-25.9	-24.1	30
1427+480	0.80	14.92	15.78	0.45	-24.9	-24.0	29
1444+407	0.85	13.72	15.19	0.26	-26.6	-25.0	39
1545+210	0.80	14.08	14.80	0.52	-26.2	-25.4	43
1613+658	0.80	12.28	12.87	0.58	-26.3	-25.6	27
1700+518	...	13.03	>14.97	<0.17	-27.5	>-25.4	~ 41

[a] $H_0 = 80$ km s^{-1} Mpc^{-1} and $q_0 = 0$

[b] Fraction of normalized PSF subtracted

[c] H magnitude of system (galaxy plus quasar nucleus)

[d] Total H magnitude of galaxy based on disk fit

[e] Fraction of total H band emission contributed by the host galaxy

[f] Total magnitude of system

[g] Total magnitude of galaxy; includes k-correction

[h] Isophotal diameter in kpc for comoving surface brightness H = 21.3 mag/sq.arcsec; $(1 + z)^4$ correction has been applied to surface brightness

[i] Uncertain

isophote of $H = 21.3$mag arcsec^{-2} (i.e. the $(1+z)^4$ correction to surface brightness has been taken into account). The corresponding surface brightness at B is $B \approx 25$mag arcsec^{-2}. The average size is 30 kpc, with 1σ scatter of 10 kpc.

3.5 Discussion

3.5.1 Galaxy Magnitudes

The mean galaxy magnitude for our low-luminosity sample is $M_H = -23.9$ mag. We have used the techniques of survival analysis (Feigelson & Nelson 1985) to investigate the hypothesis that the low- and high-luminosity samples are drawn from the same parent population of galaxies, giving proper treatment to the galaxy luminosity upper limits. The hypothesis can be rejected with a confidence greater than 99.9% for both the logrank and Gehan tests.

We can also make this comparison by omitting the radio-loud quasars because they and their hosts are among the brightest in our sample. The radio power of each quasar given by Kellerman et al. (1989) is listed in Table 3.1 (see also Miller, Rawlings, & Saunders 1993). We take as being radio-loud any quasar with power $P_{5GHz} > 10^{24.7}$ W Hz^{-1} (Woltjer 1990). By this definition, there are no radio-loud quasars in the low-luminosity sample and five in the high-luminosity sample. Including only radio-quiet objects, the two samples are found to be different with 99.3% confidence.

Finally, we make a comparison by omitting the points determined by 2-D analysis; for these objects, the galaxy magnitude often includes a contribution from a knob or companion galaxy that is inseparable from the quasar host. The two samples are still found to be different, at a level of 99.5% confidence.

Thus, the most luminous quasars seem to require their hosts to have higher H luminosities than the hosts of lower luminosity quasars. This tendency might result if the host galaxies had recently undergone very luminous starbursts, giving enhanced numbers of red supergiants and luminous asymptotic giant branch stars. An upper limit to this effect can be determined as follows. The total far-IR luminosity of the quasars is an upper limit to far-IR output produced by stars. One can use starburst models for M82 (G. Rieke et al. 1993), which has a very high ratio of 2μm luminosity to far-IR luminosity, to estimate an upper limit to the achievable ratio of H light to far-IR light. Far-IR flux densities for our quasar sample can be obtained from Sanders et al. (1989). We find that seven members of our sample—0026+129, 0052+251, 1012+008, 1302−102, 1309+355, 1322+659, and 1545+210—have upper limits to their M_H's determined in this manner that indicate that recent starbursts do not contribute significantly to their total absolute magnitudes. Seven more quasars—0923+201, 0953+414, 1048+342, 1151+117, 1307+085, 1354+213, and 1427+480—are undetected in any band by IRAS and have upper limits to their M_H's that are equal to or less than their observed M_H's; these objects probably also do not have their H outputs dominated by recent star formation. The average M_H for these 14 galaxies is -24.5. Four more quasars—1116+215, 1121+422, 1352+183, and 1700+518—were either unobserved by IRAS or unresolved by us; in only one of these cases, 1352+183, does our upper limit fall below the mean M_H for the whole sample. The remaining eight quasars—0157+001, 0947+396, 1004+130, 1202+281, 1226+023, 1402+261, 1444+407, and 1613+658—have an average $M_H = -24.9$ (or -24.8 if we exclude 3C273). For these eight objects, the upper limits to their M_H's are comparable to the values we measured; it would be interesting to investigate the possibility of strong starbursts in these galaxies using other techniques. We note, however, that

1004, 1202, and 1444 output most of their far-IR luminosity in the 25μm band, which indicates that starburst emission probably does not dominate. We conclude that there is at best only a weak correlation of stellar luminosity with potential starburst activity and that the host galaxies of the luminous quasars do in fact tend to be of higher intrinsic luminosity and hence mass than the hosts of the lower luminosity quasars.

3.5.2 Interactions

Galaxy interactions have long been thought to trigger or sustain quasar activity (Stockton 1982; Hutchings & Campbell 1983). During the course of data reduction, we noticed that six of the quasars in our high-luminosity sample have bright interacting companions or severely disturbed morphologies that make a 1-D analysis impossible. Because we had not run into such difficulties with the low-luminosity sample, we decided to investigate whether there are more interactions among high-luminosity quasars, or whether the perceived difference could be due to small-number statistics or some selection effect. For example, a galaxy called an "interacting companion" to a quasar at a redshift of 0.2 (typical of the high-luminosity sample) could be seen as separate from the quasar at a redshift of 0.1 (typical of the low-luminosity sample).

This kind of problem has already been studied in detail by Yee (1987; see also Green & Yee 1984), who obtained images of the fields surrounding low-redshift BQS quasars. His selection criteria are the same as ours and the subsample he observed includes 80% of the 45 radio-quiet objects in our combined high- and low-luminosity samples, so his results apply here. He investigated statistically the occurrence of companion galaxies within about 60 kpc projected distance from

the quasar (results scaled to $H_0 = 80$ km s^{-1} Mpc^{-1}). Though quasars were found to have companions ~ 6 times more often than expected for field galaxies, the statistical analysis indicated that the properties of a companion are not related to the quasar luminosity. First, the average luminosities of isolated and nonisolated quasars are the same. Second, the frequency of finding companions is similar for Seyfert galaxies and radio-quiet quasars. Finally, there is no observed correlation between the quasar luminosity and the tidal force of a companion as determined from the projected distance and the companion's mass (as traced by the r-band light).

To test our perception that higher luminosity quasars are more likely to have bright, interacting companions, we have carried out the following analysis for the radio-quiet objects. We consider a quasar to have a "bright, interacting companion" if the companion lies within a projected distance of 30 kpc and is brighter than $\frac{1}{10}L^*$ based on the H-band light. These criteria select out companions that are nearly as bright as the host and within about one galaxy diameter. We also include severely disturbed quasars, such as PG 1613+658, which presumably have had recent interactions with massive galaxies. These criteria are met by at least eight quasars in the high-luminosity sample (PG 0052+251, PG 0923+201, PG 0947+396, PG 1012+008, PG 1048+342, PG 1202+281, PG 1322+659, PG 1613+658, and possibly PG 0157+001) and three quasars in the low-luminosity sample (PG 0844+349, PG 1115+407, and PG 1612+261). We note that PG 1202+281 was not observed by Yee. If we combine the samples, we find that approximately 1/4 of the quasars have bright, interacting companions. Assuming Poisson statistics for observing these interacting systems, the probability for seeing only three from the low-luminosity sample is about 9%. The significance is the same for factors of two increase or decrease of the luminosity cutoff.

While this result may not be compelling, we believe it is suggestive. It is consistent with a close interaction with a massive companion being necessary to sustain the highest levels of quasar activity. This hypothesis is not contrary to Yee's findings when we consider that his definition of companion included much smaller and more distant galaxies. Our hypothesis places no restrictions or requirements on the existence of such companions.

We also resurrect Yee's suggestion that some of the most luminous quasars might have already undergone a merger so that no companion is visible today. We believe this hypothesis to be reasonable because the luminous quasars have hosts with masses roughly twice that of L^* galaxies (twice the mass of their low-luminosity counterparts) and because some of these hosts have very disturbed morphologies. The merger hypothesis can also explain why some of the most luminous quasars were observed by Yee to have small tidal parameters. Of course, it is also possible that a very massive host can support high levels of activity without the need for an interaction.

Hutchings & Neff (1992) have examined high-resolution images of 28 low-redshift quasars, including eight of the radio-quiet objects in our combined sample, for evidence of interactions. They have assigned an age and a strength to each interaction by comparing the images to numerical simulations, examining colors, etc. One of their results was that the luminous quasars are possibly associated with older interactions. The number of high-luminosity quasars we find with superimposed companions and the number of hosts with luminosities that suggest they are possible merger products lend some support to this result. Note, however, that Hutchings & Neff often see that the interactions are between galaxies of different sizes, whereas our criteria select mass ratios closer to unity.

3.5.3 Galaxy Ellipticities

In Chapter 2 we found that the hosts of the low-luminosity quasars are never seen to have axis ratio $b/a < 0.5$, despite the fact that they are consistent with being disk galaxies. This result implies that there is a selection bias against finding quasars in edge-on galaxies (see also Dunlop et al. 1993; Malkan, Margon, & Chanan 1984). For the high-luminosity sample, we have measured the axis ratios for those hosts that are not severely disturbed. We again find no galaxies with small axis ratios. However, the identification of these galaxies as spirals is uncertain. Therefore, we say simply that these results do not contradict the conclusions of Chapter 2; in other words, we find no spiral hosts at high inclination.

3.5.4 Comparison to CCD Studies

In this section, we combine our results with CCD results from the literature to investigate the $V-H$ colors of the host galaxies. The colors are compared to the colors of "normal" galaxies, which we take to have $V-H= 2.9$. This color is appropriate for all but the latest-type galaxies (Griersmith, Hyland, & Jones 1982; Aaronson 1977). All results have been adjusted to $H_0 = 80$ km s^{-1} Mpc^{-1}, and errors given are dispersions about the mean. We consider only the radio-quiet quasars, and use the visible magnitudes determined from assuming disk profiles. The radio-quiet quasars in our high-luminosity sample have hosts with $< M_H >= -24.5 \pm 0.6$ (k-corrected value).

There are two samples in Véron-Cetty & Woltjer (1990) with which we can compare. The first is the sample they observed in the i band (converted to M_V in their Table 3). This sample has the same mean quasar luminosity as our sample but

has a mean redshift $< z >= 0.4$, twice that of our sample. The average, k-corrected galaxy magnitude assuming that the galaxies are disks is $< M_V >= -21.3 \pm 0.6$. To the extent that our samples represent the same population, this implies that $M_V - M_H \approx 3.2$, not significantly different from normal galaxies.

The second sample is drawn from the list they assembled from their own observations and those of Malkan (1984), Malkan et al. (1984), Smith et al. (1986), & Gehren et al. (1984). We select the eleven quasars that meet the luminosity criterion of our sample and find $< z >= 0.3$, closer to that of our sample. The average galaxy magnitude is $< M_V >= -22.1$ with a large scatter of 1.2 mag. The corresponding color is $M_V - M_H \approx 2.4$, half a magnitude bluer than normal galaxies and similar to the galaxies in our low-luminosity sample.

The difference between the results of these two comparisons is likely due in part to the different wavelengths used for the CCD observations. The *i*-band observations by Véron-Cetty & Woltjer are less affected by recent star formation than are the shorter wavelength observations from the literature. Thus, we may expect the colors derived from shorter wavelength observations to be bluer.

Finally, we use CCD data from the literature to investigate the k-corrected colors of individual objects in our sample. The peculiar host of PG 1613+658 has a normal color, $V-H = 2.9$ (CCD data from Malkan 1984), whereas the perturbed host of PG 0157+001 has very blue color, $V-H = 1.4$ (Smith et al. 1986).

From the *B*-band data in Hutchings et al. (1989) we find $V-H = 1.5$ (PG 0052+251), > 3.4 (PG 0923+201), 2.5 (PG 0953+414), and 3.3 (PG 1012+008). We get considerably different colors if we use the *R*-band data in that paper, and for PG 1444+407, we get $V-H > 5.0$! However, the visible magnitudes are not based strictly on disk fits to the profiles, which makes the colors difficult to

interpret. Therefore, we conclude that quasar host galaxies come in a wide range of visible-to-IR colors, and that the inferred colors of course depend on the visible wavelengths observed. Anomalously red hosts may have internal extinction. The hosts that are bluer than normal can be understood in terms of the star formation scenario given in Chapter 2.

3.5.5 The Jet of 3C273

An infrared image of the jet of 3C273 (PG 1226+023) is shown in Figure 3.5, and a surface brightness profile from the quasar along the jet (width of 1.″9) is shown in Figure 3.6. For both figures, we have subtracted the galaxian light (using the best fitting $r^{1/4}$ profile) but not that of the quasar. The innermost part of the jet joins onto artifacts of the quasar image; this extension should not be considered real. Because infrared images of the jet do not seem to have been published previously, we deviate from our discussion of host galaxies to describe these data.

Previously, Becklin, Henry, & Telesco (1984) obtained aperture photometry of the jet in J (1.25μm) and K (2.2μm). Interpolating their whole-jet flux density to H (1.6μm) would predict a flux density of 190μJy. The photometry derived from our image is 174μJy, which is in excellent agreement particularly if one allows for a small contribution from the 3C273 host galaxy (which was not removed by Becklin et al. and was by us).

Our data, with a pixel-limited resolution of $\sim$ 1.″2, is closely comparable with the images of Röser & Meisenheimer (1991). Comparing our Figure 3.5 with their Figure 5, the overall morphology at 1.6μm is very similar to that at 0.65μm, except for a more prominent additional extension along the direction of the jet past the bright knot at the tip at 0.65μm. Comparing our Figure 3.6 with their Figure 13

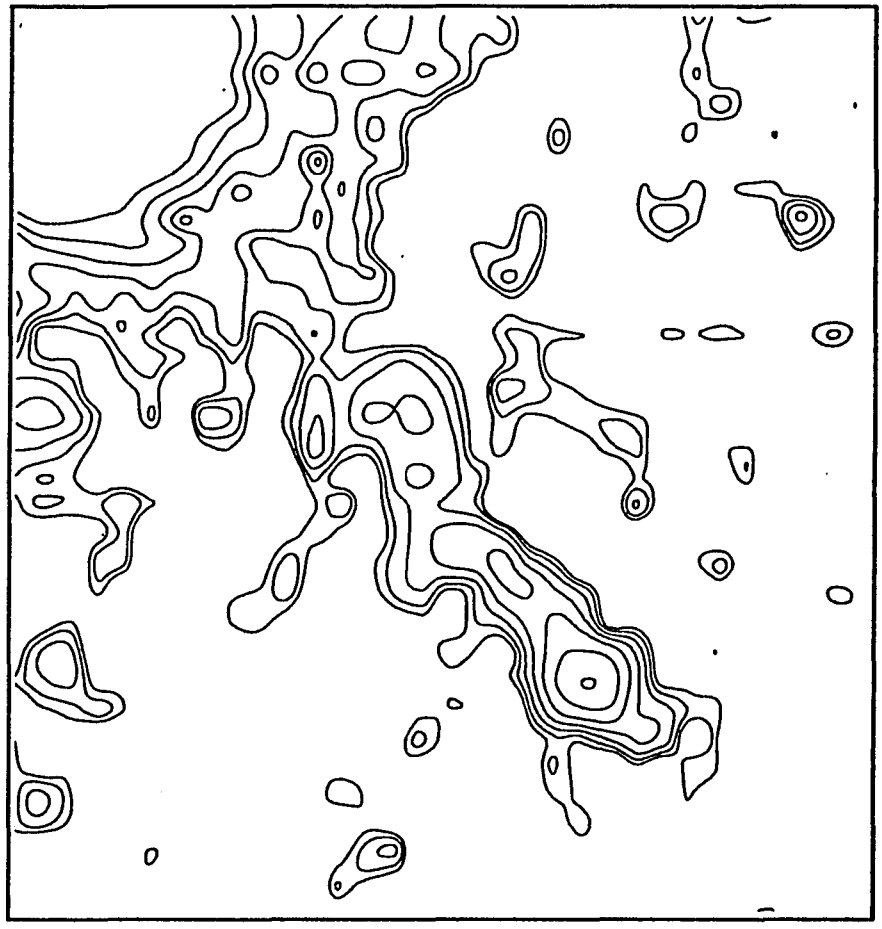

Fig. 3.5.—
Contour plot of the jet of 3C273. Lowest contour plotted corresponds to 22 H mag arcsec^{-2}, and contour spacing is a factor of $\sqrt{2}$. Box size is 21″x 21″ with North up and East to the left (note different direction from Figure 3.1).

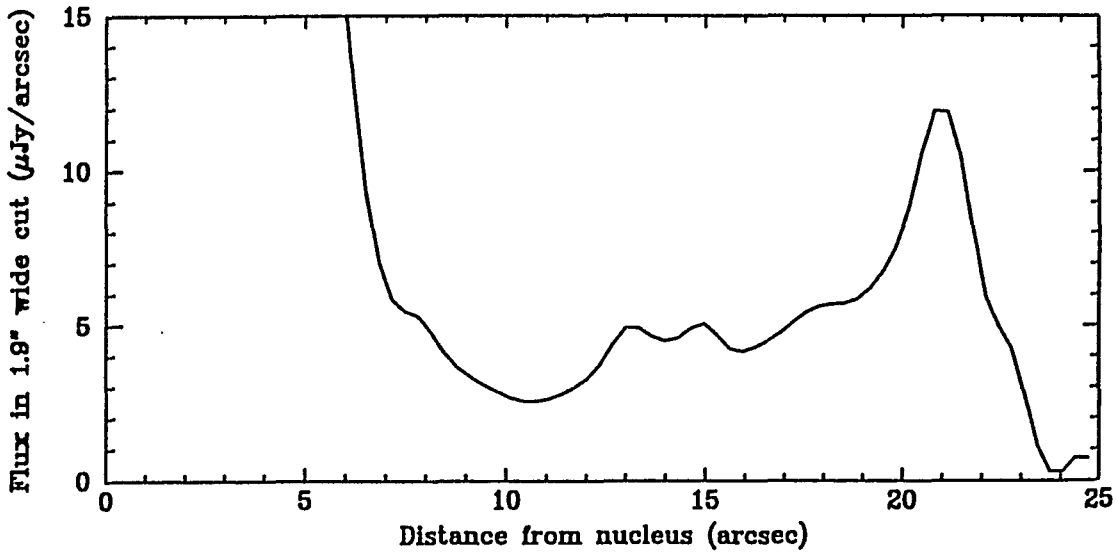

Fig. 3.6.—
Profile of the jet of 3C273 determined from a 1.″9 wide cut. The vertical scale gives flux density per arcsecond of distance along the jet. The nucleus dominates the profile at small radii.

shows a continuation of the trend they see from 0.45 to 0.86μm, that is, the bright knot near the end of the jet is relatively red compared with the rest of the jet. This statement is all the stronger for the extension past the knot. This extension would appear to coincide with the brightest radio knot, which lies about 1" beyond the brightest visible one (Thomson, MacKay, & Wright 1993).

Conway & Röser (1993) have fitted visible and radio measurements of features in the jets with synchrotron cutoff spectra. They show a progression toward low frequency for the cutoff as one moves outward from the quasar through features A through C, with a much more rapid progression for D and H (corresponding respectively to the visible and radio knots at the end of the jet). Our data confirm in the near infrared the behavior predicted by these fits and therefore support the reality of this progression. This general trend is consistent with suggestions that the radio and visible knots at the end of the jet result from rapid energy loss where

the jet is burrowing into the surrounding medium (compare with the theoretical simulations by Cox, Gull, & Sheuer 1991). The abrupt change in spectral index at the end of the jet and the lack of significant extension in the radio past the tip of the jet as defined in our infrared image both suggest a rapid increase in the density of the medium at the end of a long cavity, through which the jet otherwise proceeds with a continuous but modest rate of energy loss.

3.6 Summary

We have taken H-band images for a complete sample of 26 high-luminosity QSOs with redshift $z < 0.30$. We have detected the host galaxy for at least 23 of these objects. The average host-galaxy magnitude is $M_H = -24.6$, roughly twice as bright as that of their low-luminosity counterparts. The inferred mass, assuming there is not significant contamination of the H-band light by supergiants, is roughly twice that of an L^* galaxy. In addition, the high-luminosity quasars are possibly more likely to have close (within 30 kpc), massive (H luminosity greater than $\frac{1}{10}L^*$) companions. These results are consistent with suggestions that the highest levels of activity in radio-quiet quasars require a massive host galaxy, or a significant encounter with a massive galaxy, and that many such encounters result in mergers.

Chapter 4

THE HOST GALAXIES OF CFA SEYFERTS

We present near-IR images of 43 Seyfert galaxies from the CfA Seyfert sample. The near-IR luminosity is a good tracer of luminous mass in these galaxies. Most of the Seyferts are found in hosts of mass similar to that of L^* galaxies and ranging in type from S0 to Sc. In addition, there is a population of low-mass host galaxies with very low luminosity Seyfert nuclei. The CfA Seyferts are found to be deficient in edge-on galaxies. The hosts do not appear to have bars any more frequently than normal galaxies of the same Hubble type.

4.1 Introduction

In the previous chapters we described an imaging survey of nearby quasars. For this chapter, we have chosen a complementary sample of Seyfert galaxies for a similar analysis. Our purpose is to investigate the continuity of host properties

over a wider range of nuclear luminosity. To the extent that Seyferts and quasars represent populations with continuous distributions of properties, studying the Seyferts will tell us about the more distant quasars. The proximity of the Seyferts allows a more detailed analysis of the AGN phenomenon; from them we may hope to understand how the host galaxy funnels fuel to an active nucleus and how the central engine affects the galaxy. To minimize selection effects, we have chosen to use the well-defined, spectroscopically-selected CfA Seyfert sample (Huchra & Burg 1992) for an IR imaging survey. This sample of 48 objects contains roughly equal numbers of type 1, intermediate (1.5-1.9), and type 2 Seyferts. We also consider a preliminary sample of nearby Seyferts (R. Maiolino & G. Rieke, private communication) selected from "A Revised Shapley-Ames Catalog of Bright Galaxies" (RSA; Sandage & Tammann 1987). Like the CfA Seyferts, the RSA Seyferts are selected from a blue magnitude-limited survey and are not biased by color selection. Of the $\sim$ 64 Seyferts in the RSA sample $\sim$ 50 are not also CfA Seyferts. Though we have not obtained IR images for these 50 galaxies, we can use the RSA sample as an independent test of some of the conclusions drawn from the CfA sample.

We noted in Chapter 1 that several other groups have recently presented near-IR images of Seyfert 1 galaxies. Zitelli and collaborators (Zitelli et al. 1993; Danese et al. 1992; Granato et al. 1993; hereafter collectively called ZDG) looked at mostly Markarian Seyferts, whereas Kotilainen and collaborators (Kotilainen et al. 1992a,b; Kotilainen, Ward, & Williger 1993; Kotilainen & Ward 1994) have imaged a hard X-ray sample. The Seyfert imaging survey presented in this chapter offers several advantages. First, the CfA sample is spectroscopically-selected and is therefore not biased against Sy 2's as the other groups' samples are. Thus, we may compare host galaxies as a function of nuclear type. Second, we have

complementary low-redshift quasar samples for comparison. Third, our images were obtained with a larger array with a larger field of view. This allows more accurate sky subtraction and surface photometry of the outer parts of the galaxies. In addition, the larger fields contain stars which can be used to model the point spread function (PSF) of the nucleus.

4.2 Observations

We obtained K images of 42 of the 48 CfA Seyfert galaxies, and an H image for an additional one (I Zw 1), at the Steward Observatory 2.3 m telescope on Kitt Peak. The observations were made using a NICMOS3 infrared array camera with $0\farcs63$ pixels in roughly $1\farcs5$ seeing. The observing procedure consisted of taking a series of alternating source and sky frames (of the same exposure time) by wobbling the telescope several arcminutes between exposures. In addition, a random "jitter" component was used to vary the source position slightly from frame to frame, thus ensuring that every part of the source fell on a good pixel in at least some of the frames. The more efficient observing strategy of rastering described in the previous chapters was not useful for these nearby objects because the galaxy can cover a large part of the frame. Exposure times were chosen to keep the detector within its linear regime; times ranged from 20 to 60 seconds per frame for approximately 10 minutes of on-source integration. The sample is given in Table 4.1.

Most of the objects were observed under photometric conditions; for these objects, we flux calibrated our images using standard stars (Elias et al. 1982) observed on the same nights. We checked the photometry against published K photometry from Edelson, Malkan, & Rieke (1987) or new, unpublished

Table 4.1. CfA Seyfert host galaxy properties

Name	Sy[b]	Galaxy Type[c]	b/a	f[d]	K_{tot} mag	K_{psf} mag	$\frac{L_{gal}}{L_{tot}}$	$M_{K,gal}$ mag	M_B mag	ϵ_{bar}	D_{bar} kpc
Mkn 334	1.8	Pec	0.9	0.80	10.3	11.5	0.67	-23.8	-20.1	...	...
Mkn 335	1.0	S0/a	1.0	0.70	9.9	10.7	0.50	-24.2	-20.7	...	...
A0048+29	1.0	(R')SB(s)b	1.0	0.70	10.8	12.3	0.76	-24.7	-21.3	0.37	12.0
I Zw 1 (H data)	1.0	S?	1.0	0.85	11.4	11.9	0.38	-24.4	-22.4	...	...
Mkn 993[e]	1.5	Sa	0.3	0.75	10.1	12.8	0.91	-23.6	-19.4	...	...
Mkn 573	2.0	(R)SAB(rs)0+:	1.0	0.50	10.3	13.3	0.94	-23.8	-19.5	0.36	7.1
0152+06	1.9	SA(rs)b	0.8	0.80	10.3	13.0	0.92	-23.7	-19.9	0.55	9.9
Mkn 590	1.0	SA(s)a:	0.9	0.90	9.6	10.5	0.58	-24.8	-20.5	...	...
NGC 1068	2.0	(R)SA(rs)b	0.9[c]	...	...	...	...	-24.7[i]	-19.3	...	...
NGC 1144	2.0	RingB	0.9	0.60	9.5	11.5	0.84	-25.5	-19.8	...	...
Mkn 1243[e]	1.0	Sa	1.0	0.70	11.4	13.4	0.84	-24.1	-19.9	0.25	6.4
NGC 3227	1.5	SAB(s) pec	0.7[c]	...	...	...	...	-23.8[g]	-16.5	...	...
NGC 3362	2.0	SABc	0.9	0.50	10.4	14.5	0.98	-24.7	-21.6	...	...
A1058+45	2.0	Sa?	0.7	0.80	10.7	12.3	0.76	-24.2	-20.9	...	...
NGC 3516	1.5	(R)SB(s)0^0:	0.8	0.40	8.9	12.0	0.94	-23.6	-19.3	0.38	3.3
Mkn 744[e]	1.8	SAB(rs)a pec	0.5	0.80	10.0	11.3	0.69	-22.3	-18.1	...	...
NGC 3982[e]	2.0	SAB(r)b:	0.9	0.60	9.0	13.1	0.98	-21.9	-19.1	...	...
NGC 4051	1.0	SAB(rs)bc	0.8[c]	...	...	...	...	-23.3[g]	-16.2	...	...
NGC 4151	1.5	(R')SAB(rs)ab:	0.7[c]	...	...	...	...	-23.9[g]	-18.3	...	...
NGC 4235[e]	1.0	SA(s)a	0.3	0.60	8.4	12.2	0.97	-23.8	-19.0	...	...
Mkn 766	1.5	(R')SB(s)a:	0.8	0.70	9.9	11.6	0.79	-23.3	-19.1	0.53	5.0
Mkn 205	1.0	Pec	...	0.80	11.7	12.5	0.52	-24.7	-23.5	...	...
NGC 4388	2.0	SA(s)b: sp	0.2	0.70	8.0	11.6	0.96	-22.5[f]	-16.9[f]	...	...
NGC 4395	1.0	SA(s)m:	0.9[c]	...	...	...	...	-21.6[g]	-14.3	...	...
Mkn 231	1.0	SA(rs)c? pec	0.8	0.70	9.3	10.7	0.72	-26.3	-21.3	...	...
NGC 5033	1.9	SA(s)c	0.5[c]	...	...	...	...	-24.4[g]	-18.3	...	...
1335+39	1.8	S?	1.0	0.70	10.6	13.6	0.94	-23.8	-20.1	...	...
NGC 5252	1.9	S0	0.4	0.70	10.0	12.7	0.91	-24.6	-19.5	...	...
Mkn 266	2.0	Compact pec	0.8	0.40	11.3	13.3	0.84	-23.6	-20.9	...	...
Mkn 270	2.0	S0?	0.9[c]	...	...	...	...	...	-17.7	...	...
NGC 5273[e]	1.9	SA(s)0^0	0.9	0.70	8.8	12.2	0.95	-21.8	-16.6	...	...
Mkn 461	2.0	S	0.7	0.60	10.7	13.4	0.92	-23.1	-19.3	0.45	8.2
NGC 5347	2.0	(R')SB(rs)ab	0.8	0.85	9.7	12.1	0.90	-22.6	-18.9	0.58	10.0
Mkn 279	1.0	S0	0.7	0.90	9.9	10.6	0.45	-24.5	-20.2	...	...
NGC 5548	1.5	(R')SA(s)0/a	1.0	0.85	9.6	11.0	0.74	-24.1	-19.7	...	...
Mkn 471	1.8	SBa	0.7[c]	...	...	...	...	...	-21.0	...	...
NGC 5674	1.9	SABc	1.0	0.80	10.0	11.9	0.83	-24.7	-21.2	0.50	11.0
Mkn 817[e]	1.5	S?	0.9	0.70	10.2	11.3	0.64	-24.7	-21.1	...	...
Mkn 686	2.0	SBb	0.7	0.50	9.9	13.2	0.95	-23.7	-19.1	0.48	6.5
Mkn 841	1.5	(QSO)	...	...	...	...	...	-24.7[h]	-20.5	...	...
NGC 5929[e]	2.0	Sab: pec	0.7	0.50	10.3	12.5	0.86	-22.0	-18.1	...	...
NGC 5940	1.0	SBab	0.7	0.85	10.6	12.5	0.83	-24.8	-20.0	0.60	18.0
NGC 6104	1.5	S?	0.9	0.60	10.8	13.8	0.94	-24.3	-20.9	0.70	13.0
2237+07	1.8	SBa	0.9	0.80	10.9	12.1	0.68	-23.6	-20.6	0.46	6.8
NGC 7469	1.0	(R')SAB(rs)a	0.8	0.50	8.8	11.2	0.89	-25.0	-20.3	0.35	12.0
Mkn 530[e]	1.5	SA(rs)b: pec	0.6	0.75	9.7	11.6	0.81	-25.3	-20.5	...	...
Mkn 533	2.0	SA(r)bc pec	0.9	0.80	9.8	11.6	0.82	-25.2	-20.8	0.50	12.0
NGC 7682	2.0	SB(r)ab	0.8	0.70	10.1	12.8	0.92	-23.9	-19.6	0.50	16.0

[a] $H_0 = 80$ km s^{-1} Mpc^{-1}

[b] Osterbrock & Martel 1993

[c] Obtained from NED; usually RC3 data

[d] Fraction of normalized PSF subtracted

[e] Uncertain zero point or possibly variable

[f] If not a Virgo Cluster Member, absolute mags are $\sim$ 2 mag brighter than listed here

[g] Uncertain; derived from B magnitude

[h] Zitelli et al. 1993

[i] Derived from Aaronson 1977 K aperture photometry

K photometry from the Multiple Mirror Telescope (MMT[1]). Except in a few cases (indicated as discrepant in Table 4.1), they agreed within 15%. For the objects observed under nonphotometric conditions, we used the Edelson et al. (1987) or MMT photometry for calibration.

4.3 Data Reduction

For each set of alternating frames, a dark frame of the appropriate length was subtracted from each sky frame, and the resulting frames were median-combined to create a flatfield frame. The source frames were then sky-subtracted using averages of neighboring sky frames, and flatfielded. These images were adjusted by fractional pixel shifts to align them on the centroid of the Seyfert nucleus and combined by averaging to produce a final image for each galaxy. Bad pixels were excluded using a mask and remaining discrepant pixels were clipped during averaging. Contour plots of the Seyferts are shown in Figure 4.1. For a few of the very nearby objects only the central region of the galaxy is shown; we have no reliable sky subtraction for these objects.

For consistency with the analyses in the previous chapters, one-dimensional technique was used to subtract out the contribution of the nucleus for each Seyfert. (For NGC 1144, which has a very closely interacting companion, we had to use the two-dimensional technique described in the previous chapter.) Elliptical isophotes were fitted to each galaxy and a radial intensity profile was extracted. The fits were carried out to a level where the signal-to-noise in an annulus was $(S/N) \approx 1$; typically, this was $K \approx 20.5$ mag arcsec^{-2}, corresponding to $B \approx 24.4$

[1]A joint facility of the Smithsonian Institution and the University of Arizona

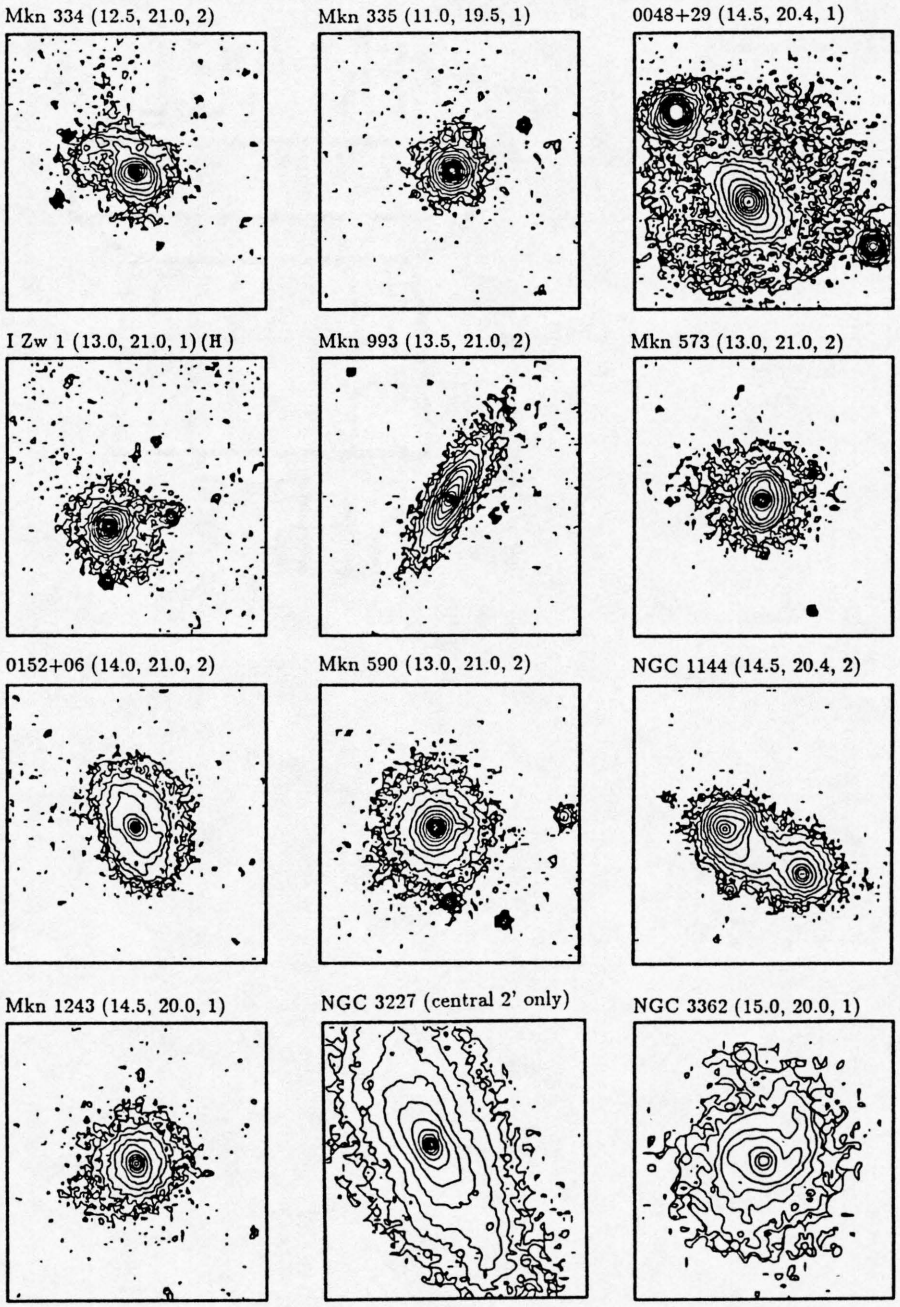

Fig. 4.1.—
K-band surface brightness contour plots of the CfA Seyferts. North is down and East is to the left. The contour interval is 0.5 mag arcsec^{-2}. The numbers above each box are brightest and dimmest contours in K mag arcsec^{-2}, and box size in arcminutes. Several objects show ghost images roughly 6″ to the south of the nucleus (e.g. Mkn 766); these have been masked during analysis. The asymmetry of NGC 5033 is likely a result of a flatfielding error; the sky frame fell on part of the galaxy.

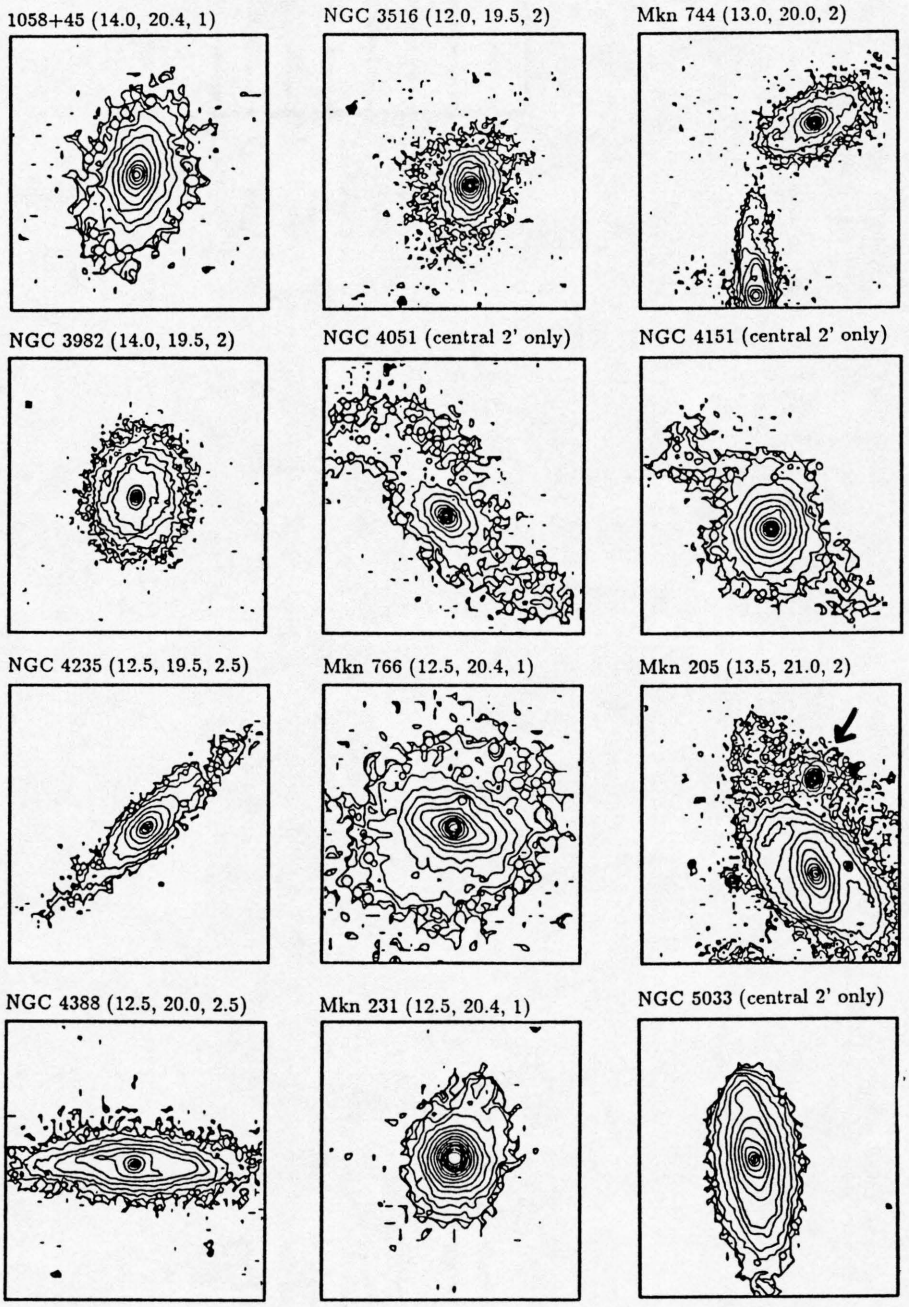

Fig. 4.1—continued

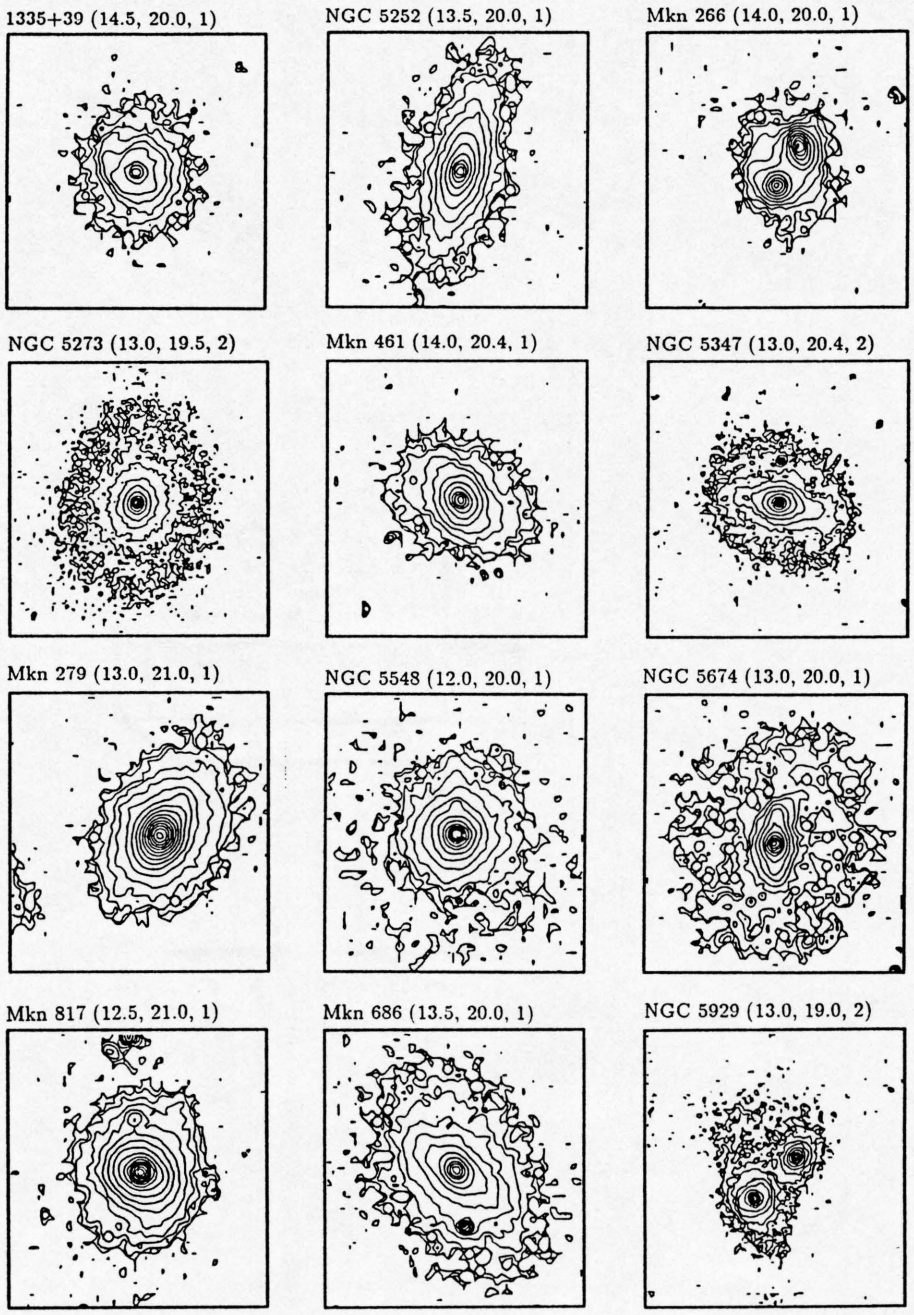

Fig. 4.1—continued

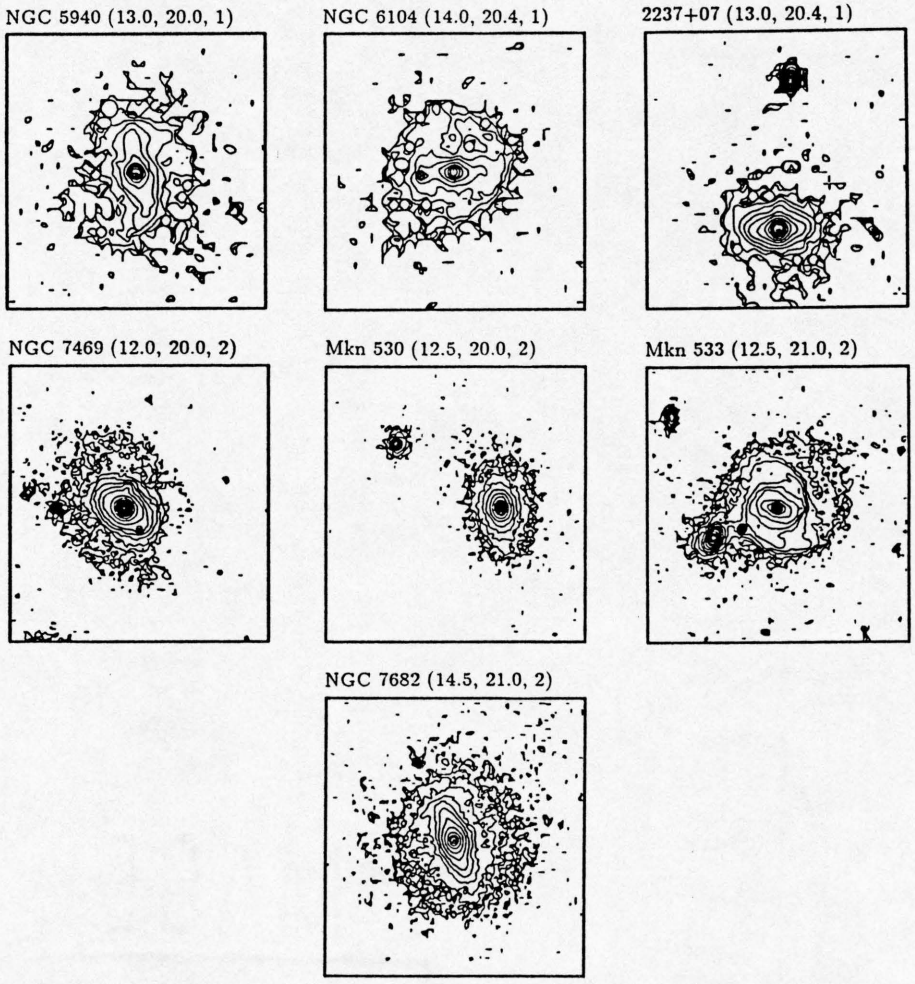

Fig. 4.1—continued

mag arcsec^{-2}, not as deep as our quasar images. An identical procedure was used on one or more high S/N stars from the same frame; these were taken to represent the PSF of each image. The radial profiles are shown in Figure 4.2.

To remove the nuclear contribution, assumed to be that of a point source, we first normalized the PSF profile to have the same central intensity as the Seyfert profile. We then subtracted progressively larger fractions of the normalized PSF from the Seyfert until the resulting profile started to turn over in the center. The fraction subtracted ranged from 0.4 to 0.9, compared to 0.7 to 0.9 for the quasars. The galaxy magnitude was then computed from the total light (obtained from aperture photometry of the image) minus the light from this fraction of the PSF. The results of this analysis are given in Table 4.1.

Our method of PSF subtraction differs somewhat from the one used by ZDG and Kotilainen et al. (1992a). Those groups performed χ^2 minimization fits to the radial profiles assuming three components: an $r^{1/4}$ bulge, an exponential disk, and a nucleus represented by a double Gaussian fit to stellar profiles. We opted not to take this approach for several reasons, the most important being that the profiles are often complicated by the presence of a bar or tidal features. Inspection of Figure 4.2 shows that in these cases, a nucleus+bulge+disk representation would prove inadequate and meaningless. Though the three-component fits probably give a fair representation of the integrated light from a galaxy, the simpler procedure outlined above performs at least as well and allows the quasars and Seyferts to be treated consistently. The important thing to note is that the conclusions drawn below are insensitive to even moderate errors in the decomposition procedure. Our procedure also differs slightly from the one we used for the quasars. For the quasars, we subtracted the PSF identically but then fit the resulting profile with an exponential disk. For the low-luminosity quasars, the disk fits were used to

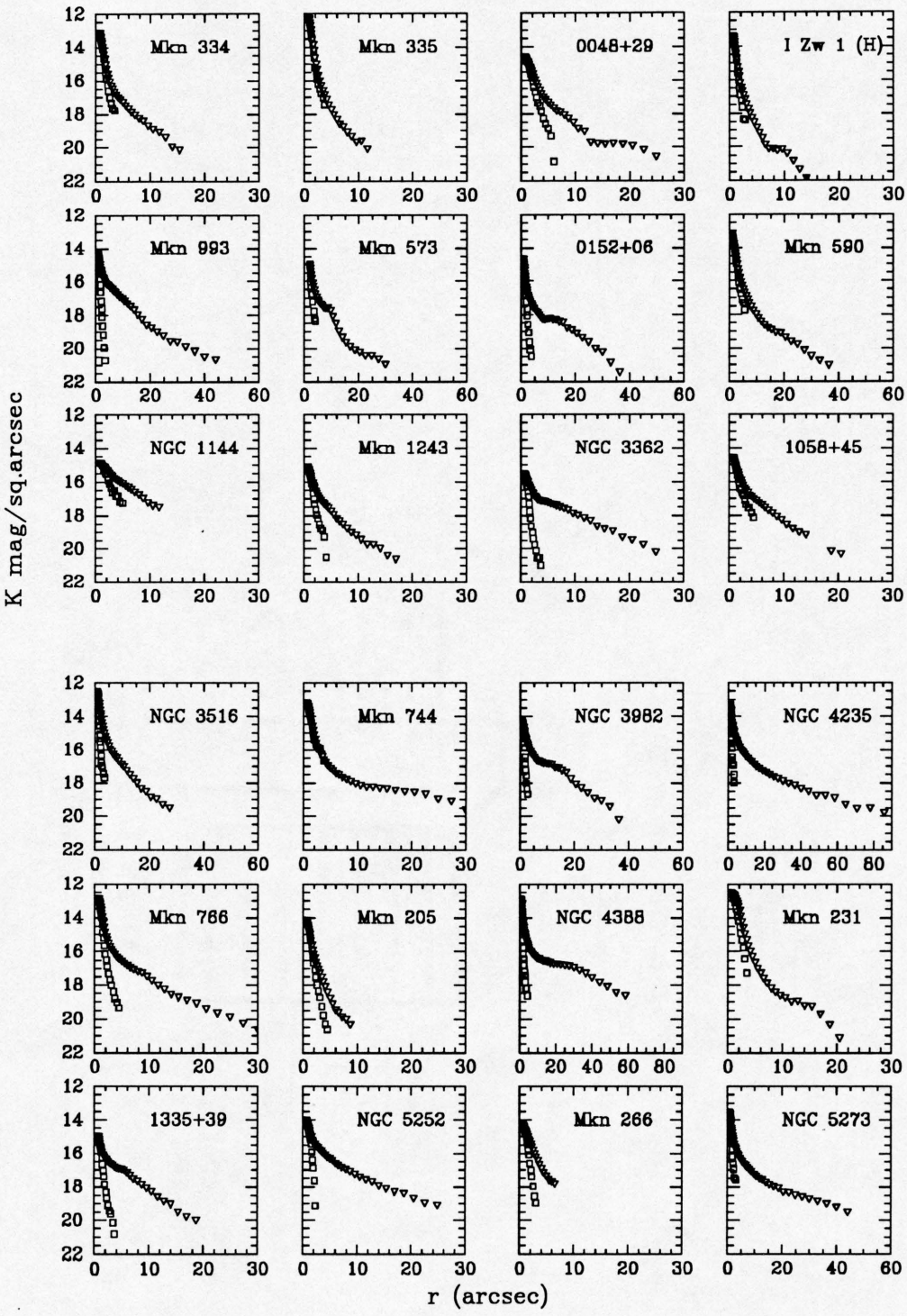

Fig. 4.2.—
Surface brightness profiles of CfA Seyferts. Triangles represent the Seyferts, squares represent stars from the same frame.

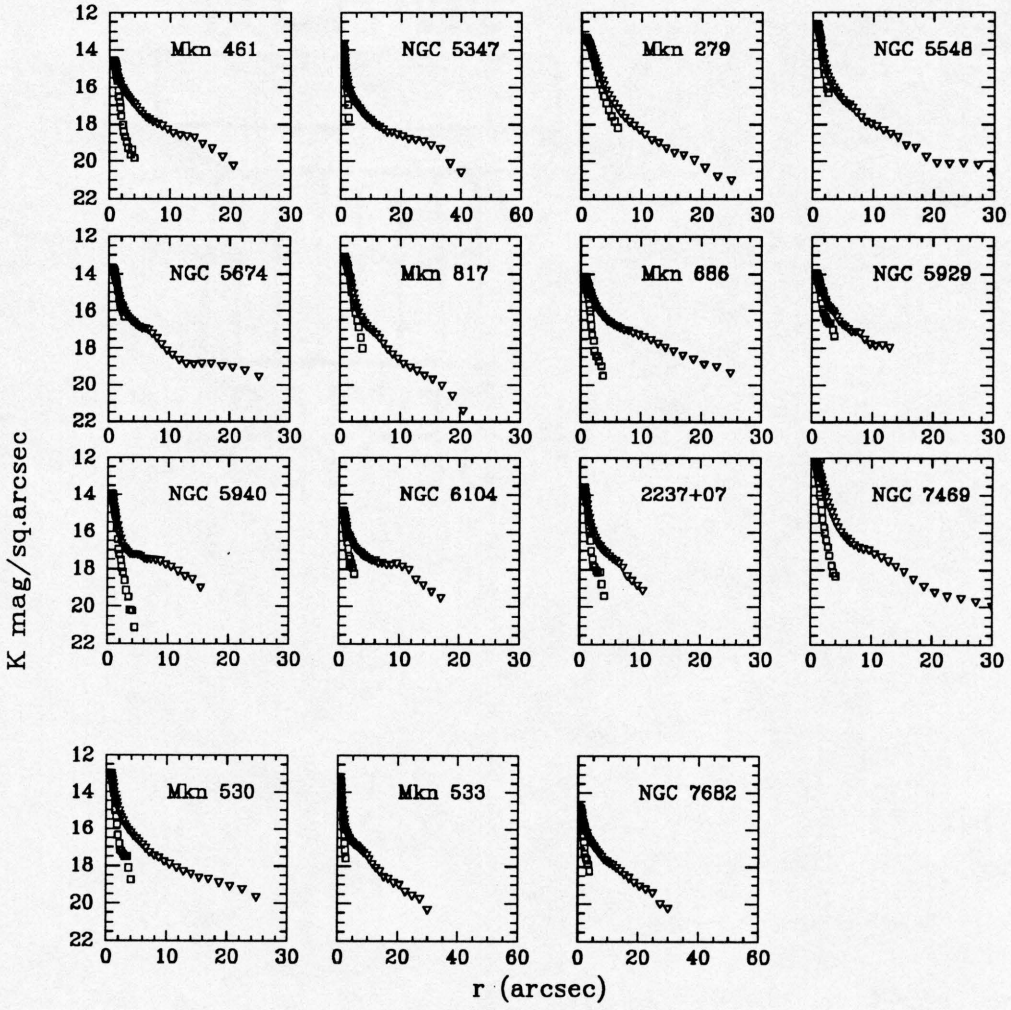

Fig. 4.2—continued

compare scale-lengths and central surface brightness with those of normal spirals. For the high-luminosity quasars, the disk fits were used simply as a convenient way of adding up the galaxy light. For the nearby Seyferts, which are seen in greater detail and often have "shoulders" in their profiles, the simpler method described above provided a slightly more accurate accounting of the galaxy light. Tests on the low-luminosity quasars showed that the two procedures result in the same galaxy magnitudes within $\approx 10\%$.

Based on standard star measurements and comparison with previous photometry, we believe the total magnitudes are accurate to 15% (unless otherwise noted in the Table). The point-source subtraction adds additional uncertainty of at most 20%; therefore, the galaxy magnitudes are accurate to about 0.3 mag.

In addition to the radial profiles, the isophote fits yielded ellipticities and position angles of the ellipses as a function of distance along the semi-major axis. As described below, these parameters can be used to search for bars in the host galaxies.

4.4 Results

4.4.1 Seyfert Galaxy Magnitudes

In most cases we have calculated galaxy absolute magnitudes from the K images assuming the distance to each galaxy to be cz/H_0 with $H_0 = 80$ km s^{-1} Mpc^{-1}. The results are given in Table 4.1. We have ignored k-corrections because the redshifts are so low; for these objects the correction would be less than 0.1 mag. We include several galaxies that have already been imaged by Kotilainen & Ward (1993) or ZDG; our galaxy K magnitudes agree within about 0.5 mag.

Some of the absolute magnitudes listed were derived by other methods. For four of the Seyferts that we observed, NGC 3227, NGC 4051, NGC 4151, and NGC 5033, the galaxies overfilled the frame of the camera. For these galaxies and for NGC 4395 (which we did not observe) galaxy magnitudes have been estimated from the total B magnitudes listed in the RSA catalog assuming $B-K=4$. These Seyferts all have low-luminosity nuclei that should not contaminate the B magnitudes significantly. Nonetheless, the inferred K magnitudes should be viewed as highly uncertain due to the unknown galaxy colors. For NGC 1068, which we did not observe, the galaxy magnitude was estimated from the K large-aperture photometry of Aaronson (1977). For Mkn 841, we used the ZDG K magnitude. We have no estimate of the galaxy magnitude for Mkn 270 or Mkn 471.

Figure 4.3 shows the absolute magnitudes of the Seyfert host galaxies. The horizontal axis plots M_B to represent the nuclear luminosity of the AGN. These magnitudes were derived from the B magnitudes listed in Huchra & Burg (1992) and supplemented by total observed B magnitudes from the Third Reference Catalogue of Bright Galaxies (RC3; de Vaucouleurs et al. 1991). In the case of the low-luminosity Seyferts, B light can have a substantial component due to stellar light, especially because some of the apertures used were large. Therefore, the Seyfert M_B values should be taken as lower (i.e. bright) limits to the nuclear luminosities. The horizontal dashed line shows the luminosity of an L^* galaxy, i.e. the luminosity at the knee in a Schechter function description of the local field galaxy luminosity function (e.g. Mobasher, Sharples, & Ellis 1993).

Two of the Seyfert 1's from the CfA sample, I Zw 1 and Mkn 205, actually have nuclear luminosities of quasars. In fact, I Zw 1 is a member of our quasar sample. The host galaxies of these two objects have magnitudes slightly brighter than the average quasar host magnitude for those nuclear luminosities, which may

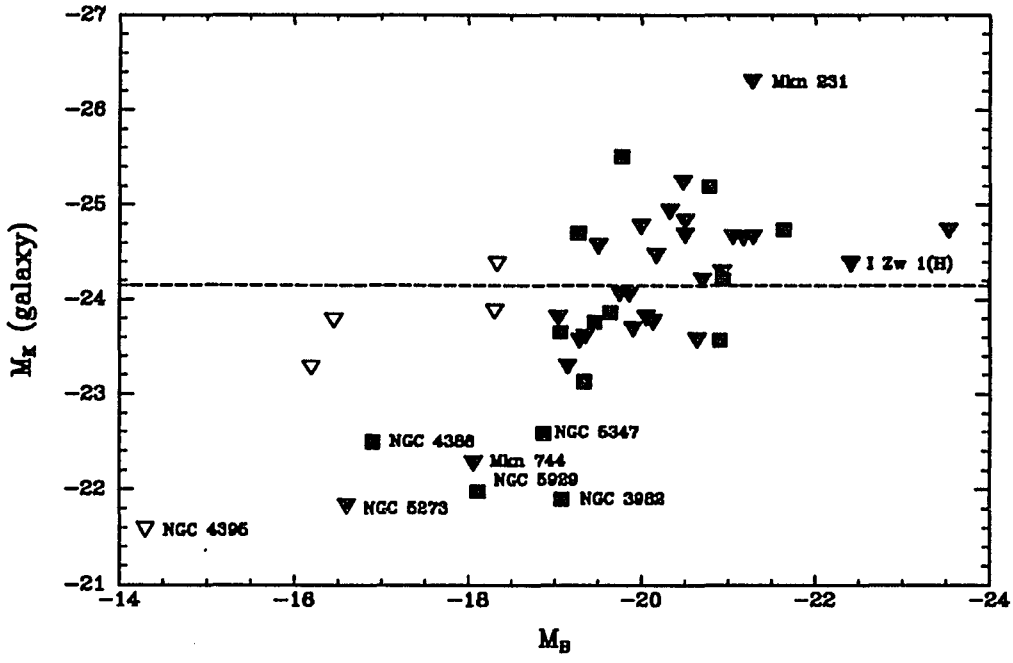

Fig. 4.3.—
Seyfert galaxy v. nuclear absolute magnitudes assuming $H_0 = 80$ km s^{-1} Mpc^{-1}. The dashed line shows the K magnitude of an L^* galaxy. The M_B's give bright estimates of the nuclear luminosities (see text). Type (1-1.9) and type 2 objects are shown by triangles and squares, respectively. Open symbols denote galaxy magnitude derived from total B magnitude; these are uncertain.

explain why they were identified as Seyfert galaxies. We show the images for completeness but omit these two objects from further analyses.

Figure 4.3 also shows that there is a shortage of high-luminosity CfA Seyfert galaxies ($M_K \lesssim -23$) with low-luminosity nuclei ($M_B \gtrsim -19$). This can be easily understood as a selection effect. A very low-luminosity nucleus against an overwhelmingly bright galaxy could be missed at the distances of typical members of the CfA survey. The gap is filled in by the Seyferts in the RSA sample; the lower average distance to the RSA galaxies makes the nuclei easier to isolate.

Perhaps the most striking feature of Figure 4.3 is the group of outlying low-luminosity galaxies containing low-luminosity nuclei. There are unfortunately some uncertainties in the placement of these points. NGC 4388 would not be in this group if we had placed it at its Hubble's law distance; we have instead placed it at the distance of the Virgo Cluster because it is thought to be a cluster member. For NGC 5273 and NGC 3982, our K-band zero points are uncertain by several tenths of a magnitude, but this is not enough to remove them from this group. For NGC 5929 and Mkn 744, both of which have interacting companions and both of which were observed on a cloudy night, the zero point uncertainties are unfortunately larger. Of the galaxies in this group, all but NGC 4388 and NGC 5347 also have low host luminosities at B. Because these galaxies are all nearby, there is a possibility that significant distance errors have biased their placement. However, unless their peculiar velocities exceed ~ -600 to -1500 km s^{-1} (depending on the galaxy), the magnitude errors determined from Hubble's law are not large enough to place these galaxies in range with the others. It would be surprising to have such large negative peculiar velocities in more than 10% of an unbiased sample such as the CfA Seyfert sample.

Finally, Figure 4.3 shows that there is no obvious difference in K magnitude between the hosts of type 1 and type 2 Seyferts.

4.4.2 Host-Galaxy Types

We list in Table 4.1 host-galaxy types collected mainly from RC3. The CfA Seyferts are primarily found in spiral galaxies ranging in type from S0 to Sc. A few are peculiar and/or interacting. Of the 37 galaxies identified as a specific type of spiral, the average and median type is approximately Sab. Figure 4.4 shows the

breakdown of galaxy classification among types 1, 1.5-1.9, and 2. The medians for each nuclear type individually are not significantly different. Thus, we see that all Seyfert types can occur over a wide range of host-galaxy bulge size. We note that there is no correlation between bulge mass (represented by the spiral type) and nuclear luminosity.

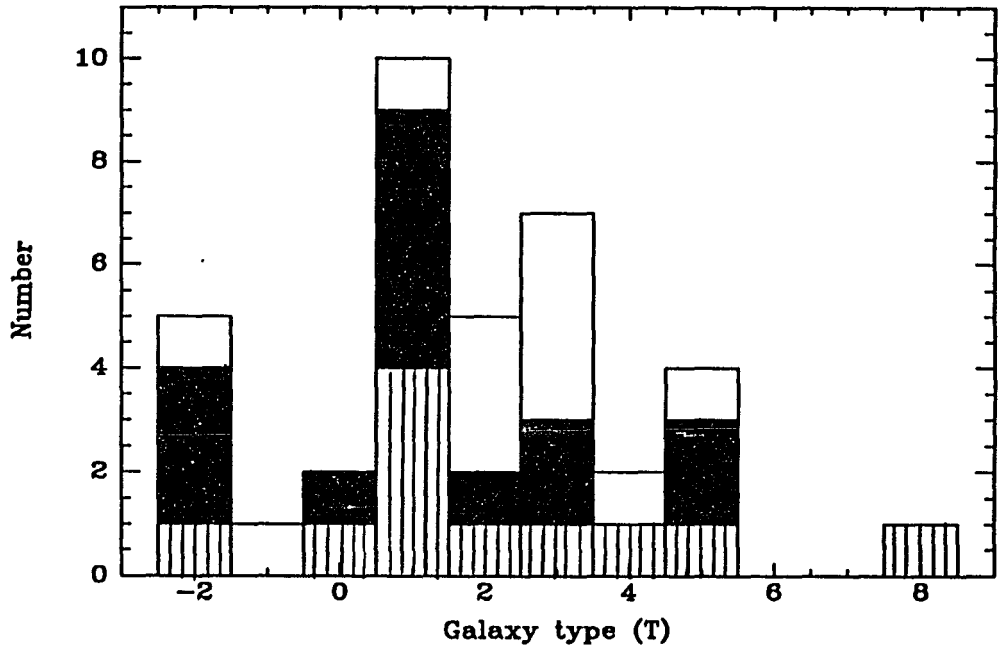

Fig. 4.4.—
Host-galaxy classifications for the 37 CfA Seyferts identified with a specific type of spiral (1=Sa, 3=Sb, 5=Sc...). The peculiar and unclassified galaxies have been omitted. Striped boxes, filled boxes, and open boxes represent Seyfert types 1, 1.5-1.9, and 2 respectively.

The anomalous dwarf Seyfert 1 NGC 4395 has by far the least luminous nucleus in this sample; its properties have recently been summarized by Filippenko, Ho, & Sargent (1993). As discussed above, there are several other low-luminosity galaxies with low-luminosity nuclei that might be considered in a class with NGC

4395. An examination of their sizes shows these galaxies also to be among the smallest in the CfA sample. Taking D_{25} (the galaxy diameter at the level of the $B = 25$ mag arcsec^{-2} level) from RC3, we find that the CfA Seyferts have $< D_{25} >= 26$ kpc with a 1σ scatter of 11 kpc. The outliers all have $D_{25} <$ kpc, except Mkn 744 which has a diameter of 20 kpc. Some of these galaxies are probably genuine dwarfs, but in other cases distance errors might have resulted in underestimates of the diameters.

4.4.3 Morphology

Axial ratios

We have computed axial ratios (b/a) for the CfA Seyferts using the results of the ellipse fits. The ratios are listed in Table 4.1. We have supplemented our observations using major and minor axis sizes listed in NED[2] (usually from RC3). For all of the galaxies for which we have elliptical isophote fits, the axis ratios are in good agreement with values derived from NED, except in one case where we had only a very shallow image. We show in Figure 4.5 the distribution of axial ratios for 42 of the 48 objects (we omit the peculiar galaxies Mkn 334, NGC 1144, and Mkn 266, the unclassified galaxy Mkn 841, and the two quasars). There are only a few galaxies with $b/a \leq 0.5$. This is very different from normal spiral and lenticular galaxies, which are seen to have a nearly flat distribution down to $b/a \approx 0.1 - 0.2$

[2]The NASA/IPAC Extragalactic Database (NED) is operated by the Jet Propulsion Laboratory, California Institute of Technology, under contract with the National Aeronautics and Space Administration

(Binney & de Vaucouleurs 1981). Thus, we find that the CfA Seyferts are deficient in edge-on galaxies.

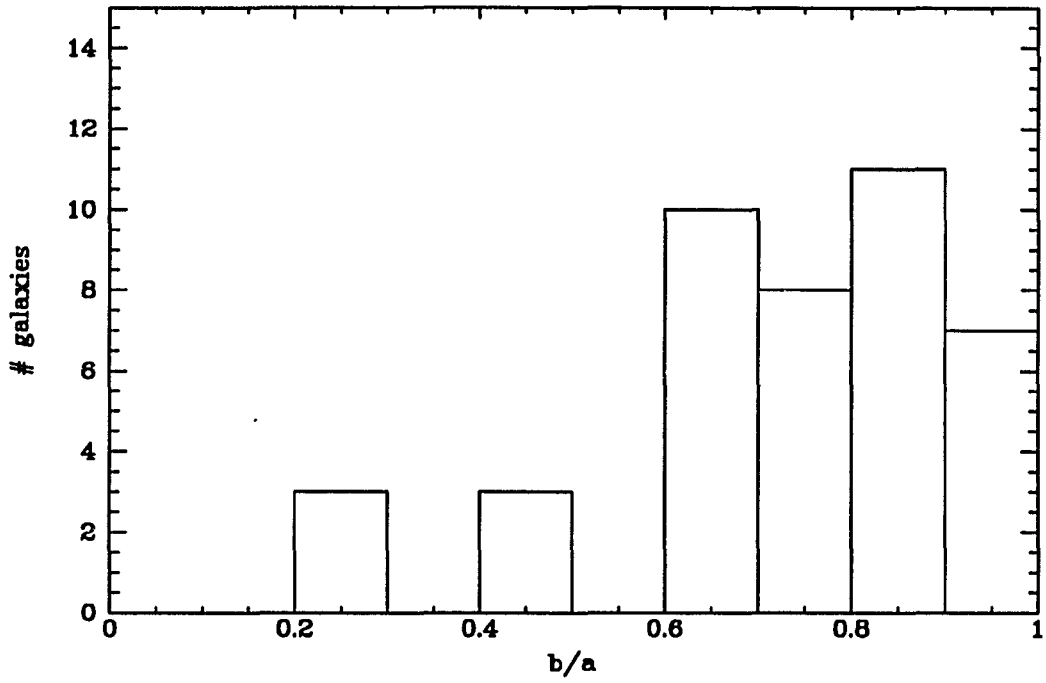

Fig. 4.5.—
Distribution of host-galaxy axis ratios for CfA Seyferts.

Bars

Because bars provide an efficient way to transport large amounts of material from the outer parts of a galaxy into the central kiloparsec, it is of interest to investigate how often a bar accompanies AGN activity. Several studies have focused on the connections between bars and nuclear activity (e.g. Heckman 1978; Simkin, Su, & Schwarz 1980; MacKenty 1990). However, CfA and RSA Seyfert samples offer a better possibility to investigate this topic with samples that are both large

and unbiased towards galaxies with very blue colors/starbursts. Star formation is commonly associated with bars so avoiding such a selection bias is important to an unambiguous result.

We have used the NED classifications (mostly from RC3) to determine the frequency of bars in both the CfA and RSA Seyfert samples. For the CfA Seyfert sample, we find 21% SB and 21% SAB type galaxies in the subsample of 42 (we again exclude the two quasars, the three peculiar galaxies, and Mkn 841). The number of SAB's is increased to 11 with the reclassification of NGC 1068 (Scoville et al. 1988) and of Mkn 270 (Simkin et al. 1980). For the $\sim$ 50 Seyferts in the RSA sample not also in the CfA sample, the fractions are 36% and 30% respectively. Comparing these fractions to the fractions for normal spirals is hampered by uncertainty in the latter. For the mix of galaxy types in these samples, the Second Reference Catalog of Bright Galaxies (RC2; de Vaucouleurs et al. 1976) has roughly 40% type SB and 25% type SAB galaxies, but the classification can be very heterogeneous (Sellwood & Wilkinson 1993). Despite the large uncertainty, there appears to be no strong preference for barred systems in these Seyferts.

Because the morphological classification system for the RSA catalog is reasonably homogeneous, counting bars in the Seyferts found in the RSA provides a cleaner test. The RSA catalog gives 36% of the Seyferts in SB systems, compared to 30% for all disk galaxies. Therefore, we conclude that there is at most a weak preference for bars.

Near-IR images highlight the mass-tracing stellar component while being less sensitive to obscuration by dust and so can reveal bars that may be weak or hidden in visible images (Block & Wainscoat 1991; Pompea & Rieke 1990). Also, the ellipse fits to the IR images allow us to quantify the physical properties of the stellar

bars in these Seyferts. From the ellipse fits we have generated plots of intensity, ellipticity, and position angle as a function of distance along the semi-major axis. We consider a galaxy to have a bar if (i) the ellipticity grows steeply to a maximum and then falls off to reveal the true inclination of the galaxy; (ii) the position angle is constant over the range of high ellipticity; and (iii) there is a shoulder in the intensity profile over the same range. We did not intend (iii) to be a necessary condition but it nearly always accompanied the first two features.

As expected, the near-IR images reveal bars in galaxies not previously classified as barred. Strong bars are seen in 0152+06, NGC 6104, and Mkn 533. Very weak bars are tentatively detected in Mkn 1243 and Mkn 461. NGC 4388 is too highly inclined for detection of a bar but we note that it has a very boxy bulge. Perhaps more surprising, we find that several galaxies previously classified as barred have no IR bars or have weak IR bars at best. NGC 3982 (classified visibly as SAB) shows a strong multi-armed spiral structure even at K; it is likely that HII regions have influenced the visible classification. For NGC 3362 (also an SAB), the K-band images show a strong, wide, two armed spiral pattern that winds close to the nucleus; while probably not a true bar, it is still indicative of a nonaxisymmetric perturbation. If Mkn 686 (SB) and NGC 7469 (SAB) contain bars, they are very weak in the IR. These latter two galaxies might have gas bars supported by a weaker (invisible) stellar bar and currently forming stars at the ends. While we have added several galaxies to the list of barred Seyferts, we find that such a perturbation is by no means a universal feature of spiral AGN hosts.

In Table 4.1 we have listed the ellipticity (defined as $1 - b/a$) and approximate size for all of the IR bars we could measure from our frames; comparison with the images in Figure 4.1 may also be of interest. The ellipticity gives some measure of the strength of the bar, while the size gives a clue to the position of

resonances in the underlying potential. We believe these values will soon be useful for comparisons with new models and observations. Three-dimensional numerical models including stars and gas are now becoming available (e.g. Friedli & Benz 1993, Heller & Shlosman 1994), and large samples of normal spirals are currently being imaged in the IR by several groups.

Outer rings

Closely related to bars in spiral galaxies are inner and outer rings. The radial flow of gas associated with a bar can cause pileups near inner and outer Linblad resonances; characterizing the rings can therefore yield additional information about the gravitational potential and fueling in AGN. Simkin et al. (1980) found a very high percentage of Seyfert hosts with outer rings (43%, compared with only 8% for a control sample of nearby RC2 galaxies).

We would like to obtain a similar count of outer rings for Seyferts in the CfA sample. The IR images, however, are ill-suited to this task; of the galaxies classified visibly as having inner or outer rings, there are only a few where we see the ring at all and those are at very low contrast. In the case of outer rings, we usually see a smooth plateau instead. Presumably the rings are made up of stars that have formed recently as a result of the bar-induced gas flow, and the IR images are insensitive to this young population. We must therefore rely on the visible classifications. NED gives the number of CfA Seyferts with outer rings as 9, or 21%. The fraction for the RSA Seyferts not also in the CfA sample is the same. This is lower than the frequency seen by Simkin et al. (1980) but higher than the frequency in their control sample. Assuming Poisson statistics, we find that the probability of finding 9 or more outer rings in this sample to be only $\sim$ 1%. The

heterogeneous classification system again adds uncertainty. Unfortunately, the RSA catalog is of little help because there are so few ringed galaxies identified there; out of more than 900 disk galaxies, only 2% are classified as ringed. For completeness, we note that the fraction of ringed Seyferts in the RSA catalog is 3%. We conclude from the RC3 classifications that there is some evidence for an excess of Seyferts with outer rings.

4.4.4 Interactions

Galaxy-galaxy interactions provide another indication of gravitational asymmetries that could trigger the flow of gas to the center of a spiral galaxy. The relationships between interactions and Seyfert activity have been studied by many groups over the last decade. One approach has been to compare samples of paired and isolated galaxies; the results are that paired galaxies have stronger nuclear emission lines, elevated rates of star formation, and higher frequencies of Seyferts (especially in close pairs but not in very disturbed systems) (Kennicutt & Keel 1984; Keel et al. 1985; Dahari 1985). Another approach has been to compare the number of companions for Seyferts and control samples of galaxies. Compared to normal spirals, nearby Seyferts seem to show a weak excess of bright companions and possibly a stronger excess of faint ones (e.g. Fuentes-Williams & Stocke 1988; Byrd, Sundelius, & Valtonen 1987). However, Markarian Seyferts do not have close companions more frequently than non-Seyfert Markarian galaxies, implying that interactions are more directly related to star formation activity than to nuclear Seyfert activity (MacKenty 1989).

We would like to determine an interaction rate for the CfA Seyferts to investigate possible sources of fueling for this sample and to compare with

our results on quasar companions. For the quasars, we considered only bright ($L > \frac{1}{10}L^*$), physical companions within a projected separation of 30 kpc; such an object would have been detected in our quasar studies and could certainly exert a significant tidal force on the AGN host. For the quasar samples, we used our images to search for companions. Unfortunately, the proximity of the CfA Seyferts means that our frames do not always cover the required area of sky; therefore we have used NED to search for companions within that separation. NED lists companions with similar redshifts to 7 of these Seyferts: NGC 1144, NGC 3227, Mkn 744, Mkn 266, NGC 5929, NGC 7469, and Mkn 533. Additionally, our frames show a companion to Mkn 279 and possible companions to 0048+29, Mkn 590, and Mkn 530; we have no redshifts for these objects. The overall rate is then $17 - 23\%$, equally divided among types 1, 1.5-1.9, and 2.

We will compare this rate to that found for the PG quasar samples in §5.4 below. However, we note here that the rate we determined for the Seyferts is not significantly higher than the corresponding rate for normal spirals. To provide a control sample for the CfA Seyferts we have used the ADS[3] to select non-Seyfert CfA galaxies with the same range and distribution of redshifts and morphological types as the Seyferts, with the restriction that they also be listed by their NGC number (most of the CfA Seyferts are members of that catalog). That yielded > 2000 galaxies. As for the Seyferts, we used NED to search for neighbors within 30 kpc projected separation. Finally, we eliminated those neighbors with redshifts differing from the primary galaxy by more than 700 km s^{-1}. The results are not sensitive to our exact cutoff; for example, there are only a handful of neighbors with redshift differences between 500 and 700 km s^{-1}. The overall rate

[3]NASA's Astrophysical Data System v. 4.0

of physical companions in this control sample is less than 9%, compared to 15% (companions found by NED only) for the Seyferts. We have not determined the luminosities of the normal galaxies' companions, but they are likely similar to the Seyfert companions found by the same technique. Assuming Poisson statistics and considering only the Seyfert companions listed by NED, the probability of finding such a high rate for the Seyferts is $\approx$ 15%. We conclude that the CfA Seyferts are only marginally more likely to have very close bright companions than normal galaxies are.

Chapter 5

COMPARISON OF QUASAR AND SEYFERT HOST GALAXIES

The Seyfert hosts from Chapter 4 are compared with the quasar host galaxies from Chapters 2 and 3. The radio quiet quasars and the Seyferts lie in similar kinds of galaxies spanning the same range of mass centered around L^*. However, for the most luminous quasars, there is a correlation between the minimum host-galaxy mass and the luminosity of the active nucleus. Radio-loud quasars are generally found in hosts more massive than an L^* galaxy. The low-luminosity quasars and the Seyferts both tend to lie in host galaxies seen preferentially face-on, which suggests there is a substantial amount of obscuration coplanar with the galaxian disk. The obscuration must be geometrically thick (thickness-to-radius ~ 1) and must cover a significant fraction of the narrow line region ($r > 100$ pc). We have examined our images for signs of perturbations that could drive fuel toward the

galaxy nucleus, but there are none we can identify at a significant level. The critical element for fueling is evidently not reflected clearly in the large scale distribution of luminous mass in the galaxy.

5.1 Introduction

In the previous chapters we have presented near-IR images of three nearby samples of AGN: low-luminosity quasars, high-luminosity quasars, and Seyferts. In this chapter, we consider the properties of all three samples together to investigate AGN host galaxies over a range of more than 10,000 in nuclear luminosity.

5.2 Host-Galaxy Luminosities and Masses

The CfA Seyferts are plotted in Figure 5.1(a) together with the k-corrected quasar host magnitudes. For the quasars, where the nucleus dominates over the stellar light, M_B should give a good measure of the AGN luminosity. As already discussed, M_B should be taken as a lower (i.e. bright) limit of the nuclear luminosity for the less luminous Seyferts. The Seyfert host-galaxy magnitudes have been adjusted to H assuming $H-K = 0.25$. This color is appropriate for all but the latest-type normal galaxies (Griersmith, Hyland, & Jones 1982; Aaronson 1977). In Figure 5.1(b) we add the galaxies from three other large IR imaging surveys in the literature. Where the samples overlap, we have used our values of the galaxy magnitudes. We include: (i) low-redshift radio-loud quasars (RLQ) and radio-quiet quasars (RQQ), selected to cover the same area in the $V-z$ plane (Dunlop et al. 1993); (ii) hard-X-ray-selected Seyferts from a flux-limited sample (Kotilainen & Ward 1994; we plot only those Seyferts more distant than

$z = 0.02$ to eliminate objects which were much larger than the IR array used in that study); and (iii) mostly Markarian Seyferts (ZDG). Unlike our Seyfert M_B's, for most of the Seyferts in these additional samples the M_B's have been derived from decomposition of visible images and should accurately represent the nuclear magnitudes. We also plot for comparison crude estimates of the magnitudes for the RSA Seyferts; the host IR magnitudes have been computed from visible magnitudes assuming $B-H$=3.7, and the nuclear magnitudes have been derived from small aperture fluxes when possible.

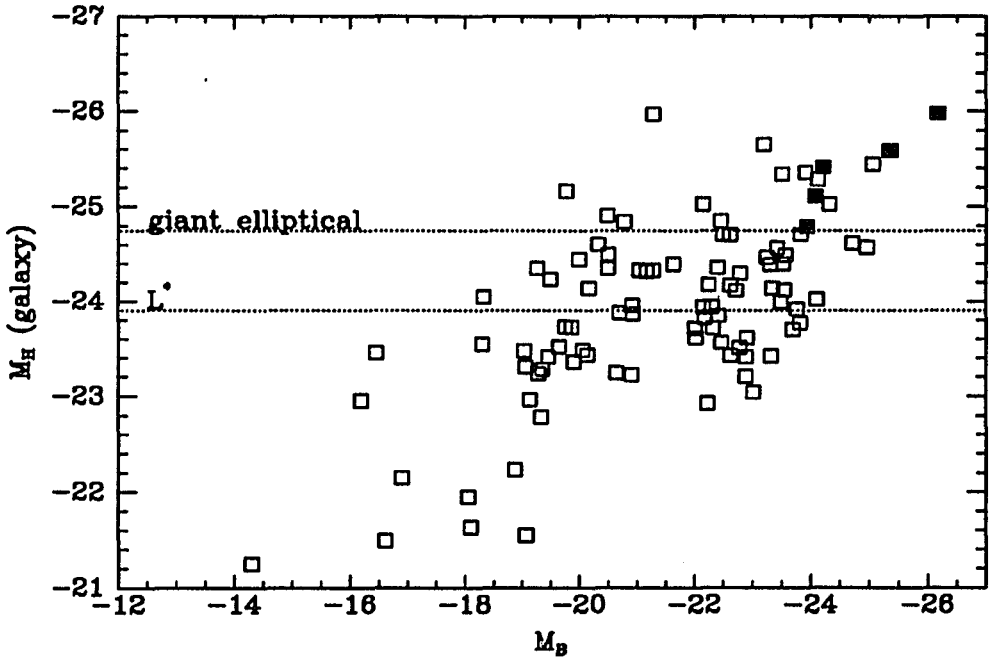

Fig. 5.1.—
(a) Galaxy v. nuclear absolute magnitudes for our three samples: low- and high-luminosity Bright Quasar Survey quasars and CfA Seyferts. Seyfert K magnitudes have been converted to H magnitudes assuming $H-K = 0.25$. Radio-loud quasars are shown as filled squares. The dashed lines show the H magnitude of an L^* galaxy and a giant elliptical galaxy. $H_0 = 80$ km s^{-1} Mpc^{-1}.

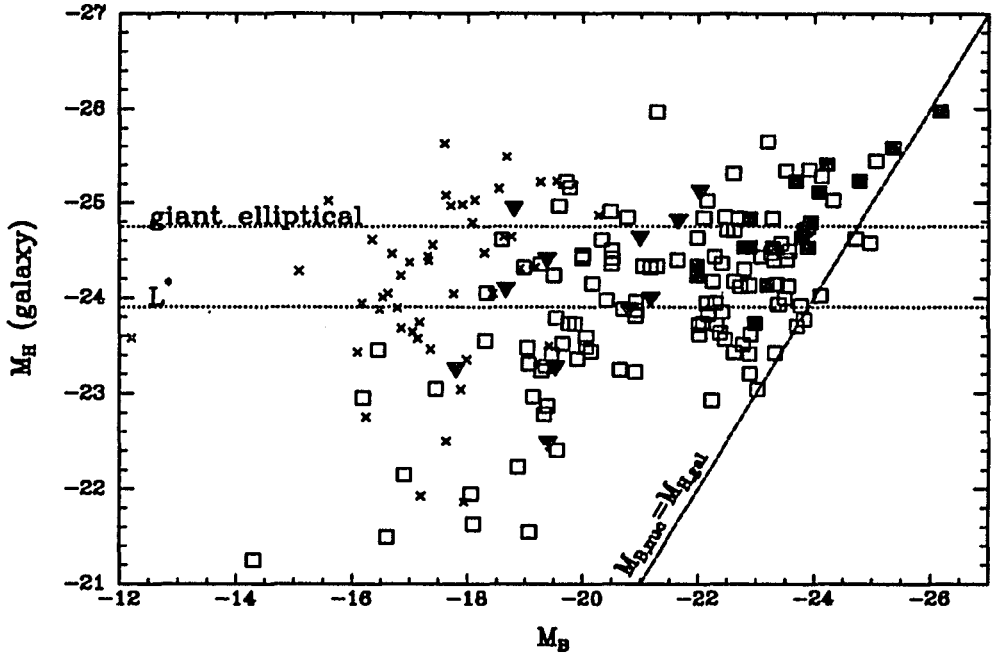

Fig. 5.1—continued
(b) same as (a) but with the addition of four samples from the literature: low-redshift radio-loud and radio-quiet quasars (Dunlop et al. 1993, adjusted to H magnitudes by $H-K = 0.25$), X-ray-selected Seyferts (Kotilainen & Ward 1994, adjusted by the colors they list), Markarian Seyferts (Zitelli et al. 1993; Granato et al. 1993, adjusted to H by the colors they list or $H-K = 0.25$ otherwise), and RSA Seyferts (estimated from visible magnitudes assuming $B-H$=3.7). Filled squares show radio-loud quasars, filled triangles show the X-ray-selected Seyferts, and crosses show the RSA Seyferts.

Despite the different techniques of sample selection and removal of nuclear light there is generally good agreement among all the samples; the properties of the ensemble seem quite well defined. The hosts of the X-ray-selected sample are identical to the CfA hosts. The Seyfert hosts cover the same range of luminosity as the RQQ hosts. For RQQ with luminosities $M_B \lesssim -23$, there seems to be a minimum host luminosity that increases with increasing nuclear power. RLQ are not generally found in hosts less luminous than an L^* galaxy. There are also a few low-luminosity host galaxies harboring very weak AGN.

The absence of luminous quasars in underluminous galaxies (the gap in the lower right corner, to the right of the diagonal line) is not a selection effect; the PG survey is complete for nuclear luminosities brighter than $M_B = -22$ at these redshifts, and the plot is not biased by galaxy non-detections. We note that a similar effect was discussed by Yee (1992) and also by Véron-Cetty & Woltjer (1990), who collected AGN host-galaxy visible magnitudes from their own images and from the literature. Our Figures 5.1(a,b) can be compared with Figure 5 from Véron-Cetty & Woltjer (1990), keeping in mind that our sample is several times larger, is composed of well-defined subsamples, and extends over a wider range in nuclear luminosity. The upturn they claim to see at high nuclear luminosities is more clearly defined in our plot. For RQQ, the minimum host luminosity envelope corresponds approximately to $M_H(\text{galaxy}) = M_B(\text{nucleus})$. To the left of the diagonal line it is possible that the absence of low-luminosity galaxies might be due to selection effects. For example, in the CfA survey, which is based on a galaxy catalog, such objects might have been missed because they would appear stellar. For the X-ray-selected and Markarian samples, the hole could result from small number statistics.

We know that the Seyfert hosts are nearly all spirals. The hosts of the RQQ

appear to be predominantly spirals covering the same range of luminosity as the Seyferts. For high-luminosity or more distant quasars, the galaxy luminosity is currently the most useful clue we have to the galaxy type. Several groups have compared images of RLQ and RQQ to look for differences in their hosts. Three recent studies have considered samples of RLQ and RQQ well-matched in apparent magnitude/redshift space to ensure that they were comparing nuclei of similar luminosity. Hutchings, Janson, & Neff (1989) found that hosts of RLQ are more luminous than their radio-quiet counterparts by 1.9 mag at B and 1.3 mag at R. Véron-Cetty & Woltjer (1990) considered only high-luminosity quasars ($M_B < -23.6$ for $H_0 = 80$ km s^{-1} Mpc^{-1}) and found the RLQ hosts to be 0.6 to 0.9 mag more luminous at i than the RQQ hosts. Dunlop et al. (1993) considered nuclei extending to lower luminosities and found that there is no difference in absolute K magnitude between RLQ and RQQ hosts. As pointed out in that paper, this last result is model dependent; if the RQQ do live in disk galaxies and the RLQ in ellipticals, then the RQQ hosts are several tenths of a magnitude less luminous than the RLQ hosts. The significance is difficult to assess because of the uncertainty in the 0.75 mag correction Dunlop et al. (1993) applied to the host magnitudes to correct for oversubtraction of the nuclear light. Figure 5.1(b) provides a new assessment of the RLQ/RQQ host question. There are RQQ hosts as luminous as the RLQ hosts for nuclei of the same magnitude. However, the RLQ hosts are nearly all above L^*, whereas there are less luminous RQQ hosts for the same nuclear magnitude. Finally, there is a minimum mass for the RLQ hosts that increases with increasing nuclear power. The slope of this cutoff is similar to that for RQQ hosts, but there is an offset of ~ 0.75 mag, i.e. a factor of ~ 2 in luminosity. These results need to be confirmed with larger numbers of RLQ. However, the data support the proposed unification of RLQ with radio galaxies

(Barthel 1989), since the hosts of radio galaxies are generally large ellipticals with IR luminosities of about $2L^*$ and similar to those of the RLQ hosts (e.g. Lilly & Longair 1984; Lebofsky & Eisenhardt 1986).

The RSA sample has added two more candidates for small galaxies containing low-power AGN: NGC 3185 and NGC 4278. Both galaxies have diameters of ≈ 10 kpc, barring distance errors. NGC 4278 is especially interesting because it is the only RSA Seyfert in an elliptical galaxy. Together with the CfA "dwarf" candidates, we believe these objects will provide an interesting topic for future study. In particular, further observations of the nuclear properties of these objects might be able to determine if Seyferts in this luminosity range have intrinsically different types of central engines than their more powerful counterparts. In addition, because these galaxies tend to be very nearby they are good targets for high spatial resolution studies.

In previous chapters we argued that the near-IR light of the quasar hosts is dominated by the quiescent stellar population and that any starburst activity is not strong enough for populations of red supergiants to boost the near-IR output significantly. We believe this is also true for the Seyferts. Fewer than half of the galaxies classified visibly as spirals show arms in the K images, and star-forming visible rings usually appear as smooth plateaus in the near-IR. If there are central starbursts in these objects, most of that light would be removed as part of the point source component and would not significantly boost our inferred galaxy magnitudes.

Since the IR light traces the mass, our results imply the following. For radio-quiet AGN, the dependence of nuclear power on host mass is very shallow. This supports the idea that these AGN inhabit the same sort of galaxy over a large

range of nuclear power. For the highest levels of nuclear activity, the minimum required host mass increases with increasing nuclear luminosity. Finally, there is a family of very low-mass galaxies that can sustain only weak nuclear activity.

5.3 Ellipticities

Since Keel's (1980) discovery that optically-selected Seyfert 1's tend to avoid edge-on disk galaxies, several groups have considered different samples of AGN and have made attempts to find correlations between nuclear properties and host inclinations. In particular, Lawrence & Elvis (1982) showed that a hard-X-ray-selected sample does not show an inclination bias. From their study of axis ratios, X-ray fluxes, and emission lines, they concluded that selection biases seen in other samples are due to obscuration in a flattened configuration parallel to the plane of the host galaxy. Because no obvious correlation of narrow line strengths/decrements with inclination was detected, the obscuring material was thought to be in or cospatial with the broad line region (Lawrence & Elvis 1982; De Zotti & Gaskell 1985). A large but ill-defined sample of Sy 1's and 2's suggested that the inclination bias also applies to Sy 2's, an indication that the obscuration extends beyond the broad line region (Kirhakos & Steiner 1990a).

To investigate this question further, we have compiled a set of AGN samples selected in different wavelength regimes. All of the samples are thought to contain similar objects in disk galaxies. Figure 5.2 shows the distribution of host-galaxy axis ratios for the 7 samples of AGN. For comparison, the distribution for normal disk galaxies is flat from $b/a = 1.0$ down to ≈ 0.2 (Binney & de Vaucouleurs 1981). The first panel shows the CfA Seyferts; we have excluded the two quasars and several peculiar galaxies, all of which have large b/a. The second panel shows the

RSA Seyferts, excluding the one elliptical. The third panel shows low-luminosity PG quasars; some are confirmed spirals, and most of the rest are consistent with being disk systems. The fourth panel shows Seyfert 1's and 1.5's, mostly UV-excess selected, from ZDG; a similar distribution was seen for Markarian Seyferts by MacKenty (1990). The fifth panel shows soft-X-ray-selected AGN from Malkan, Margon, & Chanan (1984). These authors argue that the host galaxies are likely spirals. They point out that the effects of seeing possibly led to an overestimate of axis ratios for the 3 most distant objects on the plot (all are shown with $b/a > 0.9$). The sixth panel shows hard-X-ray-selected Seyferts listed by Turner & Pounds (1989). This list includes the sample of Seyferts imaged by Kotilainen & Ward (1994); we have taken galaxy axis ratios from Kotilainen et al. (1992a) and from NED. We omit two quasars and a few Seyferts for which we do not have an axis ratio. The seventh panel shows the Seyferts from the Extended 12μm Galaxy Sample of Rush, Malkan, & Spinoglio (1993); we were able to obtained the axis ratios for $\approx 80\%$ of the sample by using NED and other sources.

It is immediately obvious that some of these samples show a strong bias against host galaxies with small axis ratios: they are the optically/spectroscopically-selected sample (CfA), the UV-selected samples (PG and Markarian), and the soft-X-ray-selected sample. All of these samples have a deficiency of axis ratios $\lesssim 0.5$, and there is no apparent difference in the cutoff ratio for the low-redshift quasars compared to the Seyferts. The RSA sample shows a slight indication of bias. The hard X-ray and mid-IR samples show no strong bias.

One way to explain these results is to have the obscuring material distributed in a flattened configuration roughly coplanar with the host galaxy's disk. To give the appropriate sharp cutoff, the obscuration must have a central hole and have a thickness-to-radius ratio of ~ 1; this corresponds to an opening half-angle of

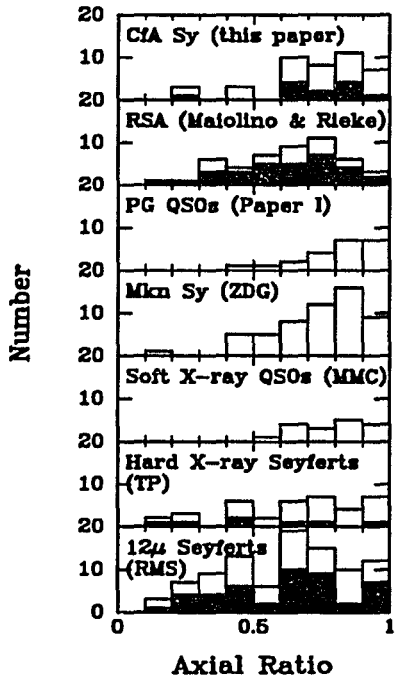

Fig. 5.2.—
Distribution of host-galaxy axis ratios for samples of Seyferts and nearby quasars (see text). Shaded boxes are narrow-lined AGN.

60° for the cone into which we can see the central engine. These data show no evidence that the opening angle changes with increasing nuclear luminosity; the cutoff is the same for the Seyferts and the quasars. The obscuring material must lie outside the continuum source to be able to hide the visible, UV, and soft X-ray continuum. The CfA sample's bias shows that the material must also be outside of most of the broad line region; we note that visibility of the continuum source was not a prerequisite for inclusion of an AGN in this sample. However, a more striking result from the distribution of CfA axis ratios is that *there is also a bias against finding Sy 2's in edge-on galaxies.* This bias implies that a significant fraction of the obscuration must lie outside part of the narrow line region. Adopting the

"standard model" for AGN, the obscuration would lie at least 100 pc from the center (probably extending further) and have a thickness of at least 100 pc.

The strongest constraint on the amount of obscuring material comes from the possibility that soft X-rays are hidden. Using the X-ray photoelectric cross sections given by Morrison & McCammon (1983), we can determine the necessary column density of obscurers. We assume that the soft X-rays are absorbed (the detection bandpass was $\sim 0.1 - 4$ keV) while the hard X-rays pass through (the detection bandpass was $2 - 10$ keV). Assuming an optical depth of unity at ~ 4 keV implies a column density of $N_H \sim 1.5 \times 10^{23}$ cm^{-2}, and a corresponding visual extinction of $A_V \sim 100$ mag! The optical depth for hard X-rays is then less than 0.3 above 6 keV so some would indeed escape. The extinction at 12μm would be several magnitudes, so we might not expect to see too many 12μm Seyferts in edge on galaxies; however, it is possible that the mid-IR flux for galaxies in the 12μm sample has a substantial contribution from star formation which complicates the interpretation. If we relax our soft X-ray constraint to give optical depth unity at only 1 keV, the column density could be ~ 30 times lower. The corresponding UV/visible extinction would still be several magnitudes, enough to hide much of the flux.

Because the column density we derive depends heavily on the bias seen for the soft X-ray sample, we now discuss this sample in more detail. In particular, we investigate the possibility that soft X-rays actually do penetrate the obscuration, but that such objects are not identified as AGN because the follow-up visible spectroscopy fails to detect the broad or narrow emission lines. If this were the case, then there would have to be a non-negligible population of seemingly "normal" galaxies detected in an unbiased soft X-ray sample. However, the selection procedure used for the Malkan et al. (1984) sample was designed to eliminate

"previously catalogued objects" (Chanan, Margon, & Downes 1981), and we are not sure if normal galaxies have been *a priori* eliminated. Fortunately there is another sample, the Einstein Medium Sensitivity Survey (Stocke et al. 1983; Gioia et al. 1984), that we can use to test this possibility. This catalog of 112 objects is an unbiased sample within a specified range of soft X-ray flux. Considering nearby objects ($z < 0.15$), we find 14 confirmed AGN and 8 identifications or possible identifications of galaxies that could harbor a hidden AGN. Of these 8 objects, at most 2 could be edge-on spirals, based on examination of their images on the Palomar Sky Survey plates. Expanding the search to more distant objects ($0.15 < z < 0.3$) we find 15 additional AGN and at most 7 galaxies. We conclude that no more than 25% of the total number of AGN can be hidden in edge-on galaxies. We assume that this statistic is applicable to the Malkan et al. (1984) AGN; both samples have similar detection methods and they result in identical finding rates for AGN. Thus, there is a strong suggestion that Einstein X-rays do not penetrate the obscuration in AGN with edge-on host galaxies.

The RSA sample requires special consideration in this discussion. Its identification criteria are similar to those of the CfA sample, but the bias against edge-on objects is not as strong. The four $b/a < 0.5$ galaxies shown with open symbols in the figure are actually type 1.9's, so the RSA sample does seem to be biased against true Sy 1's in edge-on galaxies. The small number of type 1's makes it difficult to assess the significance of this effect. For Sy 2's there is only a weak bias. However, a very important difference between the RSA sample and the others is that its galaxies are on average an *order of magnitude* closer. Therefore, the visible spectra will have less contamination from extranuclear starlight and will be better able to detect weak lines from the nuclear narrow line region. The RSA catalog does in fact have a higher fraction of Sy 2's (2%) than the CfA catalog

(0.6%). Further support comes from the result that edge-on objects from the CfA and IR samples are also relatively nearby.

We would like to look for differences in nuclear properties between AGN with host-axis ratios near 0.5 versus 1.0. The low-luminosity PG quasar sample is currently the best-studied sample available for this kind of comparison. Unfortunately, there are too few objects at high inclinations to carry out a meaningful test. Choosing the 4 objects with axial ratios $b/a \leq 0.7$, we find that they do not differ from the others in, e.g., B luminosity or visible spectral index, but this is obviously not a significant result. It will be interesting to carry out this kind of analysis with a larger sample.

To summarize, the axis ratios for the host galaxies of nearby Seyferts and quasars strongly suggest that there is a large amount of obscuration, $N_H \sim 10^{22}$ *to* 10^{23} cm^{-2}, in a layer $>$ 100 pc thick coplanar with the disk of the host galaxy at a distance of $>$ 100 pc from the central source. In a recent study of molecular line emission in NGC 1068, Tacconi et al. (1994) describe evidence for nuclear gas in a thick configuration much like the one we describe. The b/a distributions suggest that this is a common component of Seyferts and low-luminosity quasars.

We can now ask whether normal spiral disks also contain molecular gas in this configuration, or if such an arrangement is particular to AGN. We note that the column densities are much higher than observed in face-on spiral disks. There are not too many galaxies for which we know the distribution of gas and dust inside the central few hundred pc, but we can use the Milky Way as a test case. Our Galaxy contains $\sim 10^8$ $M_\odot$ of molecular gas inside the central 500 pc, some of it in a ring structure. This material is distributed in a flattened configuration coplanar

with the overall Milky Way disk; as traced by molecular line emission, this gas has a thickness of only $\sim 30 - 50$ pc (Güsten 1989 and references therein). This layer is not thick enough to meet our requirement. There are now several other galaxies known to have compact rings of molecular gas in their nuclear regions. As summarized by Sofue (1991), high-resolution CO maps show that rings with radius $r \sim 200$ pc might be a common feature of Sb/c spirals, possibly formed when star-formation activity clears gas out of the central regions of the galaxy. However, there is not yet evidence that these rings are thick.

On the other hand, there is some evidence that a thick ring can exist in a galaxy where Seyfert activity does not dominate the nuclear energetics. One example is NGC 4945, a nearby, edge-on spiral which is undergoing nuclear star formation but might also contain an obscured Seyfert. Bergman et al. (1992) have used CO line profiles to deduce the presence of a molecular ring in this galaxy. In their model, the CO emission originates in a ring with radius 220 pc and thickness 200 pc. The ring is composed of molecular clouds with an average size < 15 pc and column density $\sim 10^{22}$ cm^{-2}. A line of sight through the plane of the galaxy intercepts ~ 5 of these clouds, yielding a total extinction in the range we infer for the AGN obscurers.

The Bergman et al. (1992) ring model suggests a useful modification to our simplistic picture of obscuration in AGN. Putting the obscuring material into small clouds helps explain some of the puzzling observations. For example, the resulting patchiness of the obscuration will allow a line-of-sight directly into the broad-line region in a few objects. It can also explain the relatively sharp cutoff at an axis ratio of 0.5; each cloud is optically thick enough to cut off continuum or line flux, even if only one cloud lies along the line-of-sight.

We conclude that axis ratio distributions can provide a powerful diagnostic for studying obscuration and geometry in AGN, and we suggest that future studies of large AGN samples include axis ratio measurements. In particular, we feel that rigorous tests with soft X-ray samples and consideration of far-IR-selected samples could put further constraints on the depth to the nucleus through this large scale obscuration.

5.4 Fueling the Active Nucleus

As discussed above, the connections between Seyfert activity and galaxy perturbations (such as bars and interactions) have been popular topics for study. For more distant quasars, finding bars is problematic but the frequency of companions has been studied (see, e.g., Yee 1987).

In previous chapters we investigated the rate at which low-redshift PG quasars have close interactions with nearby (< 30 kpc projected separation), massive (H luminosity corresponding to $\frac{1}{10}L^*$) companions; a companion with these parameters undoubtedly provides enough tidal force to perturb the gravitational potential of the AGN host. The overall rate of these interactions for the combined quasar sample was found to be $\approx 23\%$. This is nearly the same as the rate (22%) of physical companions we determined for the CfA Seyferts. Therefore, we find that these AGN have close companions at a similar rate over 10 mag of nuclear luminosity. The marginal excess of such companions noted for the high-luminosity quasars is likely a result of small number statistics. The overall frequency of close, massive companions and the range of AGN host luminosities both indicate that AGN need not be triggered by the merger of two large galaxies. However, they do not rule out the possibility that minor mergers could trigger activity; recent

simulations have shown that even a small infalling satellite can drive large amounts of gas into the center of a spiral galaxy (Mihos & Hernquist 1994).

The proximity of the CfA Seyferts and the long wavelengths of our images allow us to approach the question of fueling from a more comprehensive angle. We can ask how many of these objects do not show *any* evidence for a disturbance. Taking close companions, bars, weaker oval distortions, tidal tails, and disturbed morphologies to indicate asymmetric potentials favorable for funneling gas to the center, we find no sign of disturbance in at least 7 of the 46 Seyferts: Mkn 335, Mkn 993, 1058+45, NGC 3982, NGC 4235, NGC 5252, NGC 5273, and possibly also in NGC 4395, Mkn 270, Mkn 471, and Mkn 841 (we have no images for the latter four, but they are not classified as barred and they do not have close companions). These Seyferts cover the same range of nuclear and galaxy luminosity as the sample as a whole. Given that some of the Seyferts show no evidence for a disturbance, it is relevant to ask whether a significant perturbation to the mass distribution of the host-galaxy potential is necessary for AGN activity. For example, we can speculate that these apparently undisturbed systems once contained a bar that has now disappeared. Theoretical models predict that once the bar has channeled enough ($\sim 1\%$) of the galaxy's mass into the central few hundred pc of the galaxy, the bar will dissolve on $\sim$ Gyr timescales (Friedli & Benz 1993). These models also predict it is possible for a remnant triaxial bulge to continue to support the inflow of gas through a gaseous bar. Interestingly, nearly all of the apparently undisturbed galaxies have very early types (S0-Sa); it is possible that a prominent bulge makes a weak distortion more difficult to detect. However, it is intriguing that visible bars appear to be required to feed nuclear starbursts in early-type spirals (Devereux 1993), whereas exactly the opposite seems to prevail for Seyferts.

It will be interesting to look harder in these apparently undisturbed systems

for signs of asymmetry, such as smaller companions or faint tidal tails that could have been missed in the relatively shallow IR images. It will also be interesting to compare quantitatively the properties of the outer rings and the IR bars to those in normal galaxies when IR samples become available. New models will be useful to determine if these bars should be any more efficient than those of normal galaxies at funneling gas to the galaxian centers.

However, we feel that the bulk of the observations reported here suggest we look elsewhere for the key to fueling the active nucleus, at least for the Seyferts and low-luminosity quasars. To summarize, the Seyferts do not have bars more often than normal galaxies; they are only marginally more likely to have significant interactions; a substantial number show no evidence for a disturbance even in our relatively high-resolution images of the mass-tracing component of the host; and the nuclear luminosity does not depend on the size of the bulge as determined from the spiral type. We conclude that the key to fueling the AGN need not show itself in the large (> several hundred pc scale) stellar potential of the host galaxy. An interaction or a bar can certainly drive fuel into the central kiloparsec and, statistically, star formation activity is clearly enhanced by the presence of either (e.g. Hummel et al. 1990). However, funneling the fuel more than 3 orders of magnitude closer into the central engine must ultimately depend on details of the star formation and gas dynamics invisible in the large scale, mass-tracing stellar component of the galaxy.

5.5 Summary

We have obtained and analyzed near-IR images of nearly 100 AGN host galaxies, equally divided among Seyferts and quasars, and we have compared them

to Seyfert and quasar host galaxies from the literature. We find the following.

1. Host luminosities: The near-IR light is a good tracer of luminous mass in these AGN host galaxies. There is a clear continuity of host-galaxy properties from Seyferts into radio-quiet quasars. Most of these galaxies are disk systems. For quasars with nuclei more luminous than $M_B = -23$ there is a minimum host-galaxy mass that increases linearly with increasing nuclear power. Radio-loud quasars are not generally found in hosts less massive than an L^* galaxy. There is a population of very low-mass spirals with very low-luminosity central engines.

2. Host ellipticities: There is a selection bias against finding UV-excess AGN, spectroscopically-selected AGN (both broad and narrow lined objects), and probably even soft X-ray AGN, in highly inclined galaxies. This suggests a large amount of obscuration ($A_V \sim 10 - 100$ mag), coplanar with the host galaxy's disk, having a thickness-to-radius ratio ~ 1, and covering a significant fraction of the narrow line region (> 100 pc).

3. Host morphologies: An examination of visible properties shows that Seyferts do not have bars or nearby companions any more frequently than do normal spirals. We have analyzed the IR images for signs of nonaxisymmetry that might be hidden in the visible but that could nonetheless contribute to the fueling of the central engine. We found several previously unidentified bars, but there are some AGN hosts that show no signs of perturbation even in the IR. The critical elements of the fuel supply need not be visible in the large-scale distribution of luminous mass in the host galaxy.

Chapter 6

FUTURE WORK

There are many projects which we would like to undertake to follow up the work presented here. In this chapter we describe a few we have already begun and suggest some additional ones for future work.

In Chapter 2 we found that a few of the low-luminosity quasars have been imaged with CCDs to yield host-galaxy magnitudes in the visible. The colors of these galaxies were found to be blue in $V-H$, indicative of a burst of star formation in the recent past or considerable ongoing star formation. There is great potential for modeling the stellar evolutionary history of the host galaxies of Seyferts and nearby quasars if more visible-to-infrared colors can be measured. To determine accurate colors, it is very important to treat point-source removal in a consistent manner across all wavelengths. We have already begun a program to obtain CCD images for nearby quasars from our sample. We are concentrating our efforts in two wavelengths. We have observed some galaxies in the B-band, which provides a long color baseline when combined with the near-IR data. The B images are extremely useful for detecting spiral arms and other areas undergoing star formation. We

have also observed some galaxies in the i-band, to minimize contamination from emission lines. We are hopeful that the visible-to-infrared colors will provide useful constraints for evolutionary models of galaxies containing monsters in their nuclei.

In Chapter 4 we characterized the IR structure of Seyfert galaxies through analysis such as elliptical isophote fitting. We would like to compare and contrast the Seyfert host IR properties with a control sample of normal galaxies. The ironic fact is that we do not really have a good picture of how normal galaxies look in the near-IR! The combination of large-format IR arrays with large amounts of telescope time has been sufficiently rare that there have not been many IR imaging studies of large samples of galaxies. A few groups are now presenting first results from this type of project. We have recently begun working on one survey with A. Grauer and M. Rieke, who have obtained near-IR images for ~ 50 nearby galaxies. Control sample in hand, we will look differences in the distribution of luminous matter between Seyferts and normal spirals; we will examine luminosity profiles, bar properties, etc.

In Chapters 3 and 5 we commented that the host galaxies of more distant quasars escape classification. Obviously, the superior spatial resolution of HST will be useful for determining host-galaxy morphology for distant objects. HST is also useful for probing the small-scale structure in nearby Seyferts. Of course, HST can only provide visible images as currently configured.

Throughout this work, we have been treating the active nuclei themselves as simply annoyances. It is high time to stop throwing this information away! As we have shown, even small aperture fluxes can be significantly contaminated by stellar emission at IR wavelengths. Therefore, the decompositions we have performed are crucial for obtaining accurate SEDs of the nuclei. We plan to put the nuclear

fluxes we have determined together with nuclear fluxes from other wavelengths to build up nuclear SEDs. These SEDs will be used to investigate possible emission mechanisms in the active nuclei.

Finally, one of the most intriguing results of this work is the lack of edge-on galaxies hosting AGN. These results need to be confirmed with better X-ray samples. If confirmed, our findings have interesting implications. One obvious ramification is that we have been missing roughly half of the AGN in the local universe. The space density of AGN, the fraction of galaxies with currently active nuclei, and the contribution of point sources to the soft X-ray background could all be underestimated by a factor of 2! Hard X-ray selection is one obvious way to find the "missing" objects. Infrared selection might provide another. Studying the edge-on cases in more detail could add new information on the nature and distribution of the obscuration.

REFERENCES

Aaronson, M. 1977, Ph.D. Thesis, Harvard University

Baade, W., & Minkowski, R. 1954, ApJ, 119, 206

Balick, B., & Heckman, T. M. 1983, ApJ, 265, L1

Barthel, P. D. 1989, ApJ, 336, 606

Becklin, E. E., Henry, J. P., & Telesco, C. M. 1984, ApJ, 280, 98

Bergman, P., Aalto, S., Black, J. H., & Rydbeck, G. 1992, A&A, 265, 403

Binney, J., & de Vaucouleurs, G. 1981, MNRAS, 194, 679

Block, D. L., & Wainscoat, R. J. 1991, Nature, 353, 48

Boroson, T., & Oke, J. B. 1984, ApJ, 281, 535

Boroson, T., Persson, S., & Oke, J. B. 1985, ApJ, 293, 120

Byrd, G. G., Sundelius, B., & Valtonen, M. 1987, A&A, 171, 16

Chanan, G. A., Margon, B., & Downes, R. A. 1981, ApJ, 243, L5

Conway, R. G., & Röser, H.-J. 1993, in Jets in Extragalactic Sources, ed. Röser & Meisenheimer, (Heidelberg: Springer), in press

Cox, C. I., Gull, S. F., & Scheuer, P. A. G. 1991, MNRAS, 252, 558

Danese, L., Zitelli, V., Granato, G. L., Wade, R., de Zotti, G., & Mandolesi, N. 1992, ApJ, 399, 38

Dahari, O. 1985, ApJS, 577, 643

de Vaucouleurs, G., de Vaucouleurs, A., Corwin, H. G. Jr. 1976, Second Reference Catalogue of Bright Galaxies (Austin: University of Texas) (RC2)

de Vaucouleurs, G., de Vaucouleurs, A., Corwin, H. G. Jr., Buta, R. J., Paturel, G., & Foqué, P. 1991, Third Reference Catalogue of Bright Galaxies (New York: Springer-Verlag) (RC3)

Devèreux, N. 1993, preprint, to be published in "Mass Induced Transfer Activities in Galaxies"

De Zotti, G., & Gaskell, G. M. 1985, A&A, 147, 1

Dunlop, J. S., Taylor, G. L., Hughes, D. H., & Robson, E. I. 1993, MNRAS, 264, 455

Edelson, R. A., Malkan, M. A., & Rieke, G. H. 1987, ApJ, 321, 233

Elias, J. H., Frogel, J. A., Matthews, K., & Neugebauer, G. AJ, 87, 1029

Efstathiou, G., Ellis, R. S., & Peterson, B. A. 1988, MNRAS, 232, 431

Feigelson, E. D., & Nelson, P. I. 1985, ApJ, 293, 192

Filippenko, A. V., Ho, L. C., & Sargent, W. L. W. 1993, ApJ, 410, L75

Friedli, D., & Benz, W. 1993, A&A, 268, 65

Fuentes-Williams, T., & Stocke, J. T. 1988, AJ, 96, 1235

Gehren, T., Fried, J., Wehinger, P. A., & Wyckoff, S. 1984, ApJ, 278, 11

Gioia, I. et al. 1984, ApJ, 283, 495

Goldschmidt, P., Miller, L., La Franca, F., & Cristiani, S. 1992, MNRAS, 256, 65p

Granato, G. L., Zitelli, V., Bonoli, F., Danese, L., Bonoli, C., & Delpino, F. 1993, ApJS, 89, 35

Green, R. F., & Yee, H. K. C. 1984, ApJS, 54, 495

Griersmith, D., Hyland, A. R., & Jones, T. J., AJ, 87, 1106

Güsten, R. 1989, in The Center of the Galaxy, IAU Symposium 136, ed. M. Morris (Dordrecht: Kluwer), 89

Heckman, T. M. 1978, PASP, 90, 241

Heller, C. H., & Shlosman, I. 1994, ApJ, 424, 84

Hickson, P., & Hutchings, J.B. 1987, ApJ, 312, 518

Huchra, J., & Burg, R. 1992, ApJ, 393, 90

Hummel, W., van der Hulst, J. M., Kennicutt, R. C., & Keel, W. C. 1990, A&A, 236, 333

Hutchings, J.B. 1987, ApJ, 320, 122

Hutchings et al. 1984, ApJS, 55, 319

Hutchings, J. B., & Campbell, B. 1983, Nature, 303, 584

Hutchings, J. B., Crampton, D., & Campbell, B. 1984, ApJ, 280, 41

Hutchings, J.B., & Crampton, D. 1990, AJ, 99, 37

Hutchings, J. B., Janson, T., & Neff, S. G. 1989, ApJ, 342, 660

Hutchings, J.B., Johnson, I., & Pyke, R. 1988, ApJ, 66, 361

Hutchings, J.B., & Neff, S.G. 1992, AJ, 104, 1

Keel, W. C., 1980, AJ, 85, 198

Keel, W. C. Kennicutt, R. C. Jr., Hummel, E., & van der Hulst, J. M. 1985, AJ, 90, 708

Kellerman, K. I., Sramek, R., Schmidt, M., Shaffer, D. B., & Green, R. 1989, AJ, 98, 1195

Kennicutt, R. C. Jr., & Keel, W. C. 1984, ApJ, 279, L5

Kent, S. M. 1985, ApJS, 59, 115

Kirhakos, S. D., & Steiner, J. E. 1990, AJ, 99, 1435

Kotilainen, J. K., Ward, M. J., Boisson, C., DePoy, D. L., Bryant, L. R., & Smith, M. G. 1992a, MNRAS, 256, 125

Kotilainen, J. K., Ward, M. J., Boisson, C., DePoy, D. L., & Smith, M. G. 1992b, MNRAS, 256, 149

Kotilainen, J. K., Ward, M. J., & Williger, G. M. 1993, MNRAS, 263, 655

Kotilainen, J. K., & Ward, M. J., 1994, MNRAS, 266, 953

Kristian, J. 1973, ApJ, 179, L61

Lawrence, A., & Elvis, M. 1982, ApJ, 256, 410

Lebofsky, M. J., & Eisenhardt, P. R. M. 1986, ApJ, 300, 151

Lilly, S. J., & Longair, M. S. 1984, MNRAS, 211, 833

MacKenty, J. W. 1989, ApJ, 343, 125

MacKenty, J. W. 1990, ApJS, 72, 231

Maiolino, R., & Rieke, G., private communication

Malkan, M. A. 1984, ApJ, 287, 555

Malkan, M. A., Margon, B., & Chanan, G. A. 1984, ApJ, 280, 66

Mihos, J. C., & Hernquist, L. 1994, ApJ, 425, L13

Miller, P., Rawlings, S., & Saunders, R. 1993, MNRAS, 263, 425

Mobasher, B., Sharples, R.M., & Ellis, R.S. 1993, MNRAS, 263, 560

Morrison, R., & McCammon, D., 1983, ApJ, 270, 119

Neugebauer, G., Green, R. F., Matthews, K., Schmidt, M., Soifer, B. T., & Bennett, J. 1987, ApJS, 63, 615

Osterbrock, D. E., & Martel, A. 1993, ApJ, 414, 552

Pompea, S. M., & Rieke, G. H. 1990, ApJ, 356, 416

Rieke, G. H., Loken, K., Rieke, M. J., & Tamblyn, P. 1993, ApJ, 412, 99

Rieke, M. J., Winters, G. S., Cadien, J., & Rasche, R. 1993, in SPIE Proceedings, Vol. 1946, Infrared Detectors and Instrumentation, ed. A. M. Fowler, 214

Röser, H.-J., & Meisenheimer, K. 1991, A&A, 252, 458

Rush, B., Malkan, M. A., & Spinoglio, L. 1993, ApJS, 89, 1

Sandage, A., & Tammann, G. A. 1987, A Revised Shapley-Ames Catalog of Bright Galaxies, 2nd ed. (Washington: Carnegie Institute of Washington)

Sanders, D. B., Phinney, E. S., Neugebauer, G., Soifer, B. T., & Matthews, K. 1989, ApJ, 347, 29

Savage, A., Cannon, R. D., Stobie, R. S., Kilkenny, D., O'Donoghue, D., & Chen, A. 1993, Proc. Ast. Soc. Australia, 10, 265

Scalo, J. M. 1986, Fund. Cosmic Phys., 11, 1

Schmidt, M. 1963, Nature, 197, 1040

Schmidt, M. & Green, R. F. 1983, ApJ, 269, 352

Scoville, N. Z., Matthews, K., Carico, D. P., & Sanders, D. B. 1988, ApJ, 327, L61

Sellwood, J. A., & Wilkinson, A. 1993, Reports on Progress in Physics 56, 1

Seyfert, C. K. 1943, ApJ, 97, 28

Simkin, S. M., Su, H. J., & Schwarz, M. P. 1980, ApJ, 237, 404

Smith, E. P., Heckman, T. M., Bothun, G. D., Romanishin, W., & Balick, B. 1986, ApJ, 306, 64

Sofue, Y. 1991, PASJ, 43, 671

Stocke, J. T. et al. 1983, ApJ, 273, 458

Stockton, A. 1982, ApJ, 257, 33

Tacconi, L. J., Genzel, R., Blietz, M., Cameron, M., Harris, A. I. & Madden, S. 1994, preprint

Thomson, R. C., MacKay, C. D., & Wright, A. E. 1993, Nature, 365, 133

Turner, T. J., & Pounds, K. A. 1989, MNRAS, 240, 833

Véron-Cetty, M.-P. & Véron, P. 1984, ESO Scientific Report No. 1

Véron-Cetty, M.-P. & Woltjer, L. 1990, A&A, 236, 69

Woltjer, L. 1990, in Active Galactic Nuclei, ed. T. J.-L. Couorvoisier & M. Mayor (Heidelberg: Springer-Verlag), 1

Yee, H. K. C. 1983, ApJ, 272, 473

Yee, H. K. C. 1987, AJ, 94, 1461

Yee, H. K. C. 1992, in Relationships Between Active Galactic Nuclei and Starburst Galaxies, ASP Conference Series 31, ed. A. V. Filippenko, 417

Zitelli, V., Granato, G. L., Mandolesi, N., Wade, R., & Danese, L. 1993, ApJS, 84, 185

This manuscript was prepared with the AAS LaTeX macros v3.0.